THE USE OF INERTIAL MEASUREMENT UNITS TO PERFORM KINETIC ANALYSES OF SPRINT ACCELERATION AND CHANGE OF DIRECTION TASKS

A Thesis
by
REED D. GURCHIEK

Submitted to the Graduate School
at Appalachian State University
in partial fulfillment of the requirements for the degree of
MASTER OF SCIENCE

May 2017
Department of Health and Exercise Science

THE USE OF INERTIAL MEASUREMENT UNITS TO PERFORM KINETIC ANALYSES OF SPRINT ACCELERATION AND CHANGE OF DIRECTION TASKS

A Thesis
by
REED D. GURCHIEK
May 2017

APPROVED BY:

_____
Herman van Werkhoven, Ph.D.
Chairperson, Thesis Committee

_____
Jeffrey M. McBride, Ph.D.
Member, Thesis Committee

_____
Alan R. Needle, Ph.D.
Member, Thesis Committee

_____
Ryan S. McGinnis, Ph.D.
Member, Thesis Committee

_____
Kelly J. Cole, Ph.D.
Chairperson, Department of Health and Exercise Science

_____
Max C. Poole, Ph.D.
Dean, Cratis D. Williams School of Graduate Studies

Abstract

THE USE OF INERTIAL MEASUREMENT UNITS TO PERFORM KINETIC ANALYSES OF SPRINT ACCELERATION AND CHANGE OF DIRECTION TASKS

Reed Gurchiek
B.S. Cumberland University

Chairperson: Dr. Herman van Werkhoven

Background: To further the understanding of the factors most important to accelerative running and to allow coaches to apply this knowledge in the field requires an assessment method that is accurate, convenient, and comprehensive. Inertial measurement units (IMUs) are becoming more popular in the analysis of human movement and might provide the technology to perform a more comprehensive sprint acceleration assessment because of their relatively low cost, small size, and ability to measure kinematic and kinetic data. Their ability to accurately estimate kinetic variables related to sprint acceleration performance (i.e., 3-dimensional ground reaction force, $\boldsymbol{F}$) has not been assessed. **Purpose:** The purpose of this thesis was three-fold. First was to assess the criterion validity of IMU estimates of the magnitude and orientation of $\boldsymbol{F}$ during accelerative running tasks by comparison to a force plate. The second was to determine the concurrent validity of a novel IMU-based sprint velocity estimation algorithm. The third was to determine the concurrent validity of IMU estimates of kinetic determinates of sprint acceleration performance. **Methods:** Fifteen subjects (12 male, 3 female) volunteered to participate in the first study. Twenty-eight subjects (16 male, 12 female) consisting of both collegiate level sprinters and non-sprinters participated in the second and third studies. For the

first study, step averaged, peak, and continuous ***F*** estimates were made by a single sacral attached IMU and a force plate during the initial push and first step of a linear sprint start as well as for the first step of a change of direction task (both to the right and left). The estimates were compared using root mean square error (RMSE), Pearson's product moment correlation coefficient (r), and Bland-Altman 95% limits of agreement (LOA). For the second and third studies, subjects performed three maximal effort 40 m sprints from a four-point stance. A recently validated position-time method along with the proposed IMU method gave estimates of maximal, average interval, and continuous sprint velocity (study 2) as well as kinetic determinants of sprint performance (study 3). The error in the IMU estimates was quantified by RMSE, r, and LOA. **Results:** The results from the first study suggest the IMU method is inappropriate for estimation of continuous and peak ***F*** (RMSE $\geq$ 514.67 N), however, step averaged estimates were characterized by less error (RMSE $\leq$ 169.91 N), especially for the linear sprint condition (RMSE $\leq$ 77.32 N). For the second study, the IMU estimates showed absolute percent error between 5.09% and 7.13% and significant ($p < 0.01$) correlations with reference measures ($r \geq 0.79$). Finally, for the third study, the IMU estimates of the kinetic parameters most important to evaluating sprint performance were significantly ($p < 0.01$) correlated with reference measures ($r \geq 0.73$) and characterized by relatively low bias and low RMSE. The IMU estimates were able to differentiate sprinters from non-sprinters equally as well as the reference photocell system. **Conclusion:** The results from these studies broaden the scope of IMU applications in field-based human movement analysis, especially in the context of sprint performance. Potential sources of error are detailed in each manuscript and provide a foundation from which future research may be aimed to improve these methods.

Acknowledgments

I send my sincerest thanks to all of my thesis committee members. Each of you have provided me with unique and invaluable insight into conducting robust research: Dr. Alan Needle for your help with the statistical methods and analysis of results, Dr. Jeffrey McBride for your help in understanding the fundamentals of human biomechanics especially as they relate to the kinetic and kinematic determinants of performance, Dr. Ryan McGinnis for your help with understanding rigid body dynamics and the principles of IMU data analysis, and finally, I owe a big thanks to my Thesis Chair and mentor Dr. Herman van Werkhoven for your insight into all aspects of the research process and the development of objective conclusions as well your patience for my many unplanned office visits.

Dedication

I dedicate this Thesis to my wife Zoë and my son Kadrian. I appreciate your patience through this entire project given my many late nights and for allowing the discussion of the studies' results to be the occasional dinner topic.

Table of Contents

Foreword

The three studies conducted in this thesis are described in three separate chapters (Chapters 3, 4, and 5). Each will be submitted to an international peer-reviewed journal and have been formatted according to the IEEE Citation Reference Standard.

Chapter 1: Introduction

Sprinting bouts during gameplay of many sports are often over such short distances that maximal sprinting velocity is never reached [1]. Thus, for these sports, the ability to maximally accelerate is arguably of greater value than maximal sprinting velocity. Many factors contribute to an athlete's accelerative ability that are related to both the orientation and the magnitude (F_{res}) of the ground reaction force ($\boldsymbol{F}$) as well as how these values change with increasing sprint velocity. For example, the ability to produce large magnitudes of force and forward power (P_x, where x denotes the forward direction) at high sprinting velocities has been related to better sprint acceleration performance [2–4]. The factors related to the orientation of $\boldsymbol{F}$ indicate the runner's ability to apply forces such that the forward component of $\boldsymbol{F}$ (F_x) is maximized while maintaining a sufficient vertical component (F_z) [2, 3, 5]. This has been shown to be advantageous independent of F_{res} [2, 5–9]. The ratio of force (*RF*), expressed as the ratio of the average F_x to the average F_{res} for one step, is an index that has been used to assess an athlete's ability to optimally orient $\boldsymbol{F}$ [2, 3, 5, 10]. Greater *RF*s are characteristic of athletes with greater accelerative ability [2, 3]. Further, it is important that an athlete maintain the ability to generate large magnitudes of F_x and thus also a high *RF* throughout a maximal sprint, which has been assessed using the slope of the F_x-velocity (sFV) and the *RF*-velocity curve (dRF). Some research suggests faster sprinters show a less negative dRF indicating an ability to maintain a more forward oriented $\boldsymbol{F}$ with each foot contact as sprint velocity increases [3, 5].

Improving acceleration performance involves targeting weaknesses related to both muscular characteristics and sprinting technique. Identifying weaknesses to target requires an accurate assessment method. $\boldsymbol{F}$ data must be collected for each step during a sprint to

calculate the aforementioned kinetic determinants of sprint acceleration performance (i.e., P_x, F_x, RF, dRF, sFV). The current methods used to obtain force data during accelerative running include multiple sprints over a single force plate [2, 7, 11], instrumented treadmills [3, 5, 12], and inverse dynamics with position-time or velocity-time data using equations describing sprinting dynamics [13–15]. These techniques have certain limitations and the development of a new method that can provide a more comprehensive assessment has been the focus of recent research.

Accelerometers have been used to estimate kinetic data, spatiotemporal data, and energy expenditure in various human movement tasks [16–19]. Thus, accelerometers might provide a more convenient and cost effective means to perform kinetic as well as kinematic analyses of accelerative running. Inertial measurement units (IMUs) come equipped with accelerometers, gyroscopes, and magnetometers. Data fusion algorithms are used to combine each of these sensor outputs to provide a better estimate of the desired measure [20–23]. Several studies have validated the use of IMUs to analyze dynamic human movements. This includes accurate estimates of stride and stance durations [24–26], trunk angles [22], and velocity [27] during sprinting. Others have rotated the acceleration vector measured in the sensor reference frame such that it is expressed in the world reference frame to accurately assess center of mass kinematics during jumping [28, 29] and walking [30] tasks. If the orientation of an IMU relative to a force plate is known, then IMU estimates of $\boldsymbol{F}$ using Newton's 2nd Law may be compared to that measured by the force plate [31]. To the author's knowledge, no studies have assessed the ability of a trunk mounted IMU to perform kinetic analyses of accelerative running tasks. Further, for the method to be fully comprehensive it must have the means to accurately estimate sprint velocity. IMUs have

been used to estimate running velocity for constant velocities of relatively low magnitude (≤ 3.5 m/s) [32], but it would be inappropriate to generalize the application of such a method to the acceleration phase of sprinting. To the author's knowledge, only one study has investigated the use of a single IMU to measure sprint velocity during a 100 m sprint [27]. However, the details of the algorithms employed were not given.

Thus, the purpose of this thesis was three-fold. First, to assess the criterion validity of IMU estimates of three-dimensional $\boldsymbol{F}$ compared to a force plate during accelerative tasks. Second, to develop and assess the concurrent validity of a novel IMU-based sprint velocity estimation algorithm, and third to assess the concurrent validity of IMU estimates of sprint performance variables by comparison to a recently validated position-time method. Chapter 2 provides a detailed description of the relevant research that provides the rationale to conduct the studies. Chapters 3, 4, and 5 describe the three studies separately, each formatted as a separate manuscript. Finally, the Chapter 6 summarizes the results of the studies as they relate to past and potential future research followed by the appendices.

Chapter 2: Literature Review

2.1 Current Methodologies Used to Assess Sprint Performance

The current methodologies used to assess sprint performance do so by providing estimates of several factors related to both the magnitude and orientation of the ground reaction force ($\boldsymbol{F}$) and sprint velocity. The ratio of force (RF), defined as the percentage of the magnitude of $\boldsymbol{F}$ (F_{res}) that is comprised of F_x, has been used as an index of a runner's ability to orient $\boldsymbol{F}$ such that F_x is maximized. Greater F_x and RF have been shown to be characteristic of greater acceleration ability [2, 3, 5, 6, 33]. The ability to produce high amounts of F_x and RF as sprint velocity increases, indicated by the slope of the linear relationship between F_x-v (sFV) and RF-v (dRF), is also used to characterize the maintenance of optimal technique in the acceleration phase of sprinting [2, 3, 5, 14]. Extrapolation of the F_x-v line to the x and y intercepts provide estimates of the runner's theoretical maximal velocity (v_0) and maximal forward force (F_0) respectively, which are also included in the current sprint acceleration assessment methodologies [2, 12, 15, 34]. The ability to produce large forward forces at greater sprinting velocities is well described by forward power (P_x) which has also been related to acceleration performance [2, 3, 5].

These sprint acceleration performance variables have been identified because of the ability to collect the relevant kinetic and kinematic data during the acceleration phase of sprinting and relate the variables to performance. The importance of an accurate measurement technique for accelerative running may allow coaches to profile their athletes' acceleration performance based on an objective standard. This then may be used to design their athletes' programs to target the weaknesses identified by the assessment and to evaluate the effectiveness of a program by comparing pre- and post-intervention measures. Further, an accurate assessment

technique allows researchers to study how those variables related to acceleration performance are obtained by faster runners such as their relationship with joint kinematics [35], muscular activation-deactivation patterns [12, 36, 37], and structural characteristics [38, 39] may be determined. A step-by-step kinetic analysis of accelerative running is necessary to obtain the variables related to performance. Currently, three methods have been used: (1) multiple sprints with a single force plate, (2) instrumented torque treadmills (TT) and non-motorized treadmills (NMT), and (3) inverse dynamics using position-time and/or velocity-time data and equations describing sprinting.

Cavagna et al. [11] were perhaps the first to collect kinetic data for each step during a sprinting task using force plates. Their method involved piecing together force data from multiple sprints where each sprint measured a different foot contact or set of foot contacts. Integration of the force-time curve provided an estimate of the change in velocity obtained over the foot contact and the initial velocity before force plate contact was determined using photocells.

This method has since been used by others to assess acceleration performance [2] and as a standard of comparison for validation of new measurement techniques [14]. The method used in the latter two studies only differ from the original in that the distance of the sprint was 40 m (Cavagna et al. [11]:56 m) and high speed video was used to determine initial velocity as opposed to photocells. Although this method is currently considered the gold standard, it is not without its limitations. The method assumes that the first step of the first sprint has the same force application pattern as the first step of every subsequent sprint. This assumption is not trivial because the dependence of the force-application pattern of the second step on that of the first step is unknown in these studies and arguably does exist. Rabita et al. [2] showed high

repeatability of the measured data at the sixth step (about 8 m) suggested by low coefficients of variation and high intra-class correlation coefficients. One may argue, however, that the inter-sprint repeatability of data obtained from the sixth step does not well represent the repeatability across the entire sprint. For example, Hunter et al. [8] had subjects perform multiple sprints over a single force plate placed 16 m from the start. Twenty-eight of the subjects from their study showed inter-sprint force application patterns that were different enough to relate the differences to kinematic variables. Samozino et al. [14] did not report any statistical measure of inter-step repeatability and in fact acknowledged the possibility of inter-sprint variance in force application patterns as a possible contributor to the standard error of the estimate observed for the method to which they were comparing. Thus, unless controlled for, the assumption of negligible step specific force application variance may not be made. Secondly, the method is relatively inconvenient given the time it takes to piece together the virtual sprint from multiple bouts and the cost of the equipment necessary for the analysis.

A single force plate and a single sprinting bout can be used to determine step-by-step kinetic data during a sprint if the runner's displacement relative to the force plate does not change as is this case with a treadmill. Instrumented treadmills are equipped with embedded force plates and allow one to obtain multi-step $\boldsymbol{F}$ data during a single sprint. Motorized treadmills maintain a user specified constant running speed and the kinetic variables obtained for constant-velocity running bouts have been validated for intra- and inter-individual comparisons [40–42]. As long as the belt speed is constant, the belt coordinate frame is an inertial one and thus valid $\boldsymbol{F}$ measurements would be expected [42]. However, during accelerative running, the belt is a non-inertial reference frame and the previous conclusions cannot be generalized to these conditions. Van Caekenberghe et al. [43] described what they term a "fictitious" force which

must be introduced into the kinetic equations for running on an accelerating treadmill belt. Briefly, an instrumented treadmill with a person at standstill when the belt is suddenly accelerated will register a F_x due to the belt as opposed to the result of any muscular actions within the body. The hypothesis was confirmed with experimental results [43] and has been extended beyond kinetic differences to also include kinematic differences such as joint angles and joint velocities between over-ground and treadmill accelerated running [44]. They did, however, suggest the differences may be overcome by using torque treadmills (TT). TT provide only enough torque to overcome internal belt friction while the subject provides the forces for belt acceleration. The torque setting for TT is determined by defining that which is necessary to overcome static friction of the subject's body weight on the treadmill [59, 70, 71]. Non-motorized treadmills (NMT) are similar in that there is no motor causing belt acceleration, but different in that belt friction is not compensated for [48]. Thus, compared to traditional motorized treadmills, NMT and TT have been used more extensively for sprint assessments [48]. A treadmill embedded three-dimensional force plate allows direct measurement of $\boldsymbol{F}$. A harness attached to the runner is anchored to an immovable strut behind the runner at the height of the harness attachment [47, 48]. F_x is determined either using a strain gauge attached at the strut (when the force plate only gives F_z) [49, 50] or by using the three-dimensional embedded force plate [47]. Assuming no relative movement of the subject to the anchoring strut (or wall) the force values determined by the sensor are equal to F_x [48]. A similar method has been used for over-ground sprinting where a tricycle anchors a steel rod attached to the runner's belt [51]. Simperingham et al. [48] provide an extensive review comparing the NMT and TT measurement techniques and their associated validity and reliability. Particularly important was the finding that there has been no assessment of the validity of F_x, F_z, and F_{res} determined by NMT or TT

and neither have been compared to kinetic measurements determined by over-ground running with embedded force plates [48].

To avoid the shortcomings of the previously described methods, perhaps one should seek a technique that allows kinetic data collection for every step during one over-ground sprint. The inverse dynamics approach satisfies these conditions. Furusawa et al. [13] derived an equation describing the velocity-time relationship during sprinting. The derivation is dependent on two assumptions: (1) the sprint is maximal effort and (2) a frictional force exists within the muscle proportional to the shortening velocity. Because the sprint is maximal effort, the force applied (*F'*) is also maximal and, in general, is proportional to the runner's weight:

$$F' = fma_g \tag{2.1}$$

where *f* is a dimensionless proportional constant. The frictional force (F_f') is proportional to the velocity of the sprint and the runner's mass:

$$F_f' = -\frac{m}{b}\frac{dx}{dt} \tag{2.2}$$

where *b* is in units of time and is necessary for F_f' to be in units of Newtons (*a* is used in the original paper, but is substituted by *b* here to avoid confusion with acceleration). The equation of motion relative to mass is thus:

$$\frac{d^2x}{dt^2} = fa_g - \frac{1}{b}\frac{dx}{dt} \tag{2.3}$$

the solution of which is:

$$x(t) = fa_g b\left[t - b\left(1 - e^{-\frac{t}{b}}\right)\right] \tag{2.4}$$

The velocity is determined by the first derivative of position with respect to time:

$$\frac{dx}{dt} = fa_g b\left(1 - e^{-\frac{t}{b}}\right) \tag{2.5}$$

and the acceleration by the second derivative:

$$\frac{d^2x}{dt^2} = \frac{fa_g b}{b}\left(e^{-\frac{t}{b}}\right) \tag{2.6}$$

In the original study, position-time data (obtained using photocells) were fit to eq. (2.4) to find the constants fa_g and b. The equation performed relatively well considering the average difference between observed and calculated distance was about three inches. The same constants may then be used to determine velocity-time and acceleration-time relationships using eqs. (2.5) and (2.6) respectively.

One can see as $t \to \infty$:

$$\frac{dx}{dt}_{t\to\infty} = fa_g b \tag{2.7}$$

Thus, as proposed by the authors, $fa_g b$ represents the theoretical maximal velocity (v_m) should fatigue never set in. Further, let $t = b$ and $fa_g b = v_m$, then:

$$v(b) = v_m(1 - e^{-1}) \tag{2.8}$$

and thus:

$$v(b) \approx (0.63)v_m \tag{2.9}$$

The value of b then represents the time it takes for the velocity to reach 63% of v_m, at which the authors consider v_m to have been "practically attained" (pg. 34). The equation has been used in other studies using velocity-time data obtained with a radar gun positioned behind the runner at the height of the COM where the time constant (τ) is substituted for b [14, 50–52]. Given this

substitution, the equations change according to:

$$x(t) = v_m\left(t + \tau e^{-\frac{t}{\tau}}\right) - v_m\tau \tag{2.10}$$

$$v(t) = v_m\left(1 - e^{-\frac{t}{\tau}}\right) \tag{2.11}$$

$$a(t) = \left(\frac{v_m}{\tau}\right)e^{-\frac{t}{\tau}} \tag{2.12}$$

A bi-exponential curve has been used to account for the effects of fatigue [53]:

$$v(t) = v_m(e^{-k_2 t} - e^{-k_1 t}) \tag{2.13}$$

where k_2 and k_1 represent the constants relating the decreasing acceleration due to fatigue and during the initial acceleration respectively. Others substitute $\frac{1}{\tau_1} = k_1$ and $\frac{1-v_m}{\tau_2} = k_2$ where τ_1 and τ_2 represent the time constants for acceleration and deceleration during a 100 m sprint [46, 54]. Then:

$$v(t) = v_m\left[e^{\frac{tv_m - t}{\tau_2}} - e^{-\frac{t}{\tau_1}}\right] \tag{2.14}$$

A review of the reliability and validity of radar measures to determine speed by Simperingham et al. [48] determined that intraday reliability and inter-day reliability and validity have been established with the exception of the first 5 m of the sprint. The forward lean of the trunk has been used to explain the discrepancy of the latter [55]. Other observed irregularities have been attributed to segmental movements [50].

By inverse dynamics and using eq. (2.12) along with knowledge of the runner's mass, one may estimate kinetic data. Morin and Seve [46] estimated F_x during a 100 m sprint using velocity-time data obtained by a radar gun. These forces were compared to those on an instrumented treadmill to determine differences in treadmill vs. over-ground running. Although, not validated prior to this study, the method has recently been validated by Samozino et al. [14].

They compared the variables important to acceleration performance determined by the inverse-dynamics method to the multiple sprints, single force plate method. Position-time data obtained by photocells and velocity-time data obtained by a radar gun were used to assess validity and inter-trial reliability respectively. The constants v_m and τ were found by fitting the position-time and velocity-time data to eqs. (2.10) and (2.11) respectively. Then it was possible to determine acceleration (a) using eq. (2.12) and F_x by Newton's 2nd Law:

$$ma = F_x - F_D \tag{2.15}$$

where the drag force (F_D) was estimated by:

$$F_D = \frac{1}{2} C\rho A(v_x - v_{air})^2 \tag{2.16}$$

The constants in eq. (2.16) were estimated by [56]:

$$\rho = \rho_0 \cdot \frac{Pb}{760} \cdot \frac{273}{273+T^\circ} \tag{2.17}$$

$$A = Af = (0.2025h^{0.725}m^{0.425})(0.266) \tag{2.18}$$

$$C = 0.9 \tag{2.19}$$

where ρ_0 = 1.293 kg/m is the air density of 760 Torr and 273 K, Pb is the barometric pressure (in Torr), $T°$ is the air temperature in °C, and h and m are the runner's height and mass. F_z was estimated to be the subject's bodyweight allowing the estimation of F_{res} and thus RF:

$$F_{res} = \sqrt{F_x^2 + F_z^2} \tag{2.20}$$

$$RF = \frac{F_x}{F_{res}} \tag{2.21}$$

Estimates of sFV, F_0, v_0, and dRF were made as well as maximal power determined by both the

apex of the power-velocity curve and:

$$P_{max} = \frac{F_0 v_0}{4} \quad (2.22)$$

The method was considered valid and reliable given the low standard error of the estimates, low absolute bias, and narrow 95% limits of agreement from Bland & Altman analysis. The method has since been used to investigate mechanisms of injury and the effects of injury on sprint mechanics [57, 58]. Despite the close fit of sprint performance variables determined by the multiple sprints, single force plate method, the inverse-dynamics method may not be considered a fully comprehensive assessment. The authors acknowledge the lack of the ability of the method to determine any bilateral asymmetry that may be present. Further, other kinematic variables of interest cannot be determined (joint angles, flight times, contact times, stride frequency, etc.). Thus, motivation exists for the development of a novel method that satisfies matters of convenience (time and budget), validity, reliability, and comprehensive profiling of acceleration performance. Accelerometers used in inertial measurement units may provide the technology to do so.

2.2 Accelerometers

Definitions and theory

Accelerometers measure acceleration along one, two, or three axes. Accelerometer hardware used in human movement analysis is usually based on either strain gauge, piezoresistive, capacitive, or piezoelectric technology [59]. The circuit for capacitive accelerometers consists of a silicon mass anchored to a frame by an elastic structure. The mass has attached conductive fingers aligned between frame attached conductive fingers subject to a high frequency square wave source voltage. The output voltage, taken at the mass attached conductive finger, allows one to determine the differential capacitance of the conductive finger

configuration. When the frame is accelerated, the elastic structure attaching the mass to the frame is deformed by the inertia of the mass resulting in relative movement between the mass attached conductive finger and those attached to the frame. This changes the differential capacitance which is manifest by the change in the measured output voltage. The acceleration magnitude and direction is given by the sign of the measured output voltage along with knowledge of the square wave excitation source, spring constant of the elastic anchoring structure, and the mass of the silicon structure [60]. Three single axis accelerometers can be aligned orthogonally within the unit to provide the acceleration in three dimensions. Other units use a single three axis accelerometer where the three dimensional acceleration is determined by orthogonal alignment of additional conductive fingers about those of the mass.

Biomechanics Applications

The use of accelerometers in biomechanics has been around for over 50 years [61, 62]. In 1963, Cavagna et al. [63] showed the use of accelerometers to calculate external work in walking. Today, accelerometers serve as the functional unit in activity monitors to estimate physical activity and energy expenditure [19, 64, 65]. Accelerometers have also been used to assess characteristic spatiotemporal events, postural control, and segment orientations all with methods that vary with the type and placement location of the accelerometer during walking [59]. Modern smartphones come equipped with several inertial sensors including accelerometers to perform various functions within the phone (e.g., gaming, display orientation, etc.). This has led to the investigation of their use in human movement analysis [66, 67] for estimation of step cadence, velocity, and step length [68–70]. The result has been the development of applications for clinical purposes such as the assessment of the 6-minute walk test [70], fall detection [71, 72], and pedometer counts [73].

Accelerometers have also been used to assess more dynamic movement tasks characteristic of those in sport. Their use in this context is attractive because it might provide a convenient means of monitoring player load and performance assessment. For example, accelerometers have shown the ability to deterct running fatigue [74] and contact times during steady state jogging, running, and sprinting, as well as the first, third, and fifth steps of accelerative running [75]. Other studies have estimated running speed in free living conditions [76], spatiotemporal data of ice hockey skating [77] and sprinting [78], biomechanical variables of countermovement and drop jumps [31], joint angles [79], and kinematics of the barbell high pull [80].

Kinetic data have also been estimated using accelerometers during human movement, although to a much less extent. Knowledge of the mass of a body and its acceleration allows the prediction of the force that caused the motion using Newton's 2nd Law in eq. (2.3). Perhaps the first studies to investigate the use of accelerometers in predicting forces and loads during human movement were by Janz [81] and Garcia et al. [19]. Both assessed the ability of different activity monitors, using activity counts, to predict kinetic variables during walking, running, and jumping activities. Others have used the raw acceleration output to determine resultant acceleration and its relationship with kinetic variables [82]. Rowlands and Stiles [82] showed significant relationships with average F_{res} and peak loading rate, but not peak impact force during walking, running, and jumping at different intensities. Neugebauer et al. [17] developed a prediction model for peak F_z based on preliminary data dependent on accelerometer measured average resultant acceleration over 15 second epochs, centered mass (difference between subject's mass and a reference average mass specific to the subject's sex), type of locomotion (walk or run), interaction between raw acceleration and locomotion type, and sex. The results are limited,

however, in that the model assumes steady state activity and only peak F_z predictability was assessed. Another prediction model was developed by Neugebauer et al. [16] using raw accelerations as opposed to averaged epochs allowed the prediction of peak braking forces in addition to peak F_z during walking and running. These two prediction models by Neugebauer et al. [17] and Neugebauer et al. [16] are dependent on curve fitting accelerometer data with force plate data from preliminary trials as opposed to using Newton's 2nd Law. The latter may be more generalizable and has been used more recently for kinetic analysis of hopping and heel-rise tests [83], the development of a smartphone application to estimate kinetic and kinematic variables during a sit-to-stand task [84], and to estimate eccentric and concentric forces during drop jumps and countermovement jumps [31]. The first two of these three studies suggest valid estimates given high correlation coefficients. The last, however, found significant differences between force plate and accelerometer measures with high systematic bias. They attributed the error to the fact that the orientation of the sensor relative to the world frame was changing during the jumping task.

Limitations

Accelerometers suffer in their ability to accurately predict kinetic data during human movement for several reasons. First, accelerometers, similar to most electrical devices, are accompanied by noise and bias. Although these errors may be relatively small, if the velocity or position of a body is calculated by single or double integration of the acceleration respectively, the errors become relatively large, a phenomenon known as drift [85]. Second, the accelerometer can only provide acceleration information about the specific body part to which it is attached. Placement of the accelerometer near the COM (sacrum, hip, etc.) has been used in previous studies where the accelerometer is assumed to represent the COM [16, 17, 31, 82].

However, this assumes the COM is fixed relative to the body which is not true when the limbs move. $\boldsymbol{F}$ is the result of the net joint torques about all joints within the body [18]. For example, during a countermovement jump with an arm swing the COM would be vertically displaced relative to the body for which a vertical force must be responsible [86]. This would be manifest immediately by the force plate, but not a sacrum mounted accelerometer until the vertical impulse causes vertical displacement of the temporarily fixed COM position. Studies examining the use of accelerometers in analyzing jumps have, as a result, prevented arm swinging [87]. This shortcoming, however, has not prevented the finding of significant relationships between accelerometer outputs and F_{res} during human movement tasks [16, 17, 29, 82]. Finally, the three dimensional components of $\boldsymbol{F}$ in the world frame (*W*) cannot be determined by accelerometers alone. Other studies have found accurate estimates of F_{res} during various human movement tasks, but none have decomposed the vector into component parts using an algorithm that is generalizable to any task. The accelerometer measures accelerations along each of its three orthogonal axes relative to the sensor's reference frame (*S*). In order to know these values in terms of *W* one must know the orientation of *S* relative to *W* [31]. If the relative sensor orientation is initially known and an attempt is made for this orientation to be held constant throughout the movement [80] then the accelerations about the sensor's three axes are representative of the same in *W*. However, maintaining a constant orientation would be difficult in a very dynamic task such as sprinting. Accelerometers may provide inclination angles of *S* relative to *W* during static positions. However, an accelerometer cannot provide angular orientation relative to *W* about the vertical axis (heading) and are independently not an accurate inclinometer during human movement when the accelerometer is less frequently in a static position. Inertial measurement units combine multiple sensors and fuse their data in order to

compensate for relative movement between the sensor and world reference frames potentially allowing more accurate estimates of kinetic variables using accelerometers [31].

2.3 Inertial Measurement Units

Definitions and theory

Inertial measurement units (IMUs) contain built in accelerometers, gyroscopes, and magnetometers. Gyroscopes are used to measure angular rate. Their design is similar to that of the accelerometer in that they are capacitive sensors and the output is due to movement of a mass anchored to a frame by elastic structures. For gyroscopes, however, there are two masses. One, a frame itself, is anchored to the outer frame by elastic springs permitting movement in the direction of the tangential component of the rotation. The other is anchored inside the previous by elastic springs permitting movement in the direction of the radial component of the rotation. Angular rates are derived using the Coriolis Effect. For a given angular rate (ω in *rad/sec*) , an object will have a greater tangential velocity (v_T), relative to the non-rotating reference frame, when its location is further from the axis of rotation because:

$$v_T = \omega r \tag{2.23}$$

where *r* is the distance between the object and the axis of rotation. Thus, if a radial displacement occurs during rotation, the object will also accelerate tangentially. This tangential acceleration is known as the Coriolis acceleration [60]. The force responsible for the Coriolis acceleration (F_C) can be shown to be [60]:

$$F_C = 2m\omega v_r \tag{2.24}$$

where *m* is the mass and v_r is the radial velocity. When the gyroscope is rotated, the frame mass is displaced due to inertia. This motion is resisted by the springs which anchor it to the body

frame. This force, equal to F_C, is proportional to the spring constant, K, and the displacement, d, of the frame mass. Thus:

$$2m\omega v_r = Kd \tag{2.25}$$

and by solving for ω:

$$\omega = \frac{Kd}{2mv_r}. \tag{2.26}$$

Conductive fingers attached to the frame mass are configured between those of the body frame similar to the construction of accelerometers. The differential capacitance is measured between the conductive fingers allowing the determination of d. If K is known, the angular rate, ω, may be solved for. The mass and springs attached to the frame mass are necessary to compensate for the radial component of the angular acceleration:

Magnetometers sense magnetic fields using various circuit configurations. A magnetic field vector contains components in the horizontal plane and thus a magnetometer can act as a digital compass to help determine the direction in which the sensor is headed. One common example, like that in the InvenSense MPU-9250, uses the Hall Effect. When an electrical current (i) is subject to a magnetic field vector ($\boldsymbol{B}$), the electrons in the current experience a deflection force ($\boldsymbol{F}_B$):

$$\boldsymbol{F}_B = q\boldsymbol{v}_d \times \boldsymbol{B} \tag{2.27}$$

where $\boldsymbol{v}_d$ is the drift velocity of the electrons, q is the charge, and × is the vector cross product [88]. The result of this force is the displacement of the electrons within the conducting material. The Hall Effect describes the resulting voltage due to the accumulating negative charge due to $\boldsymbol{F}_B$. The magnetometer is comprised of a conducting material of thickness (h) and Hall constant (R) subject to a known current. The potential difference (V_O) is taken across the width of the material.

Thus, the magnetic field magnitude can be solved for [89]:

$$B = \frac{V_O h}{Ri} \tag{2.28}$$

The current, and thus $\boldsymbol{v}_d$, is parallel to the axis of the conducting material (i.e., the axis of the magnetometer) and *B* determined by one single-axis magnetometer represents only the component of the magnetic field which is tangential to the sensor's axis. Orthogonal alignment of three single axis magnetometers permits knowledge of the orientation of $\boldsymbol{B}$ in $\mathbb{R}^3$.

Biomechanics Applications

The ability of an IMU to determine the orientation of the sensor frame (*S*) relative to the inertial world frame (*W*) has led to its use in biomechanics where the rigid body is a limb of the human body. If the orientation of the sensor relative to the limb is known, then one can track the movement of the limb in space which permits the ability to perform a kinematic analysis. The current gold standard for kinematic analysis is using infrared videography. The potential use of an IMU in this area of research is attractive in a practical sense because it is more convenient than the videography due to its relative low cost, relative easy set-up, decreased post-processing time, and especially the fact that it does not constrain the subject to a small area [90].

Many studies have assessed the ability of IMUs to provide accurate measurements of joint kinematics during various human tasks [20, 91] using both quaternion [21, 30, 90, 92–94] and Euler angle [22, 23, 29, 95] representations along with various Kalman Filter [22, 23, 94–98], complementary filter [85, 99], and PI controller [90] data fusion algorithms. Joint angle estimates from IMUs have been validated by comparison against some of the more rigorous reference standards such as a robotic arm [96] and an instrumented gimbal [100]. The validity of these measurements on human subjects during walking trials is supported by accurate estimates of pelvis angles [94, 101], trunk angles [98], knee joint angles [21, 92, 95], and foot joint angles

[102]. Others have validated their use in segment orientation estimations during eating and crate lifting tasks [97, 103] and running [95]. Improved accuracy has been the result of improved algorithms due to optimizing sensor calibration methods [23, 92, 104] and selection of Kalman Filter parameters [98].

The validation of these methods has led to the extension of IMU applications in biomechanics research to well beyond joint kinematics. IMUs have been used to assess military performance in a target maneuvering and acquiring task [105], the effect of fatigue due to load carriage [28, 106], and the effect of load carriage on balance [107]. Logar and Munih [18] used a system of 10 IMUs attached to different body segments to estimate $\boldsymbol{F}$ from the resultant joint torques during ski jumping. IMU predicted $\boldsymbol{F}$ were within 10% of the values obtained by a force plate [18]. Highly miniaturized IMUs embedded in baseballs and softballs have been validated for use in measuring ball flight patterns supporting the potential use of IMUs to assess pitching mechanics [108].

Several studies have assessed the ability of IMUs to collect data that would be relevant in an evaluation of sprint acceleration performance. Bergamini et al. [22] validated the use of IMUs to estimate trunk angles during a sprint start. The method showed good agreement between the IMU and videography determined trunk angles in the sagittal plane and angular velocities for the first three steps of the block start. Bergamini et al. [24] used the second derivative of the angular velocity from a trunk mounted IMU during a 60 m sprint to accurately estimate stride and stance durations. The error was low enough that it allowed the discrimination of amateur and elite sprinters. Lee et al. [25] also estimated stance, stride, and step durations using the anterior-posterior acceleration spike. Accuracy of the measurement is suggested by narrow 95% confidence intervals from Bland & Altman analysis, high correlation values, and

low standard errors and was unaffected by increased velocity [25]. Wixted et al. [26] also used the anterior-posterior acceleration trace from a trunk mounted IMU to identify foot contacts during running. McGinnis et al. [28] rotated the acceleration vector in *S* (sacral mounted IMU) to express it in terms of *W* and used the determined vertical acceleration to obtain accurate measurements of countermovement jump height. Milosevic and Farella [29] used the same technique and also found accurate measurements for both one and repetitive countermovement jumps. Lee et al. [109] found strong($r = 0.96$) and low error estimates (1.84 m/s^2) between IMU and videography measured vertical acceleration of the COM during running. Further, they were able to identify bilateral asymmetries in running gait. Esser et al. [30] rotated the acceleration vector in *S* to express it in terms of *W* during a walking task with the sensor attached to the lower back. They found good agreement between IMU and videography determined values (average error for acceleration, velocity, and position were -0.19 m/s^2, -0.012 m/s, and -0.047 cm respectively). To the author's knowledge, Parrington et al. (2016) are the only others to report the use of IMUs to estimate sprint velocity, however, the details of their data fusion algorithm was not provided [27]. If the acceleration values are used to predict kinetic variables by inverse dynamics, one might be able to obtain the relevant determinants of sprint acceleration performance using an IMU. Thus, IMUs might provide the technology to perform a more thorough evaluation of sprint acceleration performance by providing measures related to ground reaction force application technique, joint kinematics, spatiotemporal variables, and step-by-step analysis capable of identifying bilateral asymmetries. No current assessment method can by itself provide such a comprehensive evaluation.

2.4 Conclusion

Many individual and team sports focus on the development of sprinting speed in their training programs. In actual gameplay of many of these sports the distance interval over which the sprinting bout occurs is often short enough that maximal sprint velocity is never reached. Thus the ability to accelerate is arguably more valuable than one's maximal sprinting velocity. Many factors contribute to an athlete's accelerative ability that are related to both technique and muscular characteristics. Improving performance involves targeting weaknesses in both of these areas. Of particular importance is the technical application of force during foot contact with the ground. The use of step-by-step analysis of this force application technique has allowed the identification of technical patterns characteristic of athletes with greater accelerative ability. These technical characteristics provide objective standards that can be used by coaches to identify areas of improvement for their athletes. However, the current methods used to perform these step-by-step analyses are tedious, require relatively expensive equipment, and are based on assumptions that may not always be valid. A more effective measurement technique is necessary and will allow the implementation of this information in a practical setting. Further, it will allow future studies to answer questions about not just what faster athletes do different, but how they do it. IMUs are becoming more prevalent in biomechanics research. Because of their small size, wireless capabilities, and relatively low costs, IMUs may provide the technology to improve the current state of acceleration measurement techniques.

Chapter 3: The Use of a Single Inertial Sensor to Estimate 3-Dimensional Ground Reaction Force during Accelerative Running Tasks

Abstract

Inertial measurement units (IMUs) provide a potential means to estimate three-dimensional ground reaction force ($\boldsymbol{F}$) in unrestricted field assessments. In this study, the feasibility of using a single IMU to estimate $\boldsymbol{F}$ was investigated. Force plate (FP) measurements of $\boldsymbol{F}$ and estimates from the proposed IMU method were collected while subjects (12 male, 3 female) performed two tasks: (1.) a standing sprint start (SS) and (2.) a 45º change of direction task (COD). Step averaged $\boldsymbol{F}$ ($\overline{\boldsymbol{F}}$), ratio of force ($RF$), peak $\boldsymbol{F}$, and instantaneous $\boldsymbol{F}$ were compared between the FP and IMU estimates using Bland-Altman analysis, root mean square error (RMSE), and Pearson's product moment correlation coefficients (r). In general, IMU estimates of directional $\overline{\boldsymbol{F}}$ (RMSE: 45.17 N to 77.32 N for SS and 60.01 N to 169.91 N for COD) showed less error than directional peak $\boldsymbol{F}$ (RMSE: 514.67 N to 1175.07 N for SS and 428.19 N to 1150.89 N for COD) and directional instantaneous $\boldsymbol{F}$ (RMSE: 376.64 N to 476.67 N for SS and 436.44 N to 632.54 N for COD). Correlation coefficients were moderate (r = 0.50 to 0.75) to strong (r > 0.75) for most estimates except for the medio-lateral component of $\overline{\boldsymbol{F}}$ and the antero-posterior component of peak $\boldsymbol{F}$ during COD. The proposed method accurately estimated the orientation of $\overline{\boldsymbol{F}}$ (angular error: 3.4° to 9.2°), but not peak $\boldsymbol{F}$ (angular error: 26.6° to 31.0°). Valid estimates of RF from the IMU method are also suggested by significant correlations (r = 0.85, p < 0.01) and low bias (0.88%). The results of this study suggest IMUs can accurately estimate step average $\boldsymbol{F}$ during a linear sprint start, but not during change of direction tasks nor when estimating peak $\boldsymbol{F}$ or instantaneous $\boldsymbol{F}$.

Introduction

The ground reaction force vector ($\boldsymbol{F}$) is an index often used to evaluate human movement. Component and resultant (F_{res}) magnitudes of $\boldsymbol{F}$ as well as the orientation of the vector are used in both clinical [110, 111] and performance assessments [5, 112]. For example, in a linear sprinting task, the ratio of force (RF) expressed as the ratio of the forward component of $\boldsymbol{F}$ relative to the resultant magnitude where the medio-lateral component is considered negligible, is often used to assess the ability to optimally orient $\boldsymbol{F}$ during the acceleration phase of sprinting [2]. Further, the medio-lateral and vertical components of $\boldsymbol{F}$ are used to assess performance during change of direction tasks [113].

Force plates are considered the gold standard for measuring $\boldsymbol{F}$, however, movements are confined to a small area. Accelerometers have shown potential in being able to estimate $\boldsymbol{F}$ during ambulatory movements [16, 84, 114]. Their application in this context is dependent upon the assumption that the location of the accelerometer on the body is such that measured accelerations during the movement are representative of the body center of mass (COM). Under this assumption, $\boldsymbol{F}$ is derived from Newton's second law [84, 114]. Wundersitz et al. (2013) assessed the ability of an accelerometer to measure the peak vertical component of $\boldsymbol{F}$ and peak F_{res} during accelerative tasks. To determine F_z, they scaled the acceleration measured along the accelerometer's vertical axis by the subject's mass. Their results showed the sensor consistently underestimated peak F_z, yet at the same time consistently overestimated peak F_{res} (except when smoothing the signal at 10 Hz). One explanation for this finding might be that while peak F_z was underestimated, the components in the horizontal plane (peak F_y and peak F_x) were consistently overestimated and thus exaggerated the peak F_{res} estimation. The authors of this paper offer another possible explanation suggesting perhaps the sensor's coordinate frame was not aligned

with that of the force plate. If so, the true vertical component of $\boldsymbol{F}$ in the force plate frame would appear in the sensor frame as a vector having components along each axis. Then, the accelerometer would be expected to underestimate peak F_z. To appropriately compare estimated components of $\boldsymbol{F}$, the acceleration vector in the sensor frame should be rotated to the force plate frame. Inertial measurement units (IMU) have onboard accelerometers, gyroscopes, and magnetometers giving them ability to determine the 3-dimensional orientation of body segments and thus the means to express sensor referenced vectors in the inertial world frame [20]. Some have predicted $\boldsymbol{F}$ using multiple IMUs attached at each body segment by inverse dynamics [18, 115]. It is unknown, however, how well a single IMU can estimate 3-dimensional $\boldsymbol{F}$ while compensating for the changing sensor orientation.

The purpose of this study was to assess the ability of a single, sacral worn IMU to accurately measure directional $\boldsymbol{F}$ during two accelerative running tasks: (1.) a standing sprint start and (2.) a change of direction task. The validity of the measurements were determined by comparing the estimates to force plate measurements.

Methods

Subjects

Fifteen subjects (12 male, 3 female, age: 23.20 ± 2.11 yrs, height: 1.78 ± 0.09 m, mass: 75.46 ± 12.56 kg) volunteered to participate in this study. Subjects were included in the study if they were between the ages of 18 and 35 years old, reported no musculoskeletal injury in the six months prior to testing, and were able to perform accelerative running tasks pain free. All subjects provided written consent to participate and the Appalachian State University Institutional Review Board approved this study.

Instruments

The IMU used in this study was a Yost Data Logger 3-Space Sensor (YEI Technology, Portsmouth, OH). These sensors have an onboard three-axis accelerometer (range: ±24 g, noise density: 650μg/$Hz^{1/2}$, 12-bit resolution), three-axis gyroscope (range: ±2000º/s, noise density: 0.009º/s/$Hz^{1/2}$, 16-bit resolution), and three-axis magnetometer (range: ±1.3 Ga, 12-bit resolution). The IMU was set to sample at 450 Hz and data were written to a MicroSD card and later downloaded to a computer via USB for analysis. IMU estimates of $\boldsymbol{F}$ were compared to measurements made by a force plate (FP) (AMTI, Watertown, MA, sampling frequency: 1000 Hz) to determine the validity of the estimate.

Procedures

Data collection consisted of one visit to the Appalachian State University Neuromuscular and Biomechanics Laboratory. First subjects' height, mass, and percent body fat were recorded. Percent body fat was assessed to evaluate the effect that subcutaneous fat might have on IMU estimates. The Lange Skinfold Caliper (Beta Technology Inc., Cambridge, MD) was used to obtain skinfold measurements for the three-site skinfold technique (chest, abdomen, and thigh for males and triceps, abdomen, and suprailium for females) [116, 117]. Subjects' performed a five-minute general warm-up on a cycle ergometer (Monark Exercise AB, Vansbro, Sweden) before a familiarization period during which they practiced the two general movements they would be performing during data collection: (1.) a standing sprint start (SS), and (2.) a change of direction task (COD). The starting location of each task was determined such that full foot contacts with the FP were made during the different movements. Next, the IMU was attached to the sacral region using an elastic strap and athletic tape (Figure 3.1). The specific location of the sensor

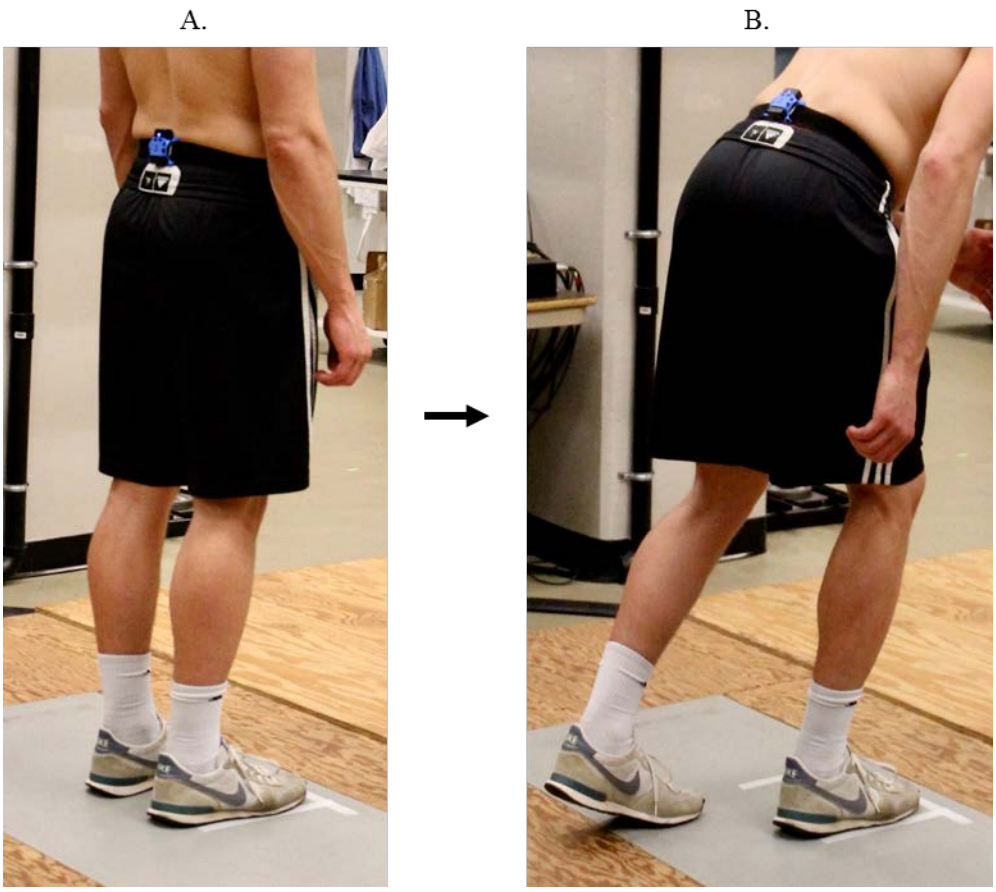

Figure 3.1: Example of a subject going through the pre-movement sequence to determine the initial IMU orientation. (A.) During the static orientation trial, subjects aligned their hips with the forward axis of the force plate. (B.) Then they assumed their standing sprint start stance for a three-second countdown before performing the movement.

was at the point of intersection of the spine with the intercristal line [118]. The latter is defined as the line connecting the left and right posterior superior iliac spines and was found via palpation [118]. The FP and IMU began recording data while the subject was off the FP. The FP was zeroed before the subject stepped on and performed a first set of two jumps separated by a five-second standing static trial. The jumps were necessary to identify the static trial during post-processing and to time-synchronize the IMU and FP signals. This first static trial was used to determine the FP estimate of the subject's bodyweight. The subject then moved to the starting location for that movement trial. Again, they performed a second set of two jumps separated by

another five-second standing static trial. During the static trial, care was taken to ensure the subject's feet and pelvis were directed straight forward and aligned parallel to the forward axis of the FP (Figure 3.1). This was necessary to later determine the initial IMU heading relative to the FP frame before the start of movement. The average gyroscope output during this static interval defines the gyroscope bias which was removed from the angular rate signal before integration. From this position, subjects' moved their preferred foot back to assume their standing start position and were instructed to remain still during a three-second countdown after which beginning the movement for that trial (Figure 3.1). Six trials were performed for both the SS and COD conditions. Three of the SS trials were performed with the subject beginning on the FP to assess the initial push of the standing sprint start. For the other three trials, subjects began behind the FP to assess the first foot contact after the initial push. For the six COD trials, a cone was placed 5 m away from the FP at about a 45º angle. Three trials were performed by cutting to the left and the other three were to the right. For all COD trials, subjects began behind the FP such that the plant foot for the cut was the first foot contact (i.e., right foot for the cut to the left and left foot for the cut to the right). A trial was repeated if the subject's foot did not clearly contact the FP.

IMU Orientation and Vector Rotation

The measurement of $\boldsymbol{F}$ in the IMU frame ($\boldsymbol{F}_S^S$) is given by scaling the acceleration vector by the subject's mass [84, 114]. It then must be rotated to be expressed relative to the FP frame ($\boldsymbol{F}_S^F$) in order to properly compare the estimate to the FP measurement of ($\boldsymbol{F}_F^F$). The quaternion notation was used to express the orientation of the IMU frame relative to the FP frame and to rotate $\boldsymbol{F}_S^S$ to $\boldsymbol{F}_S^F$. The quaternion notation describes the orientation according to the single composite rotation that would align the FP frame with that of the IMU. However, one may also

describe this single rotation according to the following two successive rotations: first through an angle α about the FP frame vertical axis and second through an angle β about an axis of unit length in the horizontal plane. This allows the determination of two angles: α representing the IMU heading (angular deviation of horizontal plane axes when the vertical axes are aligned) and β representing the IMU attitude (angular deviation of the IMU and FP frame vertical axes). Measurements during a static interval from the IMU magnetometer and accelerometer provide an estimate of the initial IMU heading and attitude respectively and thus the initial conditions from which integration may begin. To determine the orientation of the IMU throughout some movement, the quaternion orientation is time integrated using the gyroscope angular rate signal from the initial orientation. This process allows the accelerations (and therefore associated forces) measured with the IMU (corresponding to the person) to be expressed in the FP frame in order to compare with the same measured by the FP. Complete details of the computation methods, as summarized in this section, is described in Appendix A.

Data Reduction

All data analysis was performed using custom programs written in MATLAB (MathWorks, Natick, MA). First, FP and IMU data were low pass filtered at 70 Hz [24]. All data were resampled at the IMU mean sampling frequency (445.72 ± 0.55 Hz) using piecewise cubic interpolation to compare continuous data. Cross-correlation of the IMU and FP signals during the interval containing the first set of two jumps determined the time shift used to time-synchronize the two systems [31, 119]. The average force output from the FP over the stillest one-second interval between the jumps (defined as the interval during which the sum of the variance of the output from each axis of the accelerometer was a minimum) was used to estimate the subject's bodyweight (and therefore mass) in terms of the FP. The subject's mass (m) was

used to scale the IMU referenced accelerations ($\boldsymbol{a}^S$) to estimate $\boldsymbol{F}$ according to Newton's second law [84]. As mentioned in the *Procedures* section, the second set of two jumps was used to provide an initial IMU heading estimate. Although the IMU and anatomical frame vertical axes may not have been exactly aligned, because the surface of the IMU (i.e., the y-z plane) was aligned flush to the subject's skin, the assumption is made that the IMU and anatomical frame forward axes were aligned. Thus, since the anatomical and FP frame forward axes were aligned during this static trial, so were those of the IMU and FP [87]. The FP frame heading (α_0) relative to the projection of the local magnetic field vector $\boldsymbol{B}$ onto the horizontal plane $\boldsymbol{B}_H$ is then computed (Figure 3.2) [23, 119] (see Appendix A for details). From this standing orientation, the subject moved their preferred foot back to assume their standing sprint start stance with the front foot remaining stationary (Figure 3.1). The assumption is made that in this transition to stance, the subtle translation of the IMU in the FP frame is sufficiently small such that the change in $\boldsymbol{B}$ between the two locations is negligible. Again, the accelerometer and magnetometer were used to determine the IMU orientation during the stillest one second interval of the sprint start stance. This time, the IMU heading estimate relative to $\boldsymbol{B}$ ($\alpha_{s,0}$) is expressed relative to the FP heading α_0. Then, the IMU heading relative to the FP frame (α) during stance is given by (Figure 3.2):

$$\alpha = \alpha_{s,0} - \alpha_0 \tag{3.1}$$

Now, given the initial orientation, the gyroscope angular rate signal was integrated to estimate the IMU orientation at each instant during the movement. It was assumed that the time duration of the movement during which the IMU orientation need to be known (i.e., until foot off) was sufficiently small (less than two steps) such that drift error is assumed negligible and thus no data fusion techniques were implemented [94, 97]. Then, the IMU estimate of $\boldsymbol{F}$ was rotated to the

FP frame in order to directly compare the two estimates. To compare the same IMU and FP estimates of $\boldsymbol{F}$ in time, a foot contact is defined to be when the vertical component of $\boldsymbol{F}$ measured by the FP was above 10 N [2]. For the SS trials assessing the initial push from stance, the start of the movement was defined as the first instant the forward component of $\boldsymbol{F}$ measured by the FP went above 10 N.

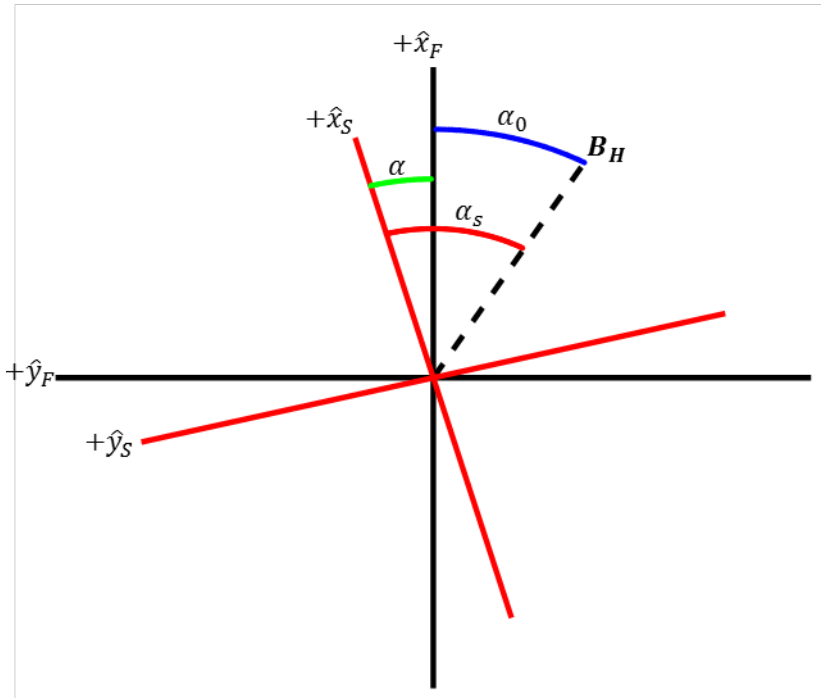

Figure 3.2: The projection of the local magnetic field vector onto the horizontal plane ($\boldsymbol{B}_H$: the dashed black line in the figure) provides a reference vector to determine first the FP heading α_0 relative to $\boldsymbol{B}_H$, then the IMU heading α_s relative to $\boldsymbol{B}_H$, and thus the IMU heading relative to FP α. The FP and IMU horizontal plane axes are the black and red solid lines respectively.

Statistical Analysis

The three components of (F_x: forward, F_y: left, and F_z: up) and the resultant magnitude (F_{res}) of the measurements made by the IMU and FP were compared in three ways: (1.) step averaged $\boldsymbol{F}$ ($\overline{\boldsymbol{F}}$), (2.) peak $\boldsymbol{F}$, and (3.) instantaneous $\boldsymbol{F}$ during the step. The ratio of force (RF) was also assessed for the SS trials to consider the potential application to assessing sprint

kinetics by [2]:

$$RF_i = \frac{\bar{F}_{x,i}}{\sqrt{\bar{F}_{x,i}{}^2 + \bar{F}_{z,i}{}^2}} \tag{3.2}$$

where i denotes the measurement system (IMU or FP) and $\bar{F}_{x,i}$ and $\bar{F}_{z,i}$ are the average F_x and F_z values over the step. The error in the IMU estimates of $\bar{\boldsymbol{F}}$, peak $\boldsymbol{F}$, and RF were quantified using root mean square error (RMSE), Pearson's product moment correlation coefficients (r), relative error (absolute percent difference), and Bland-Altman 95% limits of agreement (LOA). To evaluate the how well the IMU predicted the orientation of $\bar{\boldsymbol{F}}$ and peak $\boldsymbol{F}$ independent of the component magnitudes, the angular error (θ) of the IMU estimate of the vector was determined according to:

$$\theta = acos\left(\frac{\boldsymbol{F}_{IMU} \cdot \boldsymbol{F}_{FP}}{\|\boldsymbol{F}_{IMU}\|\|\boldsymbol{F}_{FP}\|}\right) \tag{3.3}$$

where $\cdot$ denotes the vector dot product, $\|\ \ \|$ denotes the magnitude of the vector, and θ is in degrees. The error in the IMU estimate of instantaneous $\boldsymbol{F}$ was quantified using RMSE and r. The level of statistical significance for correlation coefficients was set *a priori* at a level of 0.05. The clinical significance of the correlation coefficients were evaluated according to the following criteria: 0.00 to 0.25 (little to none), 0.25 to 0.50 (fair), 0.50 to 0.75 (moderate), and > 0.75 (strong) [120]. For the Bland-Altman analysis, the normality of the difference distributions were checked using the Shapiro-Wilk test. Data were transformed by the natural logarithm where differences were not normally distributed or showed a strong ($r \geq 0.75$) relationship with the mean of the measurements [121]. For these cases, the anti-log bias and LOA are given. To determine the effect that subcutaneous fat may have had on the IMU estimate, r was used to determine the relationships between percent body fat and relative error for each subject.

Results

Table 3.1 shows the comparison between IMU and FP measures of $\overline{\boldsymbol{F}}$ and peak $\boldsymbol{F}$ during SS and COD. Figure 3.3 shows the angular error in the IMU estimate of the orientation of $\overline{\boldsymbol{F}}$ and peak $\boldsymbol{F}$. Table 3.2 and Figure 3.4 show the comparison between IMU and FP estimates of instantaneous $\boldsymbol{F}$.

Step Averaged Forces

IMU estimates of $\overline{\boldsymbol{F}}$ and RF during SS were significantly ($p < 0.01$) correlated with FP estimates ($r \geq 0.84$) along with RMSE ≤ 77.32 N and relative error ≤ 12.88% except for $\bar{F}_y$ (r = -0.33, relative error = 341.20%). IMU estimates of $\overline{\boldsymbol{F}}$ during COD were all significantly ($p < 0.05$) correlated with FP estimates (r = 0.53 for $\bar{F}_y$-right to r = 0.94 for $\bar{F}_z$) along with RMSE ≤ 169.91 N and the relative error ranged from 5.20% for $\bar{F}_z$ to 218.02% for $\bar{F}_x$. The angular error in the IMU estimate of the orientation of $\overline{\boldsymbol{F}}$ was less than 10° for both SS and COD.

Peak Forces

IMU estimates of peak $\boldsymbol{F}$ were characterized by RMSE ≥ 514.67 N and the relative error ranged from 22.20% for peak F_z during SS to 3111.90% for peak F_y during SS. IMU estimates were significantly correlated with FP estimates only for peak F_x, peak F_z, and peak F_{res} during SS ($r \geq 0.62$, $p < 0.01$) and for peak F_z and peak F_{res} during COD (r = 0.52 and 0.57 respectively). The angular error in the IMU estimate of the orientation of peak $\boldsymbol{F}$ was ≥ 26.6º.

Instantaneous Forces

The error in the IMU estimate of instantaneous $\boldsymbol{F}$ during SS was characterized by RMSE ≥ 376.64 ± 215.54 N with correlation coefficients ranging from r = -0.24 ± 0.30 for F_y to r = 0.63 ± 0.16 for F_x. For the COD task, the RMSE ≥ 436.44 ± 175.29 N with correlation coefficients ranging from r = 0.08 ± 0.25 for F_y to r = 0.63 ± 0.25 for F_z.

Table 3.1: Comparing IMU and FP step average (top) and peak (bottom) ***F*** values. **Bold lettering denotes the antilog results of natural logarithm transformed data due to non-normality or a strong difference vs. mean relationship.** * *Denotes a significant correlation (p value given)*. LOA: Bland-Altman 95% limits of agreement, RMSE: root mean square error of IMU estimate, *r*: Pearson product moment correlation between IMU and FP measures.

			IMU	**Force Plate**					
			Mean ± SD [N]	Mean ± SD [N]	Bias [N (**antilog**)]	LOA [N or **antilog**]	RMSE [N]	Relative Error [%]	r (*p* value)
Step Average ***F***	SS	$\bar{F}_x$	219.00 ± 83.50	220.82 ± 68.83	-1.82 (**0.97**)	**0.60, 1.58**	45.17	12.88	0.84 (<0.01)*
		$\bar{F}_y$	-11.22 ± 44.23	6.54 ± 35.07	-17.77	-144.79, 109.26	66.15	341.20	-0.33 (0.08)
		$\bar{F}_z$	785.84 ± 152.02	821.34 ± 156.89	-35.50	-172.44, 101.44	77.32	6.82	0.90 (<0.01)*
		$\bar{F}_{res}$	821.16 ± 156.43	853.41 ± 162.07	-32.25 (**0.96**)	**0.82, 1.13**	75.71	6.51	0.91 (<0.01)*
		RF	26.75 ± 8.44	25.87 ± 6.44	0.88	-7.98, 9.74	4.53	12.28	0.85 (<0.01)*
	COD	$\bar{F}_x$	152.45 ± 90.98	70.88 ± 52.58	81.57	-36.92, 200.05	100.93	218.02	0.77 (<0.01)*
		$\bar{F}_y$ (Right)	-289.70 ± 96.58	-388.73 ± 89.99	99.03	-78.58, 276.64	132.18	28.42	0.53 (0.04)*
		$\bar{F}_y$ (Left)	229.11 ± 121.54	368.02 ± 92.45	-138.92	-337.41, 59.58	169.91	38.90	0.58 (0.02)*
		$\bar{F}_z$	945.76 ± 165.99	964.27 ± 145.10	-18.52	-132.30, 95.27	60.01	5.20	0.94 (<0.01)*
		$\bar{F}_{res}$	1002.27 ± 177.51	1041.72 ± 159.88	-39.45	-171.56, 92.66	77.12	6.49	0.91 (<0.01)*
Peak ***F***	SS	F_x	1024.07 ± 821.42	465.04 ± 161.06	559.03 (**1.06**)	**0.07, 16.67**	907.75	189.46	0.65 (<0.01)*
		F_y	-92.66 ± 816.48	12.92 ± 63.15	-105.58 (**0.67**)	**0.03, 13.99**	830.87	3111.90	-0.31 (0.10)
		F_z	1562.45 ± 614.32	1353.60 ± 288.29	208.85 (**1.10**)	**0.66, 1.83**	514.67	22.20	0.65 (<0.01)*
		F_{res}	2345.79 ± 908.33	1442.60 ± 286.86	903.19 (**1.55**)	**0.91, 2.63**	1175.07	60.87	0.62 (<0.01)*
	COD	F_x	259.99 ± 1164.78	107.49 ± 114.61	152.5 (**0.78**)	**0.04, 14.92**	1150.89	1214.8	0.09 (0.64)
		F_y (Right)	-648.59 ± 654.08	-622.84 ± 156.00	-25.75 (**0.52**)	**0.01, 25.17**	681.49	84.84	-0.22 (0.43)
		F_y (Left)	474.66 ± 447.40	586.74 ± 167.66	-112.08 (**0.43**)	**0.01, 27.28**	428.19	65.16	0.30 (0.27)
		F_z	1874.16 ± 575.58	1544.59 ± 247.36	329.57 (**1.17**)	**0.69, 1.99**	587.53	28.85	0.52 (<0.01)*
		F_{res}	2591.09 ± 617.30	1672.66 ± 273.74	918.43	-89.93, 1926.80	1048.51	55.34	0.57 (<0.01)*

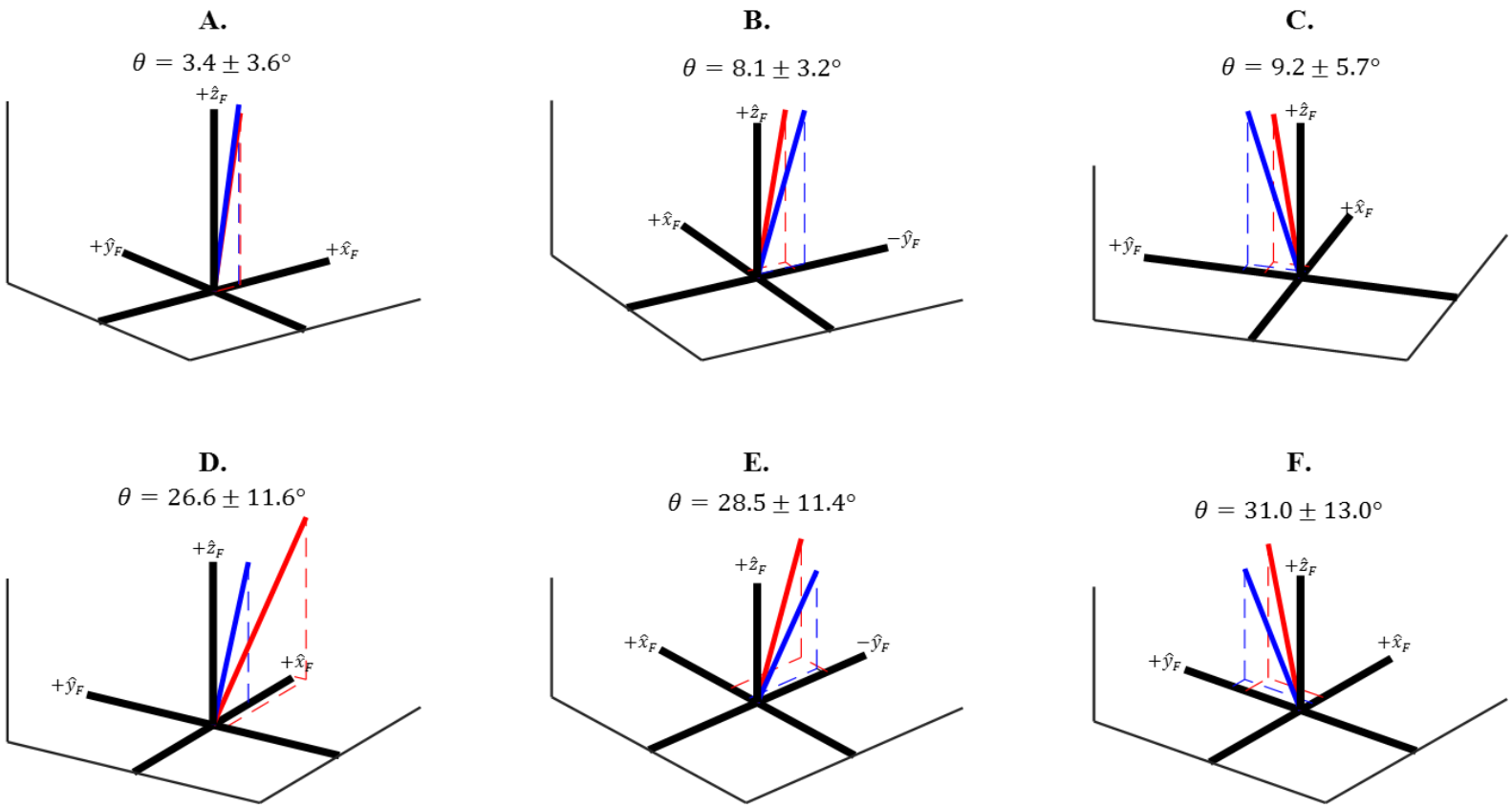

Figure 3.3: Graphical comparison of the IMU and FP estimate of $\boldsymbol{F}$. The red vector is the IMU estimate and the blue vector is the FP estimate. The vectors represent the average across all subjects. The angular error (θ) is the angle between the vectors where θ is given in eq. (3.4). The FP frame axes (solid black lines) are labeled. (A.) step averaged SS, (B.) step averaged COD (Right), (C.) step averaged COD (Left), (D.) peak SS, (E.) peak COD (Right), (E.) peak COD (Left).

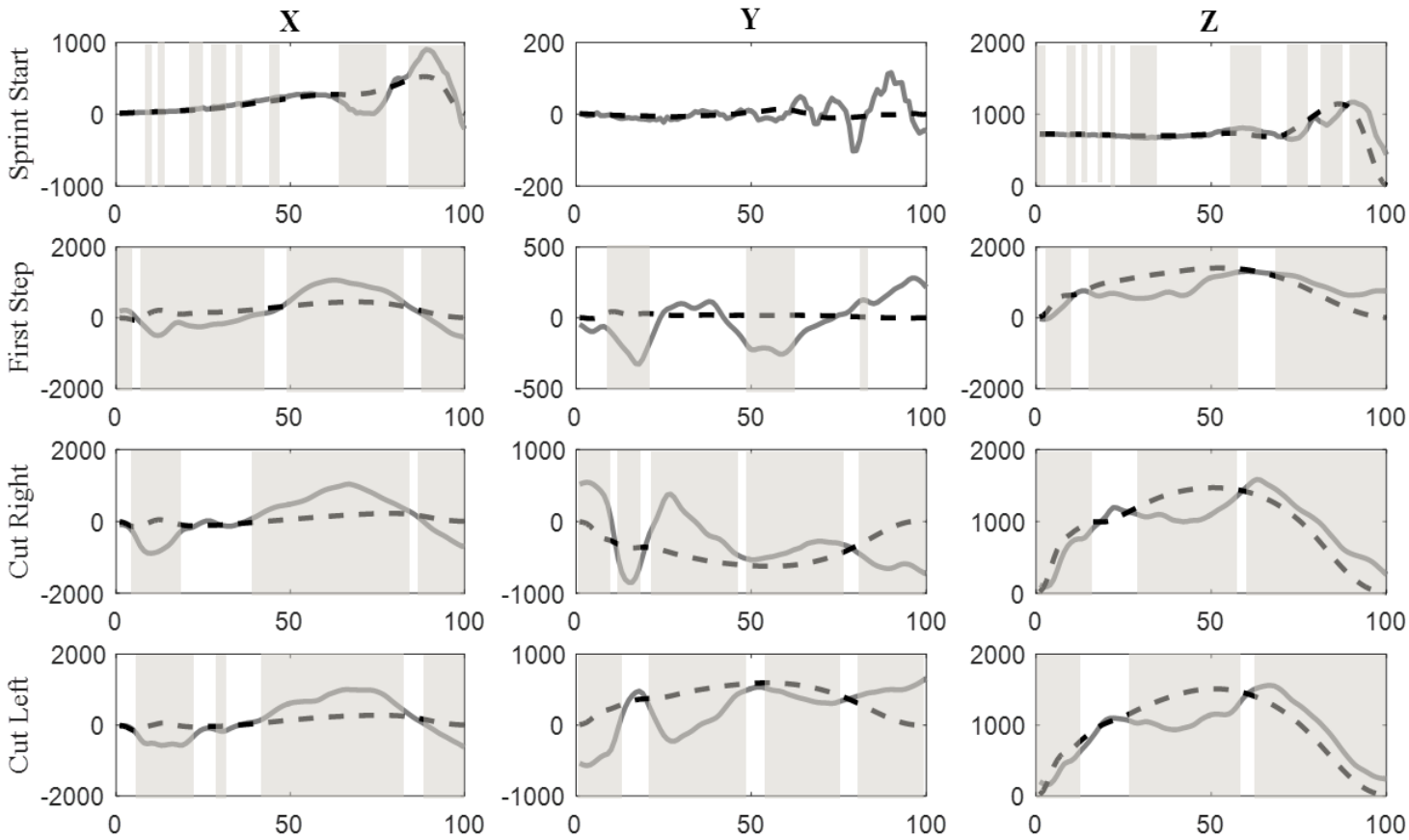

Figure 3.4: Comparison of instantaneous ***F*** between IMU and FP. Curves represent the average values across all subjects. The y-axis is force in Newtons and the x-axis is the percent of the foot contact. The solid grey curve is the IMU estimate, the dashed black curve is the FP estimate, and the shaded area denotes a significant difference between the IMU and FP estimate ($p \leq 0.05$). The left, middle, and right columns are the x, y, and z components of the ***F*** estimate. Row 1, 2, 3, and 4 are for the initial push of SS, the first step of SS, COD right, and COD left tasks respectively.

Table 3.2: Analysis of error in the IMU estimate of instantaneous $\boldsymbol{F}$ for SS (top) and COD (bottom) conditions by comparison to FP. Root mean square error (RMSE) and Pearson product moment correlations (r) are the mean ± sd of the values obtained across all subjects.

		RMSE [N]	r
SS	F_x	415.52 ± 228.74	0.63 ± 0.16
	F_y	415.84 ± 267.60	-0.24 ± 0.30
	F_z	376.64 ± 215.54	0.48 ± 0.31
	F_{res}	476.57 ± 287.02	0.47 ± 0.31
COD	F_x	632.54 ± 188.89	0.48 ± 0.22
	F_y	563.40 ± 203.24	0.08 ± 0.25
	F_z	436.44 ± 175.29	0.63 ± 0.25
	F_{res}	614.20 ± 248.41	0.46 ± 0.30

Discussion

The results from this study suggest the proposed IMU method may provide valid estimates of $\bar{F}_x$, $\bar{F}_z$, $\bar{F}_{res}$, RF, and the orientation of $\overline{\boldsymbol{F}}$ during the SS task and for $\bar{F}_z$, $\bar{F}_{res}$, and the orientation of $\overline{\boldsymbol{F}}$ during a 45º COD task. The criterion validity of the aforementioned variables is suggested by strong (r = 0.84 to 0.94) and significant ($p < 0.01$) correlations with FP estimates, RMSE between 45.17 N and 77.32 N, relative error between 5.20% and 12.88%, and average bias between -39.45 N and -1.82 N. The IMU method may also provide valid estimates of the orientation of $\overline{\boldsymbol{F}}$ suggested by angular error of 3.4º for the SS task, 8.1º for COD-Right, and 9.2º for COD-Left. The conclusion of valid estimates for these variables was further supported after a post-hoc analysis found the effect size $\left(ES = \frac{\boldsymbol{F}_{IMU} - \boldsymbol{F}_{FP}}{SD_{FP}}\right)$ of IMU and FP differences was negligible to small (ES = 0.03 to 0.25) [2]. Thus, the proposed method appears to be appropriate in applications where the step-averaged sagittal plane values or the orientation of $\overline{\boldsymbol{F}}$ are most important (e.g., analyzing performance in linear sprinting and change of direction tasks) [2, 14].

The proposed method does not appear to provide valid estimates of peak $\boldsymbol{F}$ for the SS and COD tasks, $\bar{F}_y$ during both SS and COD tasks, nor $\bar{F}_x$ during the COD task. For these estimates, the RMSE and relative error were relatively large compared to the other measures. Thus, the proposed IMU method may be inappropriate in applications where these values are of interest. However, the IMU estimates were significantly correlated ($p \leq 0.05$) with FP measures for all values except peak F_y during SS and COD, $\bar{F}_y$ during SS, and peak F_x during COD. The significant correlations suggest the method would be appropriate to compare values that were each obtained by the proposed method (e.g., to compare pre- and post-intervention, to assess the effects of fatigue, etc.).

The relative error statistic provides insight into the error in the IMU estimate relative to the magnitude of the reference measure. For this reason, some values were characterized by noticeably large relative errors compared to others, but with lesser absolute error (RMSE). For example, the relative error of the IMU estimate of $\bar{F}_x$ during COD was 218.02% while the RMSE was 100.93 N. On the other hand, relative error for peak F_z during SS was just 22.20% with RMSE 514.67 N. Thus, the appropriateness of the IMU method may depend on how much error is acceptable for a given application and should be considered before using the proposed method.

The proposed IMU method to predict $\boldsymbol{F}$ is dependent upon the assumption that the IMU location is representative of the COM. The sacral region may meet this assumption while standing in anatomical position; however, due to limb movements relative to each other during a movement, the location of the COM in the body frame will be displaced. A FP is sensitive to the force responsible for this displacement, but a sacral worn IMU has no means to sense the relative movement of body segments other than the sacrum. Thus, the poor estimates of instantaneous $\boldsymbol{F}$ are not surprising. However, the average displacement of the sacrum over some time interval

must closely resemble that of the COM and thus also the associated average acceleration over the interval. This may explain the more accurate estimates of $\overline{\boldsymbol{F}}$. The small angular differences between IMU and FP measures of $\overline{\boldsymbol{F}}$ ($\theta < 10°$, Figure 3.3) as well as the accurate estimates of RF (Table 3.1) support the validity of the orientation estimate, especially for the SS task. This was not the case for the peak values. If the observed error were to some extent due to the relative movements of the limbs, then the sacrum would be expected to experience lesser accelerations while the COM experiences greater. This must result in even greater sacral accelerations at some later time (assuming the position of the COM eventually returns to the sacral region). This may explain the inaccuracy in the estimates of peak $\boldsymbol{F}$. This explanation is also supported by the instantaneous force-time traces (Figure 3.4). Specifically, the braking portion of F_x and the decreasing end of F_z towards toe off, appear to occur slightly later in the IMU trace. Finally, the fact that the sensor was placed on the surface of the skin means that it was displaced radially from the true COM location. Consequently, rotation about an axis through the COM would appear as a linear acceleration in the sensor frame. This may explain the oscillations immediately following foot contact in the instantaneous IMU F_y trace (Figure 3.4) before the smoother pattern resembling that of the FP.

To the author's knowledge, a paper by Wundersitz et al. (2013) is the only other study comparing IMU estimates of $\boldsymbol{F}$ to FP estimates for linear acceleration and change of direction tasks [114]. Their study had several methodological differences compared to the present study: (1.) the IMU was placed on the subjects' upper back, (2.) the start of the movement trial was 5 m behind the force plate (as opposed to one step in this study), (3.) they only estimated peak F_z and peak F_{res}, and (4.) the IMU referenced estimate of $\boldsymbol{F}$ was not rotated to the FP frame. They assessed the effect of different low-pass filter cutoff frequencies on the estimate and found 10 Hz

to be optimal. The data in this study was filtered at 70 Hz [24] and thus, in what follows, the data presented in this study is compared with their data that was low pass filtered at 25 Hz (this was the closest cutoff frequency to our 70 Hz). They found the bias of the IMU estimate of peak F_z and peak F_{res} during the SS task was -226 N and 315 N respectively compared to the 208.85 N and 903.15 N bias found in this study. For the 45º COD task, the bias was -211 N for peak F_z compared to 329.17 N in this study and 576 N for peak F_{res} compared to 918.43 N in this study. The authors suggest IMU to FP frame misalignment as a potential explanation of the observed error. If this explanation were true, the actual peak F_z would appear in the IMU frame as a vector with components along at least two axes. In this case, if the estimate of peak F_{res} were perfect, peak F_z would be expected to be too low. On the contrary, if peak F_{res} were underestimated it would be unclear how much of the error in peak F_z (if any) was due to misalignment or the underestimation of the magnitude. However, the finding that peak F_{res} was consistently overestimated would suggest an expectation of overestimated component values as well. The absence of the latter further supports IMU to FP frame misalignment as a likely source of the observed error. In this study, the overestimates of peak F_{res} are reported, but contrary to the findings of Wundersitz et al., the results of this study found peak F_z was also overestimated. Although this does not rule out misalignment error, it does make it less clear than if it were underestimated.

The magnitude of the peak F_{res} overestimation was greater in our study compared to Wundersitz et al., and because rotation of the vector does not change its magnitude, other explanations are necessary to clarify this finding. These could include the higher sampling frequency used in this study (446 Hz vs. 100 Hz), the use of different sensors (Yost 3-Space vs. SPI Pro) and associated technical specifications (e.g., noise density, non-linearity, etc.), and the

location of the IMU in this study being inferior to that used in their study. The latter was also suggested by Wundersitz et al. because shock attenuation during running has been observed at more superior body segments [122], which would suggest an expectation of higher acceleration magnitudes at locations closer to the ground.

Wundersitz et al. [114] report correlations between the IMU and FP estimates for peak F_z (r = 0.12) and peak F_{res} (r = 0.35) during the SS task that were lower than that found in the present study (r = 0.65 and 0.62 respectively). These relationships were also lower in their study for the COD task (r = -0.26 for peak F_z and 0.40 for peak F_{res}) compared to significant relationships found in the present study (r = 0.52 and 0.57 respectively). As discussed previously, misalignment error may explain their finding of poor relationships for the IMU estimate of peak F_z. However, if the estimate of peak F_{res} in the present study is different from their estimate only because of a greater bias, then relationships between IMU and FP measures for peak F_{res} should not be much different between the studies. This not being the case, one explanation could be that the location of the IMU on the upper back used in their study may be subject to accelerations due to high frequency trunk flexions during the weight acceptance phase that may not have as great of an effect on an IMU mounted at the sacral region [123]. This effect may vary between subjects which would explain the observed lesser relationships and why smoothing the signal improved the relationship (high frequency trunk flexions would be removed after filtering).

Conclusion

The results from this study suggest the proposed IMU method may provide accurate estimates of $\bar{F}_x$, $\bar{F}_z$, $\bar{F}_{res}$, RF, and the orientation of $\overline{\boldsymbol{F}}$ during a linear standing sprint start and for $\bar{F}_z$, $\bar{F}_{res}$, and the orientation of $\overline{\boldsymbol{F}}$ during a 45º change of direction task, but not for any of the

other values. Step averaged forces are used to characterize performance in linear acceleration and change of direction tasks, thus the proposed method may be appropriate for these applications. The amount of acceptable error, however, may vary depending on the context and thus should be considered before implementing the proposed method. The results of this study may not be generalized to movements other than the ones used in this study or for movements over longer periods of time unless data fusion techniques are used for the orientation estimate. Future research should investigate ways to further pin-point the underlying causes of the observed errors and potential ways to compensate for these errors. This may include, for example, estimating the measured acceleration that may be due to rotation and/or compensating for relative limb movements by using more IMUs at multiple limbs.

Chapter 4: A Novel Adaptive Gain Filtering Algorithm to Estimate Sprint Velocity Using a Single Inertial Sensor

Abstract

The ability to measure sprint running velocity is useful in a performance evaluation and to guide training interventions. Inertial measurement units (IMU) are becoming increasingly popular for field-based performance assessments making them a potential attractive methodology to measure sprint velocity. In this paper, a novel filtering algorithm to estimate sprint velocity using a single IMU independent of external measurement systems is described. The proposed method is compared to a reference method using photocell position-time data. Instantaneous velocity, average interval velocity, and maximal step velocity are determined using both methods for twenty-eight subjects during a maximal effort 40 m sprint. The concurrent validity of the proposed method was assessed using Bland-Altman analysis, root mean square error (RMSE), relative error (absolute percent difference), and Pearson's product moment correlation coefficient (r). For average interval velocity, there was a slight underestimation in the first 20 m of the sprint (-0.31 to -0.12 m/s) and a slight overestimation later in the sprint (0.05 to 0.13 m/s). The concurrent validity of the proposed method may be suggested by relative errors between 5.09% and 7.13%, RMSE between 0.34 m/s and 0.67 m/s, and significant correlations ($r \geq 0.75$, $p < 0.01$) between IMU and photocell estimates. The results of the study give insight into the source of some of the errors that allow for the development of potential compensatory techniques in future research. This study broadens the scope of IMU based applications to allow performance assessments in less restricted environments.

Introduction

Sprint running velocity over short durations (i.e., during the acceleration phase) is advantageous in both individual and team sports [1] and is thus the focus of many training programs [10, 124, 125]. Accurate methods to assess sprint velocity are necessary to best evaluate an athlete's performance and to determine the effectiveness of a training program. Available techniques to assess sprint velocity include the use of photocells [13, 14, 53], lasers [55], radar [14, 50], treadmills [47, 49], and global positioning systems (GPS) [126, 127]. Lasers, radar, and treadmills are relatively expensive, limit the assessment area, and have limited validity under certain circumstances (e.g., non-constant velocity for treadmills and the initial sprint start for lasers) [43, 44, 55]. Studies investigating GPS units concerning their ability to measure sprint velocity have varying results [126–129] and their use indoors is limited [130, 131]. The use of photocells to estimate sprint velocity was first suggested by Furusawa et al. in 1927 [13] where an expression was derived for the instantaneous sprint velocity that is dependent only on position-time data [13]. The model is derived given the assumption of the force-velocity property of muscle and that the sprint is undertaken in a non-fatigued state [13]. The solution to the equation involves two constants (v_m and τ) and is related to the position (p) at some time (t) by [13, 14]:

$$p(t) = v_m \left(t + \tau e^{-t/\tau} \right) - v_m \tau \tag{4.1}$$

Then, the velocity (v) at time t is given by differentiation:

$$v(t) = v_m \left(1 - e^{-\frac{t}{\tau}} \right) \tag{4.2}$$

More recently, this method has allowed the use of smartphones to assess sprint velocity where the position-time data is obtained using smartphone video data [15].

Inertial measurement units (IMUs), are becoming more popular for field-based biomechanics data collection [20, 26, 107, 132]. An IMU is a single sensor with an on-board three axis accelerometer, three axis gyroscope, and/or three axis magnetometer. The use of IMUs in the context of assessing sprint velocity is attractive for several reasons: (1) ease of use, (2) small size, (3) low cost, (4) the assessment task is not limited to a specific area (e.g., a laboratory, a camera's field of view, etc.), (5) they can be used indoors, and (6) they potentially provide the means to allow a more comprehensive assessment (e.g., including spatiotemporal data [26], joint angles [22], and kinetics [114]). Thus, the use of an IMU to measure sprint velocity was considered in this study.

Perhaps the simplest estimation of sprint velocity using IMU data would be the following: (1) estimate the initial orientation of the IMU in the track frame, (2) time-integrate the gyroscope angular rate signal during the sprint to obtain the orientation at each instant, and (3) rotate the acceleration vector from the IMU frame to the track frame and time-integrate the component of that vector along the track frame forward axis. An estimate obtained this way is prone to error that may originate at any of these three steps due to gyroscope sensor drift [97], the effect of ferromagnetic disturbances on magnetometer estimates [133], and/or inaccurate estimates of each sensor's calibration parameters (bias, sensitivity, and/or non-orthogonality) [23]. To compensate, an external measurement (e.g., GPS, radar, video, etc.) may be used to provide a better estimate via different data fusion techniques [131, 134].

A sprint velocity measurement system requiring the use of IMUs in combination with other external measurement systems removes some of the aforementioned advantages of an IMU-only based system. However, by excluding the use of these other measurement systems the availability of reference data for error compensation is also removed. A single IMU does

provide the means to fuse orientation estimates from different on-board sensors. The accelerometer and magnetometer can provide an estimate of attitude and heading respectively that can then be fused with the estimate from gyroscope integration [23, 93]. Data fusion in this way is only valid during quasi-static intervals (intervals when the measured acceleration is representative of gravity) and when there are no ferromagnetic disturbances (such that the measured magnetic field vector is constant at each location throughout the sprint). The dynamic nature of sprinting, however, prevents the occurrence of any quasi-static interval thereby eliminating the possibility of fusing an accelerometer estimate of orientation during the sprint. Further, the ferromagnetic disturbance problem would limit the incorporation of a magnetometer orientation update, especially indoors [133]. Thus, the use of some other reference information would be necessary to provide error compensation, which would be expected to be especially necessary as the sprint progresses in time [131, 135]. Yang et al. [32] proposed a method incorporating the known behavior of the shank during certain phases of the gait cycle to compensate for drift error. However, the method was only validated for constant velocities of relatively low magnitude (≤ 3.5 m/s). Considering this, an attempt was made to investigate what other reference information might be incorporated in a sprint velocity measurement system using a single IMU. It was theorized that some characteristics of sprint running might act as natural constraints that could be used to correct IMU estimates. Namely, the following two assumptions about sprint running were made:

(I.) the heading of the runner's pelvis during the sprint is expected to be mean zero

(II.) the velocity-time relationship is expected to resemble that of eq. (4.2).

This paper describes a novel filtering algorithm incorporating these constraints to estimate sprint velocity using data from a single IMU during a 40 m sprint. An experimental protocol is

designed to determine the concurrent validity of the proposed method by comparing the velocity estimates to that obtained using photocells.

Methods

Algorithm Design

The sprint velocity estimation algorithm developed in this study consists of three basic steps. In the first step, a first estimate of the IMU orientation during the sprint is determined. During the second and third steps, the corrections given by assumptions (I.) and (II.) respectively are employed. See Table 4.1 for a summary of the proposed algorithm.

Table 4.1: Description of proposed algorithm

Step 1: Initial Estimate of IMU Orientation

-Determine static orientation

-Integrate gyroscope angular rate signal

Step 2: Correction (I.)

-Decompose composite quaternion

-Linearly detrend raw heading estimate (force to be mean 0)

-Propagate correction to determine new estimate of composite quaternion

Step 3: Correction (II.)

-Determine foot contacts

-Estimate model velocity curves based on raw velocity at each step

-Determine step at which raw velocity best resembles expected relationship

-Apply correction to next step and generate new model velocity for next iteration

IMU Orientation and Vector Rotations during the Sprint

The full details of computing the first estimate of the IMU orientation during the sprint and of rotating vectors from the sensor frame (F_S) to the track frame (F_T) are described in Appendix A. The quaternion notation is used to describe the orientation of F_S relative to F_T according to the single rotation through an angle γ about some axis $\boldsymbol{U}$, of unit length, that would

align F_T with F_S (Figure 4.1) [136]. The parameters of the quaternion (Q_γ) describing this orientation allow a parametrization of a rotation matrix that is used to transform vectors in F_S to F_T [20]. The orientation at each instant throughout the sprint is given by integrating the gyroscope angular rate signal. The initial orientation from which integration begins is determined using sensor referenced measurements of the world frame gravity and local magnetic field reference vectors. To do this, two rotations that would align the frames instead of one composite rotation are considered: first about the world frame vertical axis through an angle α (Q_α) and second about an axis in the world frame horizontal plane through an angle β (Q_β). The former is referred to as the sensor's heading and the latter the sensor's attitude. First, the accelerometer measurement of the gravity vector, which represents the coordinates of the F_T vertical axis in F_S, is used to determine the IMU attitude β and the axis ($\boldsymbol{H}$) in the horizontal plane about which the sensor may have been rotated to assume this attitude (thus giving Q_β) [93]. The local magnetic field vector ($\boldsymbol{B}$) can be used to estimate the heading of the IMU because $\boldsymbol{B}$ has a component in the horizontal plane of F_T [23]. First, the measurement of $\boldsymbol{B}$ in F_S ($\boldsymbol{B}^S$) is rotated to the horizontal plane ($\boldsymbol{B}_H$) by Q_β. The x and y components of $\boldsymbol{B}_H$ then give the IMU heading α relative to $\boldsymbol{B}_H$ (thus giving Q_α) [23]. Then, because the quaternions Q_α and Q_β are known, Q_γ is given by their quaternion product ($Q_\gamma = Q_\alpha \otimes Q_\beta$). Integration using the gyroscope angular rate signal then gives an *a priori* estimate of the IMU orientation (Q_γ^-) throughout the sprint.

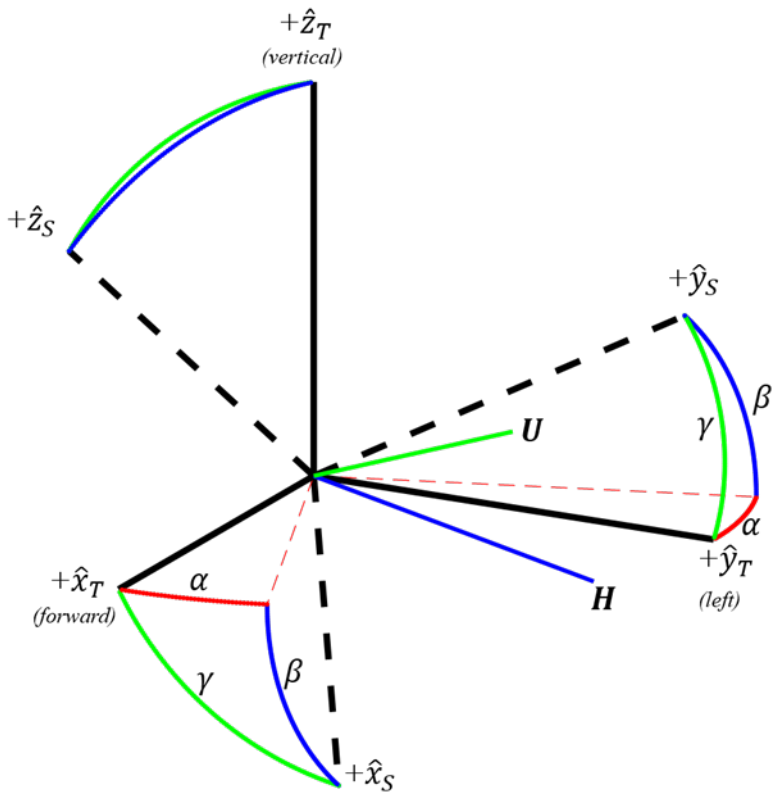

Figure 4.1: Description of frame orientations. The track frame axes are the solid black lines and the sensor frame axes are the dashed black lines. The orientation may be described by a single rotation through an angle γ (≈ 50° in the figure) about the axis ***U*** (green lines) or by two successive rotations: first through an angle α (= 20° in the figure) about $\hat{z}_T$ (red lines) and then a second rotation through β (= 45° in the figure) about the axis ***H***.

Filtering Algorithm: Correction (I.)

The first correction of the IMU estimate is given by assumption (I.); the heading of the runner (α) throughout the entire sprint should be mean zero. The first estimate of the quaternion at each instant during the sprint (Q_γ^-) is decomposed into two quaternions, Q_β and Q_α^-, such that Q_γ^- is given by their quaternion product as described previously. The derivation of the general decomposition may be found in [136] and the full details of the decomposition in the context of utilizing the correction of assumption (I.) are described in Appendix B. In short, the quaternion product $Q_\gamma^- = Q_\alpha^- \otimes Q_\beta$ allows the parameters of Q_γ^- to be expressed as linear combinations of the parameters of Q_β and Q_α^-. It is shown that because Q_β and Q_α^- have orthogonal rotation axes,

the resulting linear combinations allow the expression of the *a priori* heading estimate (α^-) in terms of just Q_γ^- parameters (which are known from integration). To employ correction (I.), α^- is linearly detrended such that it is mean zero to obtain a better heading estimate (Figure 4.2).

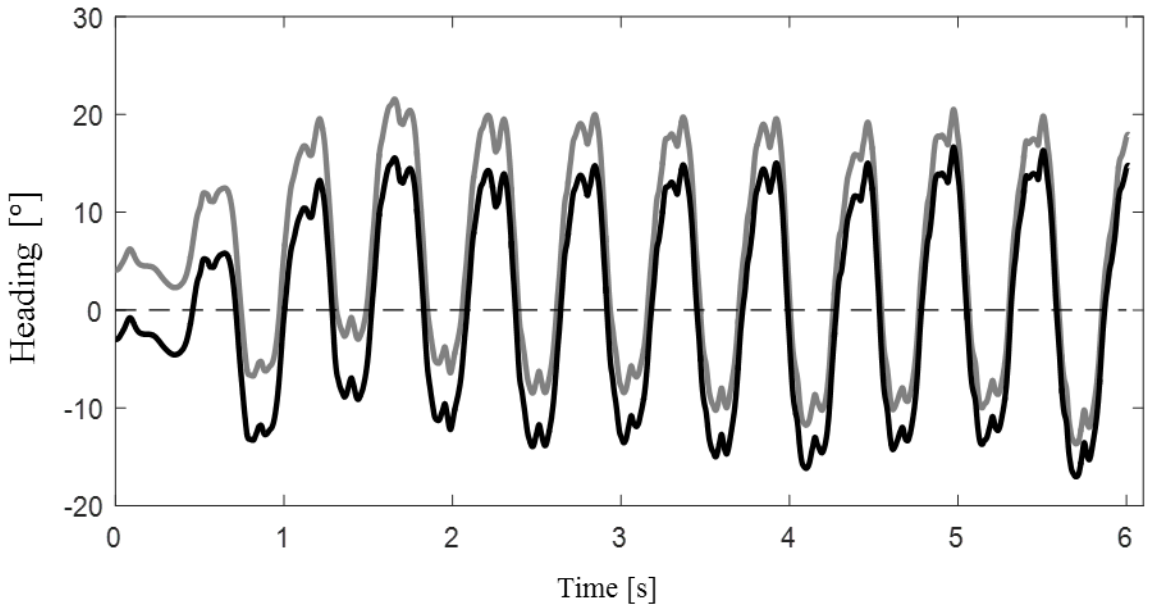

Figure 4.2: The first correction of the proposed algorithm is to force the mean zero assumption of the runner's heading. The solid grey line is the estimate obtained via integration of the gyroscope angular rate signal, the solid black line shows the detrended estimate, and the dashed line is the 0° line (the assumed average heading during the sprint).

The corrected heading (α) is then used to construct the quaternion Q_α from which the better estimate of the composite quaternion is computed (Q_γ). Then, Q_γ is used to rotate the IMU referenced acceleration vector ($\boldsymbol{a}^S$) to the track frame ($\boldsymbol{a}^T$) and the forward component of $\boldsymbol{a}^T$ (a_x^T) is then time integrated to yield an *a priori* estimate of forward velocity (v^-):

$$v^- = \int a_x^T dt \tag{4.3}$$

The time index of the sprint start (t_0) is defined as the first instant at which v^- exceeds one standard deviation above the average velocity during the interval between the beginning of stance (t_s) and the first estimate of the sprint start (t_0^-). The latter is a first estimate found by

visual inspection of v^- (the last instant before which v^- remains relatively constant during stance) and the former is defined as the end of the stillest one-second interval (interval during which the sum of the variance of each axis of the accelerometer is a minimum) during the sprint start stance (Figure 4.3).

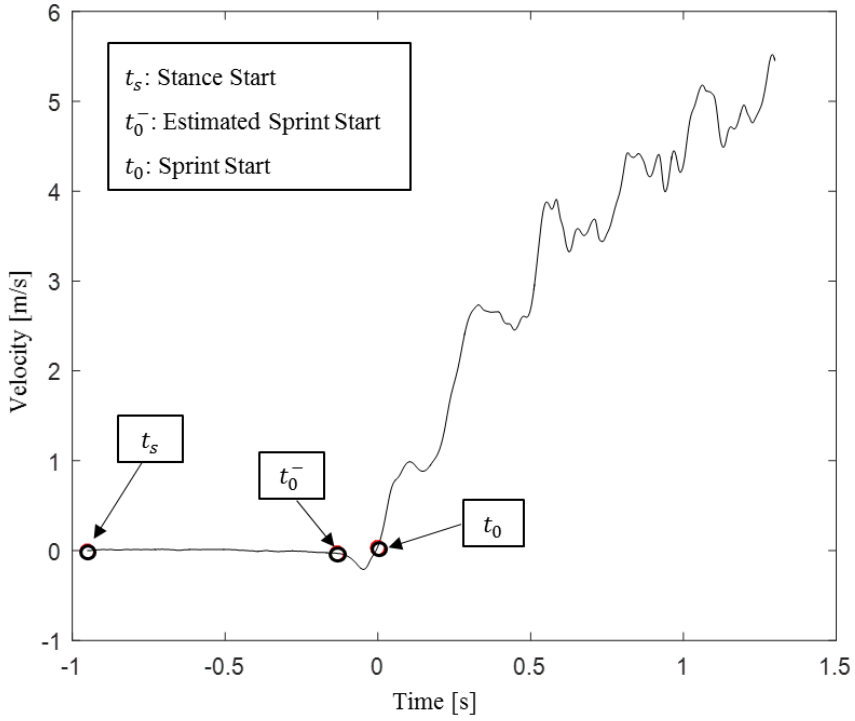

Figure 4.3: Visual inspection of the raw velocity allowed for an estimate of the beginning of the sprint start (t_0^-). The actual sprint start (t_0) was defined as the first instant after t_0^- the velocity trace went one standard deviation above the mean between stance start (t_s) and t_0^-.

Filtering Algorithm: Correction (II.)

To employ correction (II.), modeled velocity based on raw velocity through a previous step is used to provide an update to the raw velocity obtained at the current step. First, steps are identified (i.e., from one foot contact to the next) using the a_x^T and a_z^T traces according to a previously described method (Figure 4.4) [26]. Then, the idea of employing correction (II.) is that if the constants v_m and τ from eq. (4.2) characterizing any one subject's sprint velocity are

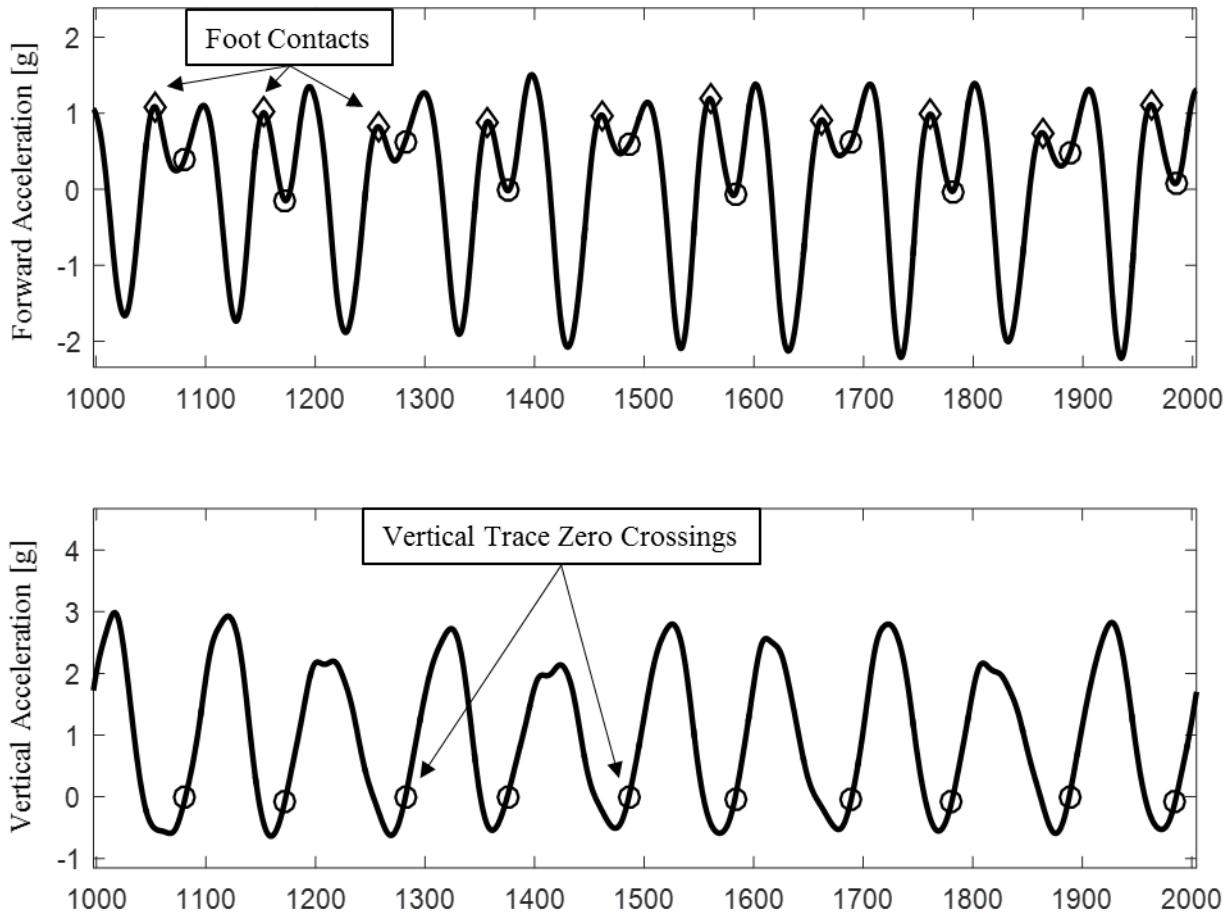

Figure 4.4: Foot contacts were identified according to a previously validated method [26]. First, zero crossings (circles) of the vertical acceleration trace (bottom) are identified. Then, the peak just prior to the zero crossing in the forward acceleration trace (top) identified the foot contacts (diamonds).

known, then the IMU raw velocity estimate may be forced to resemble the general shape of the logarithmic curve associated with these constants described in eq. (4.2). However, the only information available to estimate these constants is that from the IMU and specifically the raw velocity estimate. The problem is that if more raw velocity data (i.e., that obtained over a longer period of time) is used to estimate v_m and τ then more drift error is expected. On the other hand, if less raw velocity data is used, then there is less information available to accurately estimate the constants that best characterize any one subject's sprinting capabilities. To solve this problem, one must first determine which subset of the v^- data best resembles the expected relationship in

eq. (4.2). The subsets of v^- between the start of the sprint and each step beginning at step three were considered. It was inappropriate to begin at step one (i.e., the initial push from stance to the first foot contact) because it is biomechanically different than the rest of the steps and is not expected to be representative of the sprint capabilities throughout the remainder of the sprint [14]. Step three (i.e., using raw velocity data from the initial push to the third foot contact) was used instead of step two to avoid any potential bias in the first model estimate based on bilateral asymmetries. To determine the constants v_m and τ predicted by each of these subsets, each subset of v^- data (low-pass filtered at 1 Hz) from each step (i.e., from t_0 to the time of each foot contact) was fit to eq. (4.2) using non-linear least squares curve fitting. Low-pass filtering of v^- from pilot data at 1 Hz was shown to sufficiently remove the error due to the sinusoidal nature of the actual sprinting velocity that is not expressed in eq. (4.2). Lower bounds were placed on estimates of the constants v_m and τ in eq. (4.2) determined using previously published data [13, 14]. Three standard deviations below the mean of the values in these studies defined the lower bound for τ (τ_{min}). Then, an estimate is made for the lower bound for v_m ($v_{m,min}$) using τ_{min}, v^-, and eq. (4.2) by:

$$v_{m,min} = v^- \left(1 - e^{-\frac{t}{\tau_{min}}}\right)^{-1} \tag{4.4}$$

The normalized error associated with the curve fitting (squared norm of the residual from least squares curve fitting expressed relative to the number of samples used to generate the curve) is an index of how well the data resemble the expected relationship [137]. The subset of v^- data for which the normalized error was a minimum defines the v^- trace that best represents the expected model in eq. (4.2). The modeled velocity data (v_{mod}) at this step is then used to provide a correction at the next step. To apply the correction, the difference (d_v) between the

linear trend of v^- (l_{raw}) and the linear trend of v_{mod} (l_{mod}) from the sample at step $k-1$ (s_{k-1}) to the sample at step k (s_k) is found according to (Figure 4.5):

$$l_{raw} = \frac{v^-_{s_k} - v^-_{s_{k-1}}}{s_k - s_{k-1}}(s) + v^-_{s_{k-1}} \tag{4.5}$$

$$l_{mod} = \frac{v_{mod,s_k} - v^-_{s_{k-1}}}{s_k - s_{k-1}}(s) + v^-_{s_{k-1}}$$

$$d_v = l_{mod} - l_{raw}$$

where s is the sample expressed relative to s_{k-1}.

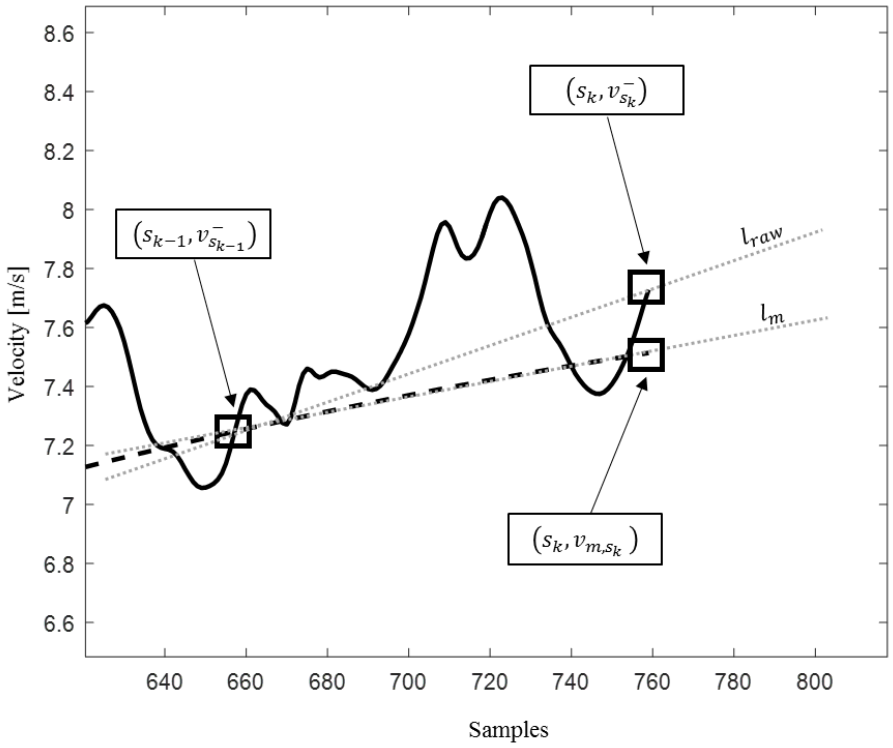

Figure 4.5: The difference between the linear trends of the raw velocity estimate (grey dotted line labeled l_{raw}) and the modeled velocity (grey dotted line labeled l_m) between a step (s_k) and the previous step (s_{k-1}) is used to correct the raw velocity estimate. The raw velocity estimate is the solid black line and the modeled velocity is the dashed black line.

The trust given to the correction d_v is dependent on the relative normalized residual error between v_{mod} generated from step $k-1$ and step k (i.e., E_{k-1} and E_k respectively). This way the v^- trace that best resembles the expected relationship in eq. (4.2) (i.e., has the smaller

normalized error) has a greater contribution to the final estimate. This relative error determines the gain (G) that scales the correction d_v to provide the best estimate of the sprint velocity (v) from step $k-1$ to step k according to:

$$G = \frac{E_k}{E_k + E_{k-1}} \tag{4.6}$$

$$v = v^- + G(d_v)$$

A new modeled velocity for step k and the associated normalized residual error is then generated using the new best estimate from eq. (4.6). The position (p) of the sprinter (distance from the start line) is then estimated by time integrating v using the trapezoidal method. Because the initial location of the IMU at the start of the sprint is actually behind the start line, an estimate is made of its initial location (p_0) using the trunk lean angle during stance (θ_s), the torso length (L_t) defined as the distance between the IMU and the seventh cervical vertebra (C7), and by assuming the location of C7 during stance in the F_T horizontal plane is near the sprint start line (i.e., is directly above the hands). The trunk lean angle θ_s is calculated given the IMU attitude relative to the anatomical frame (β_0) determined during an initial static orientation trial (see *Procedures*) and the IMU attitude during stance (β_s) by:

$$\theta_s = \beta_s - \beta_0 \tag{4.7}$$

Then p_0 and p are given by:

$$p_0 = L_t sin(\theta_s) \tag{4.8}$$

$$p = \int_0^{t_k} v\, dt - p_0.$$

The corrections continue for each foot contact as long as the condition $p < 40\ m$ is satisfied.

Experimental Set-Up

An experiment was designed to test the validity of the proposed method to estimate sprint velocity during a 40 m sprint. Five pairs of photocells (Brower Timing Systems, Draper, UT) were positioned along a 40 m straight of an indoor track to collect position-time data at 10 m, 15 m, 20 m, 30 m, and 40 m splits [14]. This timing system includes a touch sensor to initiate the timer at the start of the sprint when the sprinter's hand is lifted off the sensor. A high-speed video camera (Sensor Technologies America, Carrollton, TX) set to sample at 200 fps was used to record each subject's sprint start using MaxTRAQ software (Innovision Systems, Columbiaville, MI). The camera was positioned behind and to the left of the starting line in such a way that the IMU and hand (on the touch sensor) were within the camera's field of view (Figure 4.6). The timestamp of the frame associated with the initial forward movement of the IMU and that of the hand coming off the touch sensor were used to synchronize the two systems.

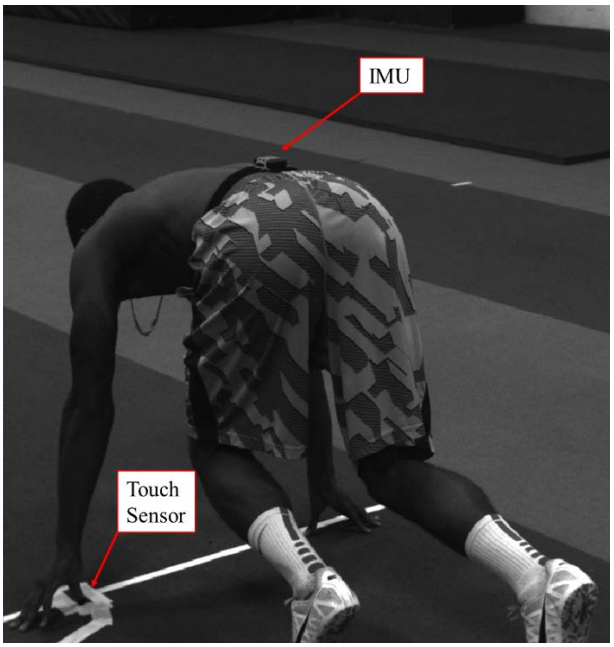

Figure 4.6: A high speed video camera was positioned behind the sprinter at the start of each sprint such that the IMU at the subject's lower back and the thumb on the touch sensor were visible. The time difference between the lift off of the thumb from the touch sensor and the initial forward movement of the IMU were used to time-synchronize IMU and photocell data.

Subjects

Twenty-eight subjects (12 female, 16 male, age: 20.9 ± 2.3 yrs, height: 1.73 ± 0.09 m, mass: 71.1 ± 11.7 kg) volunteered to participate in this study. Subjects were recruited from both a collegiate level track team and a general student population and were included in the study if they were between the ages of 18 and 35 years old, reported no musculoskeletal injuries within the six months prior to testing, regularly participated in physical activity, and were able to perform maximal effort sprints pain free. All subjects provided written consent to participate. The Appalachian State University Institutional Review Board approved this study.

Inertial Measurement Units

The Yost Data Logger 3-Space Sensors (YEI Technology, Portsmouth, OH) were the IMUs used in this study. These units have an onboard three-axis accelerometer (range: ±24 g, noise density: 650μg/$Hz^{1/2}$, 12-bit resolution), three-axis gyroscope (range: ±2000º/s, noise density: 0.009º/s/$Hz^{1/2}$, 16-bit resolution), and three-axis magnetometer (range: ±1.3 Ga, 12-bit resolution). Sampled data from each sensor (445.72 ± 0.55 Hz) were written to a MicroSD card along with the associated timestamp. Data from different trials were stored as separate files and were downloaded to a computer via USB after data collection for data analysis.

Procedures

Data collection consisted of one testing session in the Appalachian State University Biomechanics Laboratory and indoor track. Subjects' standing height, torso length, and mass were recorded. Torso length was taken to be the linear distance between the point of intersection of the intercristal line with the spine and C7. The former is defined as the point where a line joining the left and right posterior superior iliac spines meet the spine (found via palpation) [118]. Torso length was necessary to determine the initial location of the sensor relative to the

sprint start line (see *Filtering Algorithm: Correction (II.)*). Subjects were then taken through a general and sprint specific warm up. To finish the sprint specific warm up, subjects performed sprint starts from a four-point stance (two hands and two feet) without blocks to familiarize themselves with the sprint start they would be using during testing (Figure 4.6). Next, the IMU was attached to the lower back of each subject using an elastic strap and tape. The location of the IMU on the spine was at the intersection of the aforementioned intercristal line (Figure 4.6) [27]. After the IMU began recording data, subjects stood at the start line and performed a jump followed by a five second standing static trial followed by another jump. During the static trial, care was taken to ensure the subjects' feet and pelvis were aligned parallel to the forward axis of F_T while standing straight up and still as possible. The jumps allowed the identification of this static trial when visually observing the accelerometer data during post-processing. The static trial was necessary to initially align F_S with F_T and the anatomical frame later during stance. Subjects then assumed their four-point stance with one hand placed on the touch sensor (Figure 4.6). They were instructed to be as still as possible and were given a three second countdown before the start of a maximal effort 40 m sprint. This sequence was repeated twice more for three total sprints for each subject. The equations used to model sprint velocity given position-time data assume the sprinter is in a non-fatigued state. Thus, each subject was given a minimum of three minutes rest between sprints or until they felt fully recovered.

Data Reduction

Each subjects' anthropometric data and the split times of their fastest 40 m sprint were saved to a Microsoft Excel sheet. A custom MATLAB program (MathWorks, Natick, MA) was written to process photocell position-time and IMU data. The photocell split times were fit to eq. (4.1) to obtain the constants v_m and τ using non-linear least squares curve fitting. These

constants were then used to estimate each subject's instantaneous velocity according to eq. (4.2) for time domain $t: t_0 \rightarrow t_{40}$ (where t_i is the time at position i) of equally spaced discrete time values according to the mean IMU sampling frequency. The IMU estimate of sprint velocity was given according to the previously described algorithm. The initial standing static orientation trial allowed the determination of the IMU attitude relative to the anatomical frame (β_0) using the accelerometer [93, 106]. The trunk lean during stance is then given according to eq. (4.7) to determine the initial location of the IMU relative to the sprint start line by eq. (4.8). Because the surface of the IMU (i.e., the y-z plane) was aligned flush to the subject's skin, the assumption is made that F_S and anatomical frame forward axes were aligned. Further, because the anatomical frame and F_T forward axes were aligned during this static orientation period, so also were the forward axes of F_S and F_T. Thus, one could estimate the heading (α_0) of the track frame relative to the local magnetic field vector given β_0 (see *IMU Orientation and Vector Rotations*). The heading of the IMU relative to this local magnetic field vector during the sprint stance (α_s) is then determined accordingly given the stillest one second interval during stance. Finally, the initial estimate of the IMU heading α relative to the track frame is then given by:

$$\alpha = \alpha_s - \alpha_0. \tag{4.9}$$

This initial heading estimate is dependent upon the assumption that the local magnetic field vector is the same at both locations (i.e., at the subject's sacrum when standing at the sprint start line and when in their four point stance). However, any error due to this assumption is later removed by correction (I.). The gyroscope bias was determined during the standing static interval before each trial and removed from the angular rate signal before integration.

Statistical Analysis

The maximal step velocity (maximal average velocity from one foot contact to the next) and average interval velocity for the 0 m – 10 m, 10 m – 20 m, 20 m – 30 m, and 30 m – 40 m intervals were compared between methods. The absolute error in the IMU estimate was quantified using using root mean square error (RMSE) and relative error (absolute percent error). The Pearson product moment correlation coefficient (*r*) was used to determine how well the IMU estimate scaled with that of the reference photocell method. Finally, Bland-Altman 95% limits of agreement (LOA) were used to assess the reliability of the method. The error in the IMU estimate of instantaneous velocity for each subject was quantified using RMSE and *r*. The average RMSE and *r* values across all subjects was then determined to assess the ability of the IMU method to estimate instantaneous velocity. For the Bland-Altman analysis, the normality of the difference distributions were tested using the Shapiro-Wilk test [121]. Data were transformed using the natural logarithm if differences were not normally distributed or showed a strong (≥ 0.75) relationship with the mean of the measurements [121]. For these cases, the anti-log bias and LOA are given. Statistical significance for all statistical tests was set *a priori* at a level of 0.05.

Results

The split times of the subjects' best 40 m sprint were: $t_{10} = 2.02 \pm 0.16\ s$, $t_{15} = 2.72 \pm 0.24\ s$ $t_{20} = 3.35 \pm 0.31\ s$, $t_{30} = 4.57 \pm 0.46\ s$, and $t_{40} = 5.81 \pm 0.61\ s$. The range of RMSE of the IMU maximal and average interval velocity estimates was between 0.34 m/s and 0.67 m/s and the relative error was between 5.09% and 7.13% (Table 4.2). IMU estimates of maximal and average interval velocities showed significant ($p < 0.01$) relationships ($r = 0.79 – 0.83$) with photocell estimates (Table 4.2). Table 4.3 and Figures 4.7 and 4.8 show the results of

the Bland-Altman analysis. All measurement differences were normally distributed and showed no linear trend with the measurement means and thus no data were transformed. The bias in the IMU estimate of maximal and average interval velocities were between -0.31 m/s and 0.13 m/s (Table 4.3). The RMSE for instantaneous velocity was 0.70 ± 0.26 m/s and the average correlation coefficient was $r = 0.97 \pm 0.01$. Sample velocity-time curves comparing the methods are shown in Figure 4.9. Figure 4.10 shows group averaged velocity and position vs time data.

Table 4.2: Comparison of average interval and maximal velocity estimates from the IMU and photocell method. ***Denotes significance at the 0.01 level.* Relative error: absolute percent difference between IMU and photocell estimates, RMSE: root mean square error between IMU and photocell estimates, *r*: Pearson product moment correlation between IMU and photocell estimates.

		Relative Error [%]	RMSE [m/s]	*r*
Avg. Interval Velocity:	0m - 10m	5.09 ± 4.08	0.34	0.81**
	10m - 20m	5.51 ± 4.54	0.56	0.83**
	20m - 30m	6.11 ± 5.50	0.60	0.80**
	30m - 40m	7.02 ± 4.16	0.66	0.79**
	Max Velocity	7.13 ± 4.42	0.67	0.80**

Table 4.3: Results from the Bland-Altman analysis assessing the agreement between IMU and photocell estimates of average interval and maximal velocity (all units m/s). LOA: Bland-Altman 95% limits of agreement. **Denotes a significant bias at the 0.05 level.*

		IMU	Photocell		
		Mean ± SD	Mean ± SD	Bias	LOA
Avg. Interval Velocity:	0m - 10m	4.71 ± 0.35	4.94 ± 0.43	-0.23	-0.73, 0.27
	10m - 20m	7.48 ± 0.72	7.79 ± 0.85	-0.31	-1.24, 0.62
	20m - 30m	8.05 ± 0.93	8.17 ± 0.97	-0.12	-1.30, 1.06
	30m - 40m	8.33 ± 1.06	8.27 ± 1.02	0.05	-1.25, 1.36
	Max Velocity	8.42 ± 1.07	8.29 ± 1.02	0.13	-1.19, 1.45

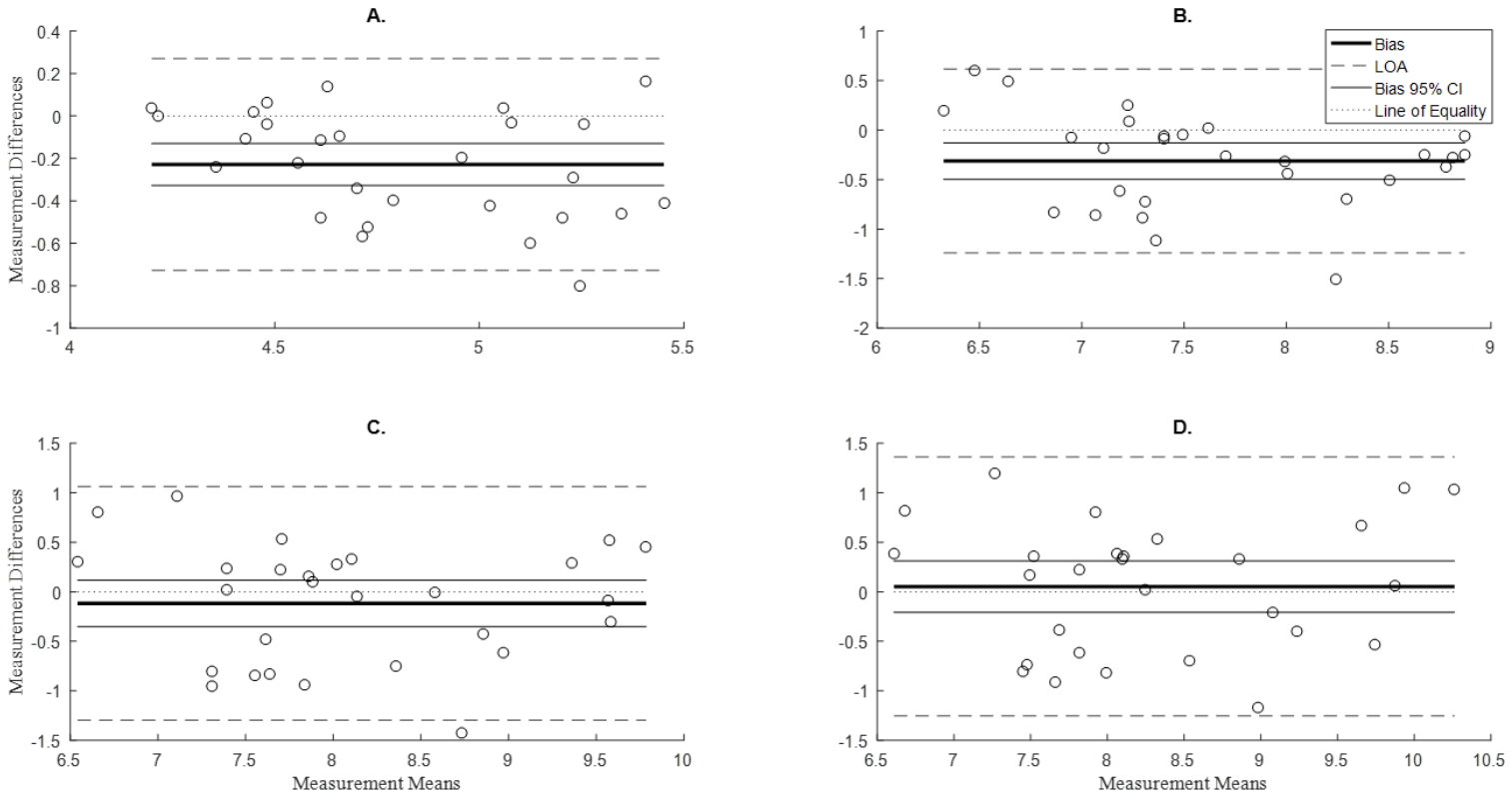

Figure 4.7: Bland-Altman plots of average interval velocity. (A.) 0 m – 10 m, (B.) 10 m – 20 m, (C.) 20 m – 30 m, and (D.) 30 m – 40

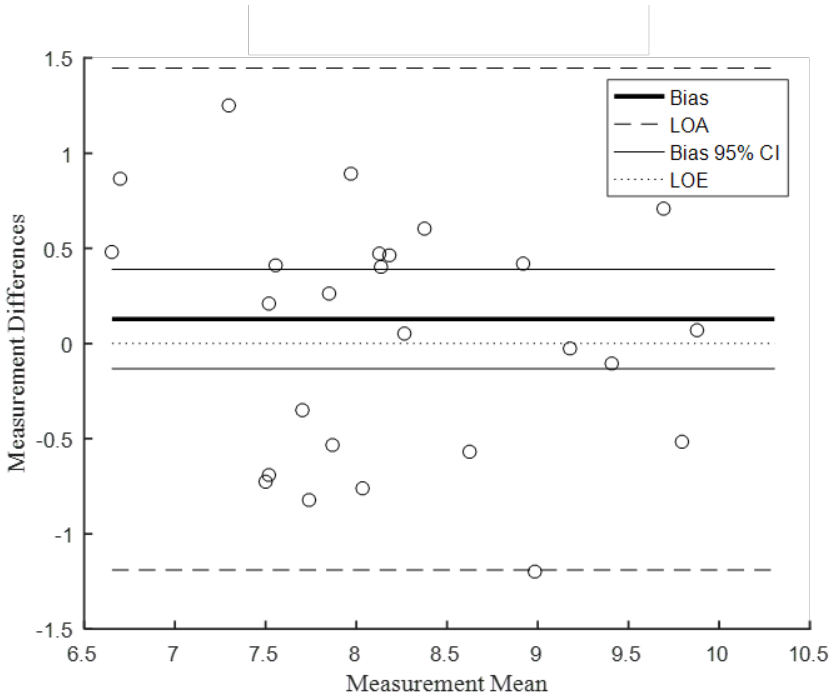

Figure 4.8: Bland-Altman plots comparing the IMU and photocell estimates of maximal sprint velocity.

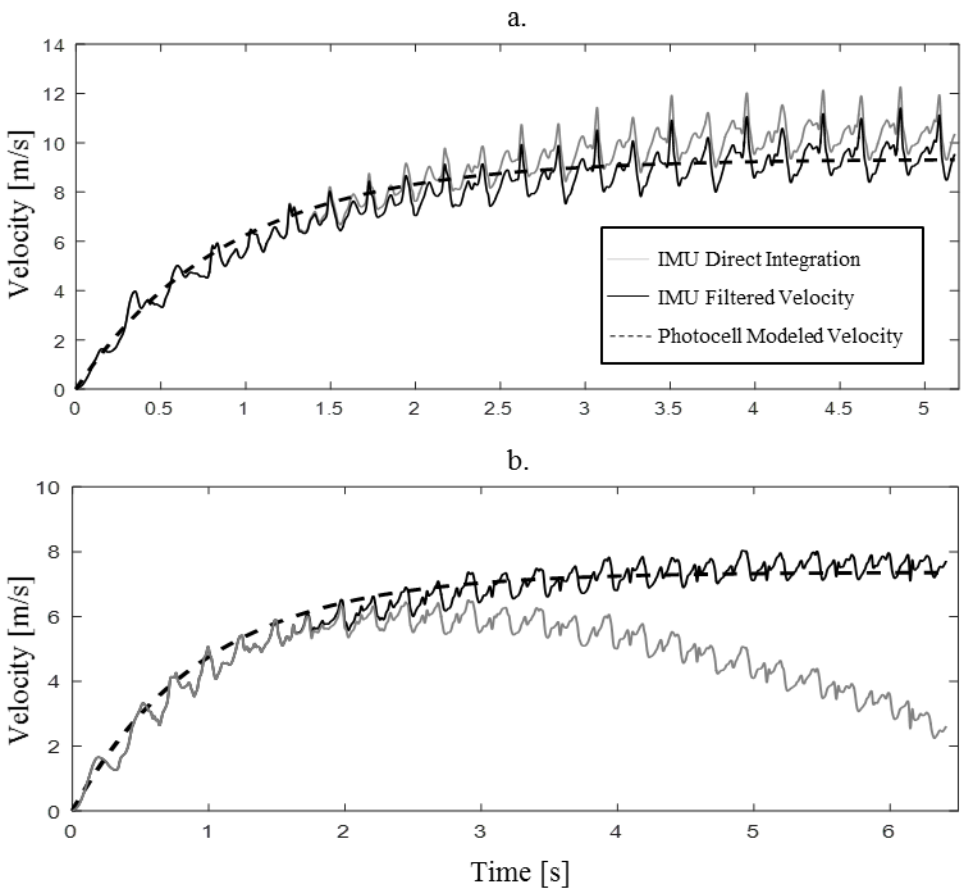

Figure 4.9: Comparing raw velocity obtained from direct integration (solid grey line), filtered velocity according to the proposed algorithm (solid black line), and model velocity obtained from the reference photocell method (dashed black line). Each curve represents a single subject. (a.) an example where direct integration overestimated the true velocity, (b.) an example where direct integration drastically underestimated the true velocity.

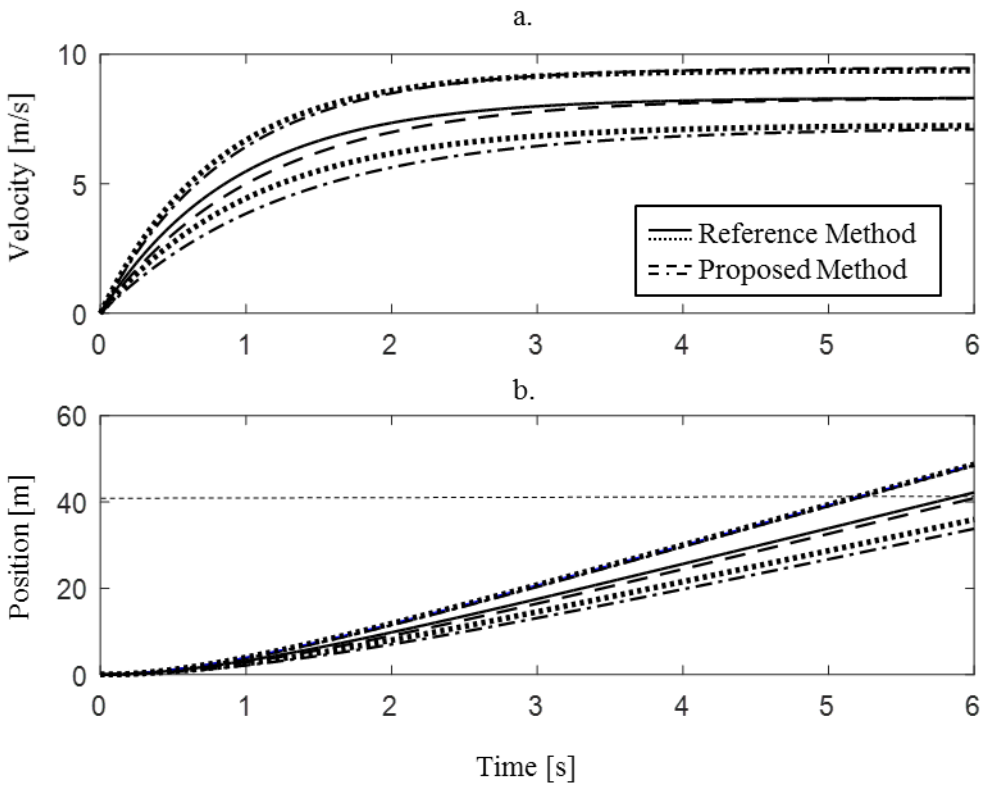

Figure 4.10: The average model velocity (a.) generated from the IMU method (dashed line) was compared to the reference photocell method (solid line) as well as the corresponding sprint distance (b.). The dotted and dashed-dot lines show the standard deviations of the photocell and IMU method sprint data respectively. The proposed IMU method accurately estimated the constant v_m, but significantly underestimated the time constant τ, which may explain some of the error in the velocity estimates early in the sprint. The position graph shows this resulted in a slight overestimation of t_{40} for the IMU method (average t_{40} photocell: 5.80 s, average t_{40} IMU: 5.94 s).

Discussion

This paper describes a novel filtering algorithm to estimate sprint velocity during a 40 m sprint using data from only a single IMU. The algorithm makes corrections by forcing known constraints characteristic of sprint running on the IMU estimate. These constraints were (I.) the heading of the sprinter must be mean zero during the sprint (aligned with the track) and (II.) the velocity-time characteristics of the sprint should resemble that of eq. (4.2). The Bland-Altman plots show a small bias from the IMU estimates for the average interval and maximal sprint velocity estimates (between -0.23 m/s and 0.13 m/s). The velocity estimates from the IMU

method were more consistent during the first 20 m compared to estimates later in the sprint (more narrow LOA), but had a slightly greater bias. The relative error and RMSE slightly increased later in the sprint with the greatest error being in the maximal velocity estimate (7.13% and RMSE = 0.67 m/s). This error was similar to the RMSE of the instantaneous sprint velocity estimate (RMSE = 0.70 m/s). Previous studies using lasers to measure sprint velocity suggest the actual instantaneous velocity of a sprinter is sinusoidal in nature (due to the braking forces at foot contact) [50, 54]. This was also seen in the IMU estimates (Figure 4.9), but it is not, however, expressed in the model of eq. (4.2). This may explain some of the error in the instantaneous velocity estimate, but it is unknown to what extent. This would not at first be expected to have as much of an effect on the estimated maximal step velocity. This is because the sinusoidal nature would be cancelled after averaging over the interval between subsequent foot contacts. However, error in the estimate of the foot contacts may have resulted in an inaccurate averaging window that included velocity data above or below the actual mean, which may explain some of the error in the maximal step velocity estimate.

Modeled data generated from estimates earlier in the sprint provided updates to raw estimates later in the sprint. Thus, one may expect there to be a relationship between errors in the estimate early in the sprint (0 m – 10 m) compared with those from later (30 m – 40 m). However, a post-hoc analysis showed no such relationship (r = 0.08). In theory, if the raw estimate from the IMU very closely resembles that from eq. (4.2), but with a consistent bias, the algorithm has no way of detecting the error. It relies on the divergence of the raw estimate from the expected model to make corrections. This hypothesis was not tested directly, but may be suggested by the strong correlations and narrow range of relative errors (5 –7%). The strong

relationships suggest the proposed IMU method may be able to discern the sprint velocity capabilities equally as well as the reference method.

Ultimately, the best estimate of sprint velocity using the proposed IMU method would be when the filtered IMU velocity and photocell position-time data yield the exact same modeled velocity-time curve. This is equivalent to determining the same constants v_m and τ in eq. (4.2). Therefore, a post-hoc comparison was performed comparing these constants characterizing the sprints of each subject determined by both methods. The results suggest inaccurate estimates of the time constant τ may have contributed more than the constant v_m to the error in the estimated velocity. The IMU estimate of v_m (8.32 ± 1.15 m/s) was nearly exactly the same as the reference measurement (8.32 ± 1.05 m/s). However, the τ estimate from the IMU method (1.09 ± 0.21 s) was significantly greater ($p < 0.01$) than the reference estimate (0.93 ± 0.13 s). This can be seen in the resulting model velocity-time curves and distance-time curves given these constants (Figure 4.10). This graphic comparison and the results from the Bland-Altman analysis (Table 4.3) seem to suggest consistent underestimates early in the sprint may have resulted in greater estimates of the model time constant τ. It is unclear what led to these underestimates. One potential explanation is that low pass filtering the raw velocity signal removed greater velocities early in the sprint and resulted in a bias towards a lesser velocity. The raw velocity was low pass filtered in an attempt to remove the natural sinusoidal nature of the true velocity when generating model curves. Without low-pass filtering, velocities later in the sprint would have been associated with greater error in the curve fitting. This would suggest a velocity-time curve markedly different from the *a priori* expectation described in eq. (4.2) and lessen the contribution of these estimates to the final velocity prediction according to eq. (4.6). Future research should focus on developing techniques to compensate for this error. Another potential

explanation is that there was error in the reference estimates before 10 m. The average 10 m time for this subject sample was 2.02 s before which there was no position-time data that may provide a better velocity estimate before 10 m. The position-time splits chosen in this study were in accordance with previously published study designs [14], but perhaps incorporating split times before 10 m would enable the testing of this potential source of error in future research.

To the author's knowledge, the study by [27] is the only other to present results assessing the validity of sprint velocity estimates (average interval velocity and peak velocity) from a sacral worn IMU. They, however, used data from a 100 m sprint and a much smaller sample size (five male sprinters). The authors state the use of propriety algorithms and other constraints applied to correct the estimate, however the details were not given. The results from our study are comparable with those from [27] with both showing strong relationships (≥ 0.75) between IMU estimates and reference measurements for both average interval and maximal sprint velocity (with the exception of the 0 m – 10 m split from their study where $r = 0.32$).

The corrections provided to the initial raw velocity estimates were based on modeled data from eq. (4.2). Therefore, the limitations of the model are also limitations for the method described here. Namely, the sprint must be performed in a non-fatigued state and must occur in a straight line. Thus, for example, the technique may not be used to assess the sprint velocity through the curve of the track because the average heading of the runner is not zero in this case. Also, it is possible that the IMU attitude estimate obtained from direct integration was subject to drift error. No corrections were made on the attitude estimate because it cannot be assumed to be mean zero like the heading estimate. Errors in the attitude estimate may result in an insufficient rotation of the sensor referenced acceleration vector such that after integration the velocity estimate is under or overestimated. However, the fusion of previous model data with raw data

later in the sprint could compensate for this error. An example where this may have occurred is shown in Figure 4.9b where the raw velocity from direct integration was noticeably underestimated. The error was detected, however, by the filtering algorithm and likewise corrected while still maintaining the sinusoidal waveform. Finally, this method has not been tested for use in sprints longer than 40 m. For longer sprints, beyond the acceleration phase, eq. (4.2) may be an inappropriate model because there is no expression for any potential decrease in sprint velocity that may occur later in the sprint. An alternate model to eq. (4.2) that is bi-exponential, has been proposed that could potentially account for this possible decrease [48]. Future research should investigate the use of this model, or a modified version incorporating the bi-exponential model, to estimate sprint velocity for longer sprint distances.

Conclusion

Wearable sensors are becoming increasingly popular for field-based performance assessments. The sprint velocity estimation method described in this paper broadens the scope of IMU applications in this context. The results from the Bland-Altman analysis, low relative errors, low RMSE, and strong correlations suggest the validity of the proposed IMU method. Post-hoc analyses suggest potential sources of the errors that may be targeted in future research. The error in the estimation of instantaneous velocity is likely due to the sinusoidal nature of true sprinting velocity that is not expressed in the reference method. Further, the small errors did not prevent the method from differentiating sprint velocity capabilities of sprinters and non-sprinters equally as well as the reference method. Other reference information that does not diminish the convenience aspect of the proposed method (e.g., onboard GPS for outdoor use) may be included to further improve the measurement and eliminate some of the limitations in this study. This should be the focus of future research.

Chapter 5: Concurrent Validity of an IMU-based Method to Estimate Kinetic Determinants of Sprint Performance

Abstract

Inertial measurement units (IMUs) are becoming more popular in field-based human movement analysis, however, an IMU-based system to measure specific sprint-related kinetic parameters has not been reported. The purpose of this study was to determine the validity of a novel IMU-based system to estimate these kinetic parameters by comparison to a recently validated photocell method. Twenty-eight subjects (sprinters and non-sprinters) performed three 40 m sprints with a single IMU attached to their sacral region. Position-time data along with subject anthropometrics and atmospheric data (temperature and barometric pressure) was used to estimate the magnitude and orientation of the ground reaction force ($\boldsymbol{F}$) and velocity (v). The proposed IMU method uses an estimate of the IMU's orientation to express sensor referenced acceleration in the track frame to then estimate $\boldsymbol{F}$ and v. Sprint performance variables of each subject's best sprint were compared between the two methods using root mean square error (RMSE), Pearson's product moment correlation coefficient (r), and Bland-Altman analysis. The IMU method gave valid estimates of directional $\boldsymbol{F}$ and power measures most relevant to performance compared to the photocell method supported by relatively low RMSE and bias and significant correlations ($p < 0.01$). The IMU estimate of the next best predictors of performance showed significant correlations ($r = 0.78$ - 0.79, $p < 0.01$) with photocell estimates. Inaccurate estimates were observed only for those variables that were least related to performance. The proposed method, which requires a single IMU, may be considered an appropriate means to estimate the sprint performance variables that are most important to an evaluation. Future research should investigate the incorporation of other parameters to improve the scope of the assessment and some of the observed error.

Introduction

Recent research in sprinting biomechanics has identified several kinetic parameters to be key determinants of sprint acceleration performance [2, 138]. Newtonian mechanics lead to an expectation that the forward component (F_x) of the ground reaction force ($\boldsymbol{F}$) underlies the primary mechanism by which one accelerates their center of mass (COM) forward during a sprint. This theory has been supported empirically from sprint data of a broad range of performance capabilities (elite sprinters to untrained subjects) [2, 3, 5, 6, 8, 9]. In several of these studies the percentage of $\boldsymbol{F}$ that is comprised of F_x, called the ratio of force (RF), has been used as an index of one's technical ability to optimally orient $\boldsymbol{F}$ to maximize F_x. An evaluation of acceleration performance must also consider how these technical parameters change with increasing velocity (v). Due to the force-velocity property of muscle [13, 139] and lesser foot contact times [2, 33], F_x and RF would be expected to decrease with increasing sprint velocity. This negative force-velocity trend in sprinting is well described by a linear relationship [2, 14, 47] and the slope of this line (sFV for F_x-v and dRF for RF-v relationships) has been used to assess sprint performance and ballistic tasks in general [2, 3, 5, 140]. Another parameter highlighting force-velocity capabilities during sprinting is average and maximal forward power ($\bar{P}_x$ and P_{max} respectively) which has also been shown to be a determinant in sprint performance [2, 3, 141].

These kinetic parameters are traditionally measured using a force plate. To assess a sprint with in ground force plates one would either have to line the entire sprint distance with force plates or perform multiple sprints such that each sprint measures a different foot contact or set of foot contacts; the combination of which provides a virtual single sprint [2, 11, 14, 138]. These methods are not the most appropriate in non-research settings because of the high cost of

the equipment and because the method is tedious and time consuming. Instrumented treadmills may also be used [47], but they too are expensive and may alter acceleration mechanics compared to that over ground [43].

In 2015, Samozino et al. [14] validated a simple method (requires one 40 m sprint in field conditions) to estimate kinetic determinants of sprint acceleration performance. The technology required to perform the assessment is much more affordable relative to the aforementioned methodologies. Their method only needs accurate and sufficient position-time or velocity-time data which they obtained using photocells and radar respectively. More recently in [15], smartphone video data was shown to be able to accurately estimate position-time information that may be used in the method proposed by Samozino et al. The method uses a macroscopic model of the sprinter's COM kinematics during the sprint derived by Furusawa et al. in 1927 [13]. The photocell method proposed by Samozino et al. fits position-time data to ultimately estimate net forward acceleration of the COM. Using Newton's 2nd Law and environmental information, the propulsive forward force can be estimated. Kinetic estimates from the method showed good agreement with the same from a force plate suggesting its validity. Although this method has shown promise since its validation [57, 58], it is limited in its ability to provide a comprehensive assessment due to its macroscopic nature. In the original validation study, Samozino et al. report the step-by-step comparison of the estimates of $\boldsymbol{F}$ showed the force plate values are scattered about the values predicted by the model. They attribute this error to inter-step variability that may be present due to a bilateral asymmetry or inter-sprint variability. Further, other parameters important to sprint performance cannot be determined using the photocell method. These other parameters include, for example, step frequency [3], joint angles [35], and the braking force at foot contact [142].

Inertial measurement units (IMUs) may provide the means to develop a more comprehensive sprint assessment system. IMUs are small, low-cost sensors that allow unrestricted field-based performance assessments. IMUs house onboard three-axis accelerometers, gyroscopes, and magnetometers, the combination of which has allowed several different applications in biomechanics research such as joint kinematics [20, 22], identification of foot contact events [24, 26], as well as kinetic parameters during running and jumping [17, 31]. Three-dimensional estimates of $\boldsymbol{F}$ are possible with an array of IMUs attached at each segment by traditional inverse dynamics [143]. However, an elaborate array of sensors begins to make the method less applicable to non-research settings due to cost and greater set-up time. In Chapter 3, it was shown that despite several limitations it might be possible to use a single IMU to estimate step-average directional and resultant $\boldsymbol{F}$ during a linear sprint start. More important to sprint assessment applications was the finding that the IMU method gave valid estimates of the orientation of $\boldsymbol{F}$ and specifically RF. Likewise, Chapter 4 described the possibility of using a single IMU to estimate sprint velocity using an adaptive gain filter implementing the velocity model described by Furusawa et al. [13]. With estimates of $\boldsymbol{F}$ and velocity, one may potentially be able to estimate those parameters that are most important to assess sprint acceleration performance. These methods require a single IMU strapped to the lower back and thus provide an attractive methodology to users in field-based settings for the purpose of research and/or sport. However, the validity of an IMU based methodology to assess sprint performance is unknown. Thus, the purpose of this study was to investigate the use of a single IMU strapped to the lower back to assess sprint acceleration performance. Sprint performance variables from the proposed IMU method were compared to those derived from the aforementioned photocell method.

Methods

Subjects

Subjects were recruited from both a collegiate level track team (male and female sprinters) and the general student population and were included in the study if they were between the ages of 18 and 35 years old, reported no musculoskeletal injuries within the six months prior to testing, and could perform maximal effort 40 m sprints pain free. Twenty-eight subjects (12 female, 16 male) volunteered to participate. The Appalachian State University Institutional Review Board approved this study and all subjects gave written consent to participate.

Experimental Protocol

The experimental protocol used to validate the proposed method was designed similar to that described by Samozino et al. (2015) [14]. In their study, they validated the photocell method by comparison to a force plate. Here, the force plate method is replaced with the proposed IMU method. Five pairs of photocells were set up to collect position-time data at 10 m, 15 m, 20 m, 30 m, and 40 m splits during a maximal effort sprint. Subjects performed three sprints with a minimum of three minutes rest between subsequent sprints or until they felt fully recovered. Prior to any maximal effort movements, subjects were taken through a standardized general and sprint specific warm-up. The warm-up ended with 10 m sprint starts from the four-point stance they would be using during testing. An IMU was attached to the sacral region (i.e., the point of intersection of the spine with the intercristal line) using an elastic strap and tape. The intercristal line connects the left and right posterior superior iliac spines and was found via palpation [118]. Before taking their sprint start stance, subjects performed two jumps with a five-second standing static trial in between. The jumps were necessary to accurately determine

the start and end of the static trial which was used during data post-processing to determine initial IMU orientation.

Instruments

The IMUs used in this study were Yost Data Logger 3-Space Sensors (YEI Technology, Portsmouth, OH). These units have an onboard three-axis accelerometer (range: ±24 g, noise density: 650µg/$Hz^{1/2}$, 12-bit resolution), three-axis gyroscope (range: ±2000º/s, noise density: 0.009º/s/$Hz^{1/2}$, 16-bit resolution), and three-axis magnetometer (range: ±1.3 Ga, 12-bit resolution). Sampled data (445.72 ± 0.55 Hz) were stored as separate files to an on board memory and were downloaded to a computer via USB after data collection for post-processing. Position-time data during the sprint were obtained using photocells (Brower Timing Systems, Draper, UT). The photocell timer was initiated at the instant the sprinter's hand lifted off a pressure sensor located at the sprint start line. A high-speed video camera (Sensor Technologies America, Carrollton, TX) recorded the sprint start at 200 fps using the MaxTRAQ software (Innovision Systems, Columbiaville, MI). The camera was positioned behind the runner such that the hand on the pressure sensor and the IMU attached to the subject's lower back were clearly visible in the camera's field of view. The times associated with the lift of the hand off the pressure sensor and the first movement of the IMU at the start of the sprint were used to time-synchronize the photocell and IMU data (see Chapter 4). Environmental temperature and barometric pressure were measured using the Vantage Vue weather console (Davis Instruments Corporation, Hayward, CA) which were necessary to estimate the drag force (see *Data Analysis*).

Data Reduction

To compare IMU based results with the reference photocell method position-time data obtained using the photocells were fit to the model proposed by Furasawa et al (1927), where:

$$p = v_m\left(t + \tau e^{-\frac{t}{\tau}}\right) - v_m\tau \tag{5.1}$$

$$v = v_m\left(1 - e^{-\frac{t}{\tau}}\right) \tag{5.2}$$

$$a = \left(\frac{v_m}{\tau}\right)e^{-\frac{t}{\tau}} \tag{5.3}$$

In eqs. (5.1) – (5.3), the position (p), velocity (v), and acceleration (a) are related to the time after the start of the sprint (t) according to the two constants v_m and τ. The photocell method proposed by Samozino et al. fits position-time data to eq. (5.1) to estimate v_m and τ from which the net forward acceleration of the COM is given from eq. (5.3). Then, the net forward force ($F_{N,x}$) is given by the subject's mass (m) and the net forward acceleration a from eq. (5.3) according to Newton's 2nd Law:

$$F_{N,x} = ma \tag{5.4}$$

This net force is the sum of F_x and the drag force (F_D) where:

$$F_{N,x} = F_x + F_D \tag{5.5}$$

and:

$$F_D = -CA\rho(v - v_{air})^2 \tag{5.6}$$

In eq. (5.6), $C = 0.9$ is the coefficient of drag (values vary between 0.8 and 1.0 in wind tunnel experiments so the average is used [42]), A is an estimate of the runner's frontal area, ρ is the air density, and v_{air} is the wind velocity relative to the ground [14]. The frontal area A is estimated given the runner's height (h) in meters and m in kilograms according to,

$$A = (0.2025h^{0.725}m^{0.425})0.266 \tag{5.7}$$

and the air density ρ is given from the barometric pressure (P) in Torr, the temperature (T) in ℃, and the air density ρ at 760 Torr and 273℃ (ρ_0 = 1.293 kg/m) according to:

$$\rho = \rho_0 \left(\frac{P}{760}\right)\left(\frac{273}{273+T}\right) \tag{5.8}$$

Using this method, F_x and v can be estimated. Further, F_z (vertical component) and F_{res} (resultant force) is estimated by assuming F_z to be equal to bodyweight over a complete step interval. From this, ratio of force (RF) can be calculated as:

$$RF = \frac{F_x}{\sqrt{F_x^2 + F_z^2}} \cdot 100 \tag{5.9}$$

In eq. (5.9) the denominator approximates the resultant magnitude F_{res} where the lateral component is considered negligible [2, 14].

An IMU estimate of velocity could also predict the constants v_m and τ which allow an estimate of $\boldsymbol{F}$ in the same way as the photocell method. However, in this study, $\boldsymbol{F}$ was estimated according to the method described in Chapter 3 to avoid the shortcomings of using a macroscopic model. That is, it is assumed that the location of the IMU at the sacral region provides a sufficient approximation of the COM location during the sprint. Then, the accelerometer measurement of the acceleration vector represents the net acceleration of the COM in the sensor frame. The orientation of the IMU during the sprint is obtained initially during stance using the accelerometer and magnetometer and then by integrating the angular rate measured by the gyroscope during the sprint (see Chapters 3 and 4). An estimate of the orientation then allows the sensor referenced COM acceleration vector to be rotated and expressed in terms of the track frame. Sensor estimates obtained over time are subject to drift error and noise, especially during a very dynamic task like sprinting. Thus, acceleration is time-integrated to get a raw estimate of velocity which is then filtered according to the method

described in Chapter 4. The filtered velocity is then differentiated to provide a better estimate of the net forward COM acceleration. At this point, the IMU provides an estimate of v from the filtering algorithm (Figure 5.1) and also $\boldsymbol{F}$ according to eqs. (5.4) – (5.8).

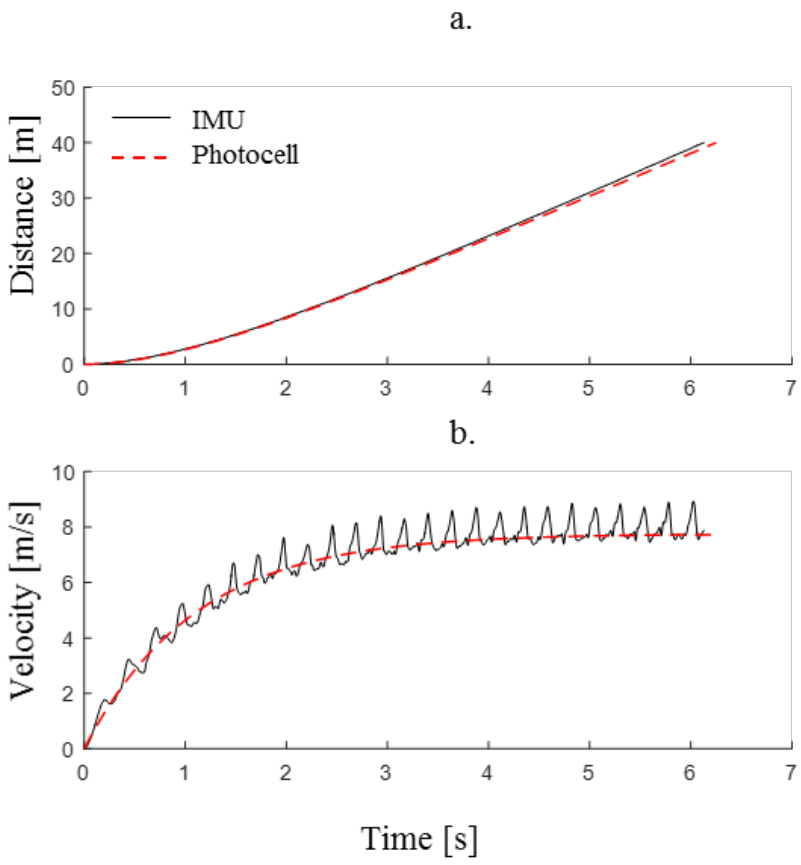

Figure 5.1: Comparison of position-time (a.) and velocity-time (b.) estimates from the IMU method (solid black line) and reference photocell method (dashed red line) for a typical subject.

Performance Variables

Foot contact events are determined using the antero-posterior acceleration trace according to the method described by Wixted et al. [26]. Then, photocell and IMU estimates of F_x, F_z, and v are averaged over each step (i.e., one foot contact to the next) [14]. Forward power (P_x) at each step is given by the product of step averaged F_x and v. RF is given according to eq. (5.9)

and the slope of the linear relationship between RF and step averaged v provides an estimate of dRF. The denominator in eq. (5.9) provides an estimate of F_{res} where the lateral component of $\boldsymbol{F}$ is assumed negligible [14]. The slope of the linear F_x and v relationship determines sFV and extrapolation of this line to the intercepts of the *x* and *y* axis provides an estimate of the theoretical maximal forward force (F_0) and velocity (v_0) respectively. Average values of F_x, F_{res}, RF, and P_x over the whole sprint ($\bar{F}_x$, $\bar{F}_{res}$, $\overline{RF}$, and $\bar{P}_x$ respectively) were determined as well as the maximal forward power output (P_{max}). The latter was taken to be the peak of the second order polynomial obtained using the quadratic relationship between the step averaged P_x and v values [2, 14].

Statistical Analysis

Data from each subject's best sprint (fastest 40 m time) were compared between methods. Per step variables (F_x, F_z, F_{res}, and RF) were compared between methods using root mean square error (RMSE), Pearson's product moment correlation coefficient (*r*), and Bland Altman 95% limits of agreement (LOA) for repeated measures [144]. Variables that describe the entire sprint ($\bar{F}_x$, $\bar{F}_{res}$, $\overline{RF}$, $\bar{P}_x$, P_{max}, F_0, v_0, sFV, and dRF) were compared between methods using RMSE, *r*, and LOA. Correlation coefficients were used to determine the strength of the relationship between performance variables and sprint performance (i.e., 40 m time: t_{40}) using estimates from the reference photocell method. Further, because there was an equal number (n = 8) of male sprinters (S) and non-sprinters (NS), a two-sample, independent t-test was used to determine any differences between the performance variables of each group for both methods. For the Bland-Altman analysis, data were transformed using the natural logarithm where differences were not normally distributed (determined by the Shapiro-Wilk test) or where a strong relationship ($r \geq 0.75$) was observed between the differences and means of the

measurements [121]. In these cases, the anti-log bias and LOA are given. The bias was considered significant ($p \leq 0.05$) if the line of identity lie outside the 95% confidence interval of the mean bias [121]. The clinical significance of correlation coefficients were determined *a priori* according to the following criteria: 0.00 to 0.25 (little to none), 0.25 to 0.50 (fair), 0.50 to 0.75 (moderate), and > 0.75 (strong) [120]. A level of significance was set *a priori* at 0.05 for all statistical tests.

Results

Subject anthropometrics and split times are shown in Table 5.1. The repeated measures Bland-Altman analysis show the bias in the IMU estimate of per step variables F_x, F_z, F_{res}, and RF were 6.13 N, -2.74 N, -4.29 N, and 1.14%, respectively. The LOA, reported by (lower limit, upper limit) were the following: F_x (-145.93 N, 158.56 N), F_z (-231.12 N, 225.63 N), F_{res} (-247.56 N, 238.98 N), and RF (-13.34%, 15.62%). IMU estimates were significantly ($p < 0.01$) correlated ($r = 0.70$ to 0.91) with photocell estimates of all per step variables and RMSE was 7.4% for per step RF and RMSE was between 79.52 N to 124.2 N for per step $\boldsymbol{F}$ (Figure 5.2). Significant correlations ($p < 0.05$) were found between all performance variables and sprint performance (i.e., t_{40}) except for sFV and dRF (Table 5.2 and Figure 5.3). IMU and photocell estimates were significantly ($p < 0.01$) correlated ($r = 0.71$ to 0.89) for all performance variables except dRF (Table 5.2). The Bland-Altman analysis showed low, insignificant bias and narrow LOA for $\overline{RF}$, $\bar{F}_x$, $\bar{P}_x$, and v_0, but not $\bar{F}_{res}$, P_{max}, F_0, sFV, or dRF (Table 5.2). Both methods found $\overline{RF}$, $\bar{F}_x$, $\bar{F}_{res}$, $\bar{P}_x$, P_{max}, and v_0 to be significantly different ($p < 0.01$) between male sprinters and non-sprinters (Table 5.3). Figure 5.4 shows the compares IMU and photocell estimates of the various performance characteristics throughout the 40 m sprinting task.

Table 5.1: Subject anthropometric characteristics and 40 m split times. ***Denotes a significant difference between Male S and Male NS at the 0.01 level.*

	Female (n = 12)	Male (n = 16)	Male S (n = 8)	Male NS (n = 8)
Age [yrs]	20.33 ± 2.15	21.38 ± 2.45	19.63 ± 1.60**	23.13 ± 1.81
Height [m]	1.67 ± 0.08	1.78 ± 0.06	1.76 ± 0.06	1.80 ± 0.07
Mass [kg]	61.06 ± 5.87	78.64 ± 8.84	76.44 ± 5.80	80.84 ±11.08
t_{10} [s]	2.11 ± 0.12	1.95 ± 0.16	1.83 ± 0.06**	2.07 ± 0.14
t_{15} [s]	2.84 ± 0.18	2.62 ± 0.24	2.42 ± 0.05**	2.81 ± 0.18
t_{20} [s]	3.53 ± 0.22	3.23 ± 0.30	2.97 ± 0.05**	3.48 ± 0.22
t_{30} [s]	4.83 ± 0.35	4.38 ± 0.42	4.04 ± 0.06**	4.71 ± 0.33
t_{40} [s]	6.14 ± 0.50	5.56 ± 0.58	5.07 ± 0.07**	6.05 ± 0.42

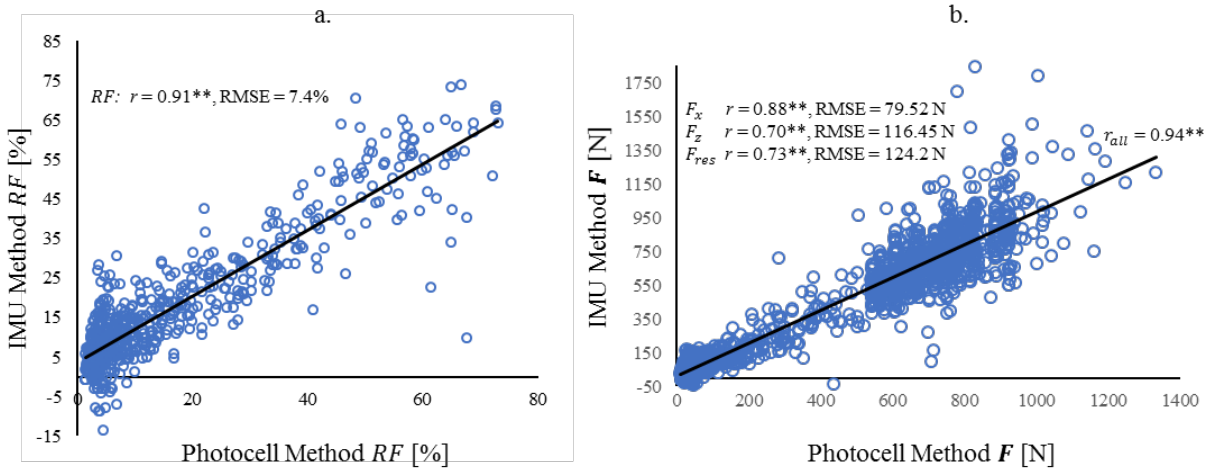

Figure 5.2: Comparison of per step estimates of directional ***F*** and *RF* between the IMU and photocell methods: (a.) *RF* and (b.) ***F***. ***Denotes a significant relationship at the 0.01 level.*

Table 5.2: Comparison of performance variables estimated by the IMU and photocell method.

	IMU	Photocell					
	Mean ± SD	Mean ± SD	t_{40} r	Bias	LOA	RMSE	r *(IMU vs. Photo)*
$\overline{RF}$ [%]	16.29 ± 3.26	15.72 ± 3.07	-0.93**	0.57	-2.62, 3.77	1.70	0.87**
$\bar{F}_x$ [BW]	0.18 ± 0.04	0.18 ± 0.04	-0.93**	0.00	0.03, 0.04	0.02	0.89**
$\bar{F}_{res}$ [BW]	1.03 ± 0.02	1.04 ± 0.01	-0.87**	-0.01(**0.99**)*	**0.97, 1.02**	0.02	0.79**
$\bar{P}_x$ [W/kg]	7.68 ± 2.68	7.88 ± 2.63	-0.95**	-0.20	-2.95, 2.55	1.39	0.86**
P_{max} [W/kg]	14.18 ± 3.35	19.32 ± 4.99	-0.91**	-5.14*	-11.41, 1.13	6.02	0.78**
F_0 [N]	562.2 ± 172.7	652.2 ± 189.1	-0.59**	-90.0*	-315.8, 135.8	144.6	0.80**
v_0 [m/s]	8.75 ± 1.34	8.56 ± 1.11	-0.97**	0.19	-1.61, 1.99	0.92	0.73**
sFV [N/m/s]	-65.2 ± 21.90	-76.22 ± 21.06	0.12	11.01*	-21.15, 43.17	19.51	0.71**
dRF [%/m/s]	-7.85 ± 1.96	-9.49 ± 1.41	-0.32	1.64*	-2.36, 5.65	2.59	0.30

*,**Denotes significance at the 0.05 and 0.01 level respectively.* **Bold lettering denotes antilog of natural logarithm transformed data due to non-normality.** , t_{40} *r*: relationship between each variable and performance (40 m time), LOA: Bland-Altman 95% limits of agreement, RMSE: root mean square error of IMU estimate, *r*: Pearson product moment correlation between IMU and photocell estimate of each variable.

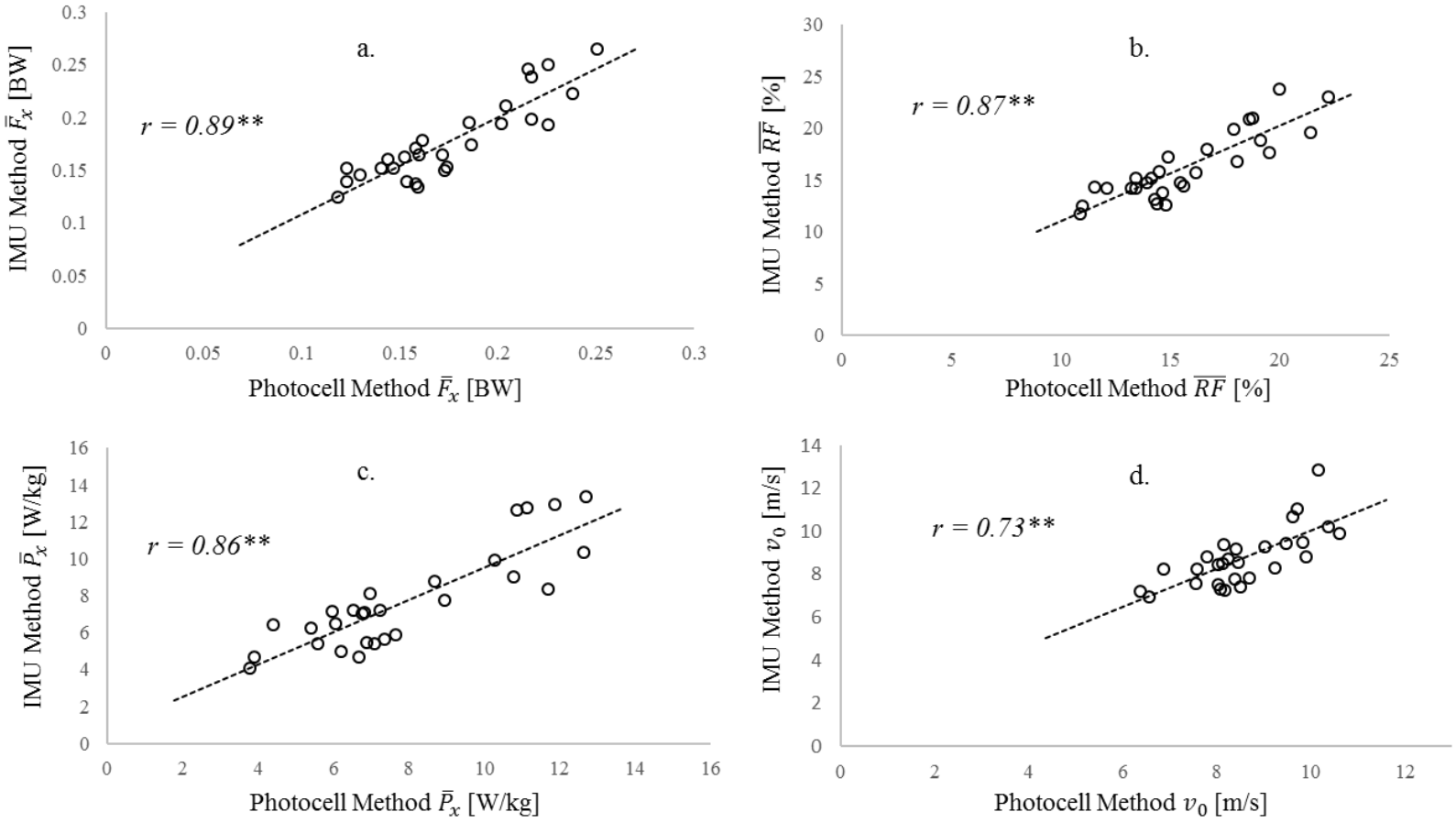

Figure 5.3: Relationships between IMU and photocell estimates of the four variables that showed the best relationships with performance (i.e., 40 m time): (a.) $\bar{F}_x$, (b.) $\overline{RF}$, (c.) $\bar{P}_x$, and (d.) v_0. ***Denotes significance at the 0.01 level.*

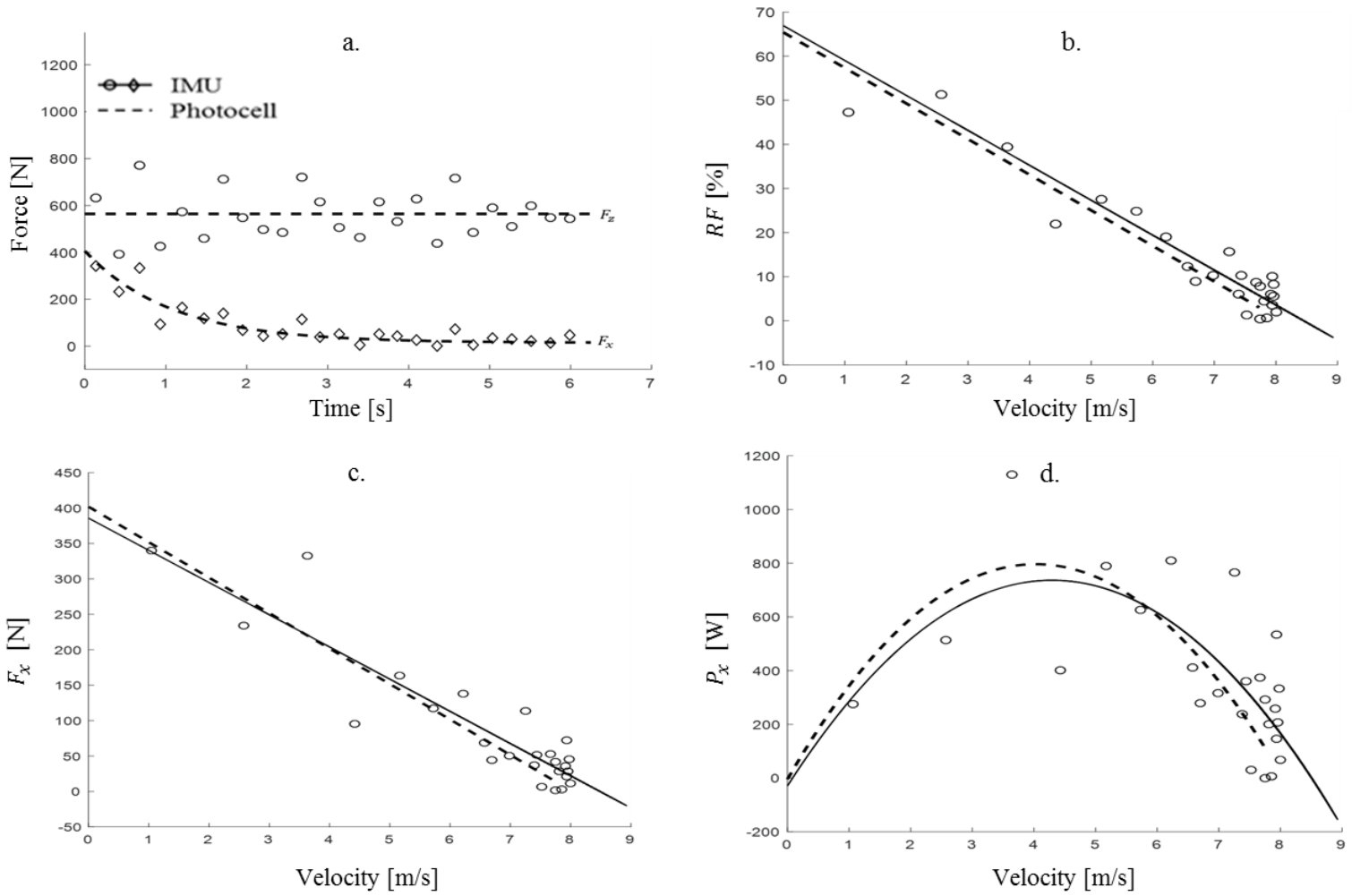

Figure 5.4: Comparison of estimated force-time, force-velocity, RF-velocity, and power-velocity made by the IMU method (individual data points) and photocell method (dashed line) for a typical subject: (a.) F_x- t and F_v - t, (b.) RF-v and dRF, (c.) F_x- v and sFV, and (d.) P_x- v. Solid line indicates best fit to performance variable of interest

Discussion

The results from this study suggest the proposed IMU method can accurately estimate those performance variables that were most important to determining sprint performance. The IMU estimates showed a systematic bias for five of the nine performance variables. However, those four for which it did consistently provide an accurate estimate ($\overline{RF}$, $\bar{F}_x$, $\bar{P}_x$, and v_0), were the most relevant to differentiating sprint performance (i.e., given the relationship with t_{40} determined by the reference method). In addition to an insignificant bias, the validity of the IMU estimate for these four variables is further supported by narrow LOA, low RMSE, and significant correlation coefficients (Table 5.2 and Figure 5.3). Of the other five performance variables, only $\bar{F}_{res}$ and P_{max} showed strong relationships with sprint performance. Even though the proposed IMU method showed a systematic bias in the estimate of these two variables, they did show strong, significant relationships ($p < 0.01$, $r = 0.79$ and 0.78 respectively) with estimates from the photocell method. This suggests the proposed method may be able to detect changes in these parameters between sprints or subjects equally as well as the reference method. The other three variables were F_0, sFV, and dRF. Our results suggest these were the least relevant to evaluating sprint performance. First, they were the only variables whose correlation with t_{40} was less than $r = 0.70$. Second, the S and NS groups were significantly different ($p < 0.05$) only for the other six variables, but not F_0, sFV, and dRF. The significant difference between groups was found given estimates of performance variables from both methods. This suggests the IMU method can differentiate performance between sprinters and non-sprinters equally as well as the photocell method. Of these three variables, the best predictor of sprint performance was F_0 (relationship with t_{40}: $r = -0.59$) of which the IMU estimate showed a strong, significant relationship with the photocell estimate ($r = 0.80$, $p < 0.01$). The other two (sFV and dRF)

showed at the most fair and insignificant relationships with t_{40} (r = 0.12 and r = -0.32 respectively).

Our finding that $\overline{RF}$, $\bar{F}_x$, and $\bar{P}_x$ are the most relevant kinetic parameters in differentiating sprint performance is also supported by the results reported by Rabita et al. (2015) [2]. They assessed differences in elite and sub-elite sprinters using the same (and more) sprint performance variables as those used in this study with the exception of sFV. Also in accordance with our findings was that dRF was not very effective in differentiating sprint performance. In their study, the effect size of the difference between the dRF capabilities of elite and sub-elite sprinters was the fifth lowest out of fourteen kinetic parameters assessed and the correlations to sprint performance were insignificant. The differences in v_0 between the elite and sub-elite sprinters had an even lower effect size than dRF, which is contrary to the findings of our study. This may be due to the differences in the populations being compared. The split times of our collegiate level male sprinter group suggest they are somewhere between the elite and sub-elite sprinters they tested, but closer to the elite. It may be the case that v_0 is too similar between skilled sprinters in general and that other measures are necessary to distinguish performance at these higher levels. In contrast, it may be argued that the superior sprint capabilities of skilled sprinters would be expected to result in them having higher v_0 compared to non-sprinters; a conclusion supported by our data. Although the effect sizes of v_0 were negligible comparing the elite and sub-elite sprinters in the study by Rabita et al., it was significantly correlated to sprint performance which is in agreement with the results from this study. Similar findings were found in the study by Morin et al. (2012) where v_0 showed strong relationships with sprint performance given a subject sample of much more varied levels of sprint ability [3].

In addition to Rabita et al. [2], other studies suggest similar conclusions concerning the importance of $\overline{RF}$, $\bar{F}_x$, and $\bar{P}_x$ in discerning sprint acceleration performance [3, 5]. However, contrary to our data and that of Rabita et al., others have found dRF to be a strong predictor of performance [3, 5]. This could be due to differences in how sprint performance was quantified. Our index was t_{40} whereas the authors in [3, 5] used maximal speed, mean speed, and four-second distance during a 100 m sprint. An argument can be made for the expectation that a less negative dRF would characterize better sprinters. As sprint velocity increases, the backward velocity of the stance leg before foot contact would need to also increase in order to prevent unwanted negative braking forces [8]. This would suggest faster shortening velocities of the leg musculature. Consequently, the force generating capabilities would be expected to be diminished due to the force-velocity property of muscle [13, 139]. With lesser ability to generate force, the direction of $\boldsymbol{F}$ must be directed more vertically such that the observed decrement does not result in an insufficient vertical impulse (and therefore flight time) necessary to optimally reposition the leg for the next foot contact [8]. In addition to the decrement due to the force-velocity property of muscle, this vertical impulse may also be diminished because of a lesser contact time at increasing velocities [2, 145, 146]. For these reasons, dRF (and sFV for that matter) would be expected to be appropriate indices of sprint performance. In theory, they indicate the maintenance of optimal technique as sprint velocity increases. It is unclear why neither the photocell method nor the IMU method did not show significant differences between the S and NS groups for these variables. It is worth noting, however, that the difference in dRF between the S and NS groups was more noticeable given the estimates from the IMU method (26% greater in S compared to NS) compared to the photocell method (only 8% greater in S compared to NS) and the difference approached significance in the IMU estimate (p = 0.057),

but not in the photocell method (p = 0.304). The same was true for sFV where the differences between S and NS groups were more noticeable in the IMU estimates (24%) compared to the reference photocell method (8%).

Step by step estimates of RF, F_x, F_z, and F_{res} made by the IMU showed moderate to strong and significant ($p < 0.01$) relationships with the reference photocell method (r = 0.91, r = 0.88, r = 0.70, and r = 0.73 respectively). Visual inspection of these relationships provides some insight into understanding potential sources of error. The photocell method of predicting $\boldsymbol{F}$ is dependent upon the prediction of COM acceleration in eq. (5.3). For all values of t in eq. (5.3), the acceleration is positive. Thus, due to its macroscopic nature, the model is incapable of detecting a negative braking force. For longer sprints well past the acceleration phase, a bi-exponential equation may be more appropriate for its ability to estimate decreasing velocity later in the sprint [48]. However, even in a 40 m sprint, it is possible that a single step could have a net negative value. Figures 5.2 and 5.4 show the IMU method did predict several of these instances. These values appear to occur near the end of the sprint where a negative braking force may be expected, especially in unskilled sprinters. A direct comparison to a force plate is necessary to delineate the true error in the IMU estimate for these values.

From Figure 5.4 it is evident that the IMU values appear scattered about the photocell estimate similar to what was observed for force plate values in the original validation study for the photocell method [14]. However, when comparing our IMU vs. photocell curves to the force plate vs. photocell curves provided by Samozino et al. [14], the scattering of IMU estimates appears more drastic. This may explain the finding of wide LOA in the IMU estimate of per step force values, but with a low bias. Samozino et al. [14] did not perform the Bland-Altman analysis on per step variables, but only for variables over the entire sprint. Thus, it is unknown

how these LOA compare to that which describe photocell estimates compared to the gold standard force plate. The scattering of IMU estimates about the true value is of less concern once the values are averaged over the entire sprint. This explains the finding of low bias for per step variables and most per sprint variables. Samozino et al. [14] suggest inter-step variability as a potential causal factor underlying the observed scattering of force values between subsequent steps. One drawback of the photocell method, therefore, is that it is not able to detect bilateral asymmetries. The IMU method likely can detect these differences, but the difference appears to be exaggerated. This may be due to an inaccurate determination of foot contacts. This would result in an inappropriate averaging window within which IMU estimates would then be either under or overestimated. If this is the case, a potential compensation for this observed error may be to average force estimates over two steps instead of one, but at the expense of the ability to detect inter-step differences. This should be the focus of future research.

The proposed IMU method to assess sprint performance is a combination of those described in Chapters 3 and 4. Those IMU-based methods provide estimates of 3-dimensional step averaged $\boldsymbol{F}$ and estimates of sprint velocity respectively. Each were subject to their own limitations and, therefore, also describe limitations inherent in the method proposed here. Namely, the IMU has no means to estimate limb movements relative to the point of IMU attachment at the sacral region. These limb displacements result in COM displacements which the IMU cannot immediately detect. However, averaging over the interval between subsequent foot contacts may overcome this problem. This then requires an accurate detection of foot contact events. Any inaccuracies in these estimates will result in an over or underestimate of the desired value. Also, the IMU is radially displaced from the true COM location. Thus, rotation of the body about an axis through the true COM manifests itself in the IMU frame as a linear

acceleration which will corrupt kinetic estimates. Finally, the velocity filtering algorithm described in Chapter 4 is only appropriate for sprints along a straight line less than or equal to 40 m and undertaken in a non-fatigued state.

Conclusion

Recent research efforts in sprint acceleration mechanics and the development of field-based assessment methodologies have made notable progress [138]. In fields other than specifically sprint acceleration ability, IMUs have also proven to be especially useful in both kinematic and kinetic analyses of human movement [18, 147]. Compared to other sprint assessment technologies, IMUs are small, low cost, do not affect the user's movement, do not restrict the movement to a specific area, and show the potential to provide a more comprehensive assessment. Chapter 3 suggests the criterion validity of RF and sagittal plane step-averaged $\boldsymbol{F}$ estimates in the sprint start from a single IMU. Chapter 4 suggests the validity of a novel filtering algorithm to estimate maximal, instantaneous, and average interval velocity also from a single IMU. This study built upon those two to show the validity of an IMU-based method to provide valid estimates of those kinetic parameters most important to sprint acceleration performance. Future research should focus on improving the scope of the assessment by including other parameters (e.g., step frequency, joint angles, etc.) as well as novel ways to improve IMU estimates of $\boldsymbol{F}$ and velocity during sprinting. Potential methods worth investigating involve using additional IMUs to estimate limb movement to improve $\boldsymbol{F}$ estimates, onboard GPS to improve velocity estimates outdoors and for longer sprints, and ways to compensate for the radial displacement of the IMU from the true COM location.

Chapter 6: Conclusion and Future Directions

Recent research efforts have improved IMU-based methodologies for use in biomechanics applications. These improvements allow unrestricted field-based performance assessments which could lead to their more frequent use by coaches and practitioners outside of traditional laboratory settings. The objective of this thesis was to investigate the use of IMUs to perform kinetic analyses of accelerative running tasks and specifically the acceleration phase of sprint running. Chapter 3 described an IMU-only method of estimating 3-dimensional ground reaction force and the comparison of those estimate to the gold standard force plate. Peak and instantaneous force estimates from the IMU method were inaccurate, but step-average, sagittal plane values during the linear standing sprint start task and the orientation of the vector were considered valid by comparison to the force plate. The finding that the IMU method accurately estimated the ratio of force was especially promising in the context of assessing sprint acceleration performance. Chapter 4 described a novel IMU-only based method of estimating sprint velocity. The method was validated against a photocell method for maximal velocity, average interval velocity, and instantaneous velocity. The estimates were characterized by significant correlations with photocell estimates and absolute percent difference less than 8%. Chapter 5 described an IMU-only based method of estimating sprint acceleration performance variables. The method builds on those described in Chapters 3 and 4 and was compared to a recently validated photocell method. The IMU method was shown to provide valid estimates of those sprint acceleration performance variables that were most important to sprint performance. Further, the IMU method differentiated sprinters from non-sprinters equally as well as the photocell method.

The methods described in all of these studies use a single IMU attached at the lower back. More accurate estimates may have been found if multiple IMUs or other external measurement systems were incorporated, however, in this study, a single IMU is used such that the method would be easy to use and low cost. In each study, potential error sources are described that may be used to direct future research. Ultimately, whoever finishes the race first is all that matters and thus, arguably the most important sprint acceleration performance variable is the final sprint time. The IMU method described in Chapter 4 overestimated the final sprint time by 0.14 s on average. This may be too large for a coach to be willing to remove the use of photocells or some other timing system. Combining an accurate timing system with the proposed IMU method to estimate the other kinetic performance variables may allow the coach to best determine the weaknesses of the athlete to then target in training. Of course, if a timing system is going to be used, one could simply use the photocell method and no IMU at all. On the other hand, fusion of IMU data and photocell data may provide an even more robust evaluation system. In this context, a single photocell or a simple handheld timer (resources a coach may likely already have) may be used to estimate final sprint time and then provide an external measurement to later correct the IMU estimate. An IMU-based method may also provide the means to perform a more comprehensive sprint assessment for its ability to potentially estimate other parameters important to sprint performance. For example, although not directly assessed in the study of Chapter 5, it was possible to estimate average step frequency using the IMU which was significantly correlated with t_{40} (r = -0.73) and also significantly different ($p < 0.05$) between the sprinters (step frequency: 4.58 ± 0.29 Hz) and non-sprinters (4.18 ± 0.31 Hz). IMUs may also be used to estimate joint angles such as trunk lean [22, 99] which has been shown to be a determinant of acceleration ability [9]. For example, although not directly assessed in Chapter

5, it was possible to estimate hip rotation angles and forward trunk lean during the sprint. The latter showed significant correlations with both RF (r = 0.90) and F_x (r = 0.89). Thus, one might expect the decreasing trend of RF with velocity to be related to trunk lean. Indeed, it was found that one could use the slope of the linear relationship between trunk lean and velocity (similar to dRF but with trunk lean instead of RF) as an index of the sprinter's ability to maintain forward trunk lean with increasing velocity. Results from a t-test suggest the sprinter group maintained a significantly ($p < 0.05$) less negative trend (-6.12 °/m/s) compared to the non-sprinter group (-7.85 °/m/s). The use of IMUs for these purposes should be the focus of future research as well as novel ways to improve IMU estimates of ground reaction force and velocity during sprinting.

References

[1] M. Spencer, D. Bishop, B. Dawson, and C. Goodman, “Physiological and metabolic responses of repeated-sprint activities,” *Sports Med.*, vol. 35, no. 12, pp. 1025–1044, 2005.

[2] G. Rabita *et al.*, “Sprint mechanics in world-class athletes: A new insight into the limits of human locomotion,” *Scand. J. Med. Sci. Sports*, vol. 25, no. 5, pp. 583–594, Oct. 2015.

[3] J.-B. Morin *et al*, “Mechanical determinants of 100-m sprint running performance,” *Eur. J. Appl. Physiol.*, vol. 112, no. 11, pp. 3921–3930, Nov. 2012.

[4] A. E. Chapman and G. E. Caldwell, “Kinetic limitations of maximal sprinting speed,” *J. Biomech.*, vol. 16, no. 1, pp. 79–83, 1983.

[5] J.-B. Morin *et al*, “Technical ability of force application as a determinant factor of sprint performance:,” *Med. Sci. Sports Exerc.*, vol. 43, no. 9, pp. 1680–1688, Sep. 2011.

[6] M. Otsuka *et al*, “Effect of expertise on 3D force application during the starting block phase and subsequent steps in sprint running,” *J. Appl. Biomech.*, vol. 30, no. 3, pp. 390–400, Jun. 2014.

[7] N. Kawamori *et al*, “Relationships between ground reaction impulse and sprint acceleration performance in team sport athletes,” *J. Strength Cond. Res. Natl. Strength Cond. Assoc.*, vol. 27, no. 3, pp. 568–573, Mar. 2013.

[8] J. P. Hunter *et al*, “Relationships between ground reaction force impulse and kinematics of sprint-running acceleration,” *J Appl Biomech*, vol. 21, no. 1, pp. 31–43, 2005.

[9] F. Kugler and L. Janshen, “Body position determines propulsive forces in accelerated running,” *J. Biomech.*, vol. 43, no. 2, pp. 343–348, Jan. 2010.

[10] R. G. Lockie *et al*, “Effects of sprint and plyometrics training on field sport acceleration technique,” *J. Strength Cond. Res. Natl. Strength Cond. Assoc.*, vol. 28, no. 7, pp. 1790–1801, Jul. 2014.

[11] G. A. Cavagna *et al*, “The mechanics of sprint running,” *J. Physiol.*, vol. 217, no. 3, pp. 709–721, 1971.

[12] J.-B. Morin *et al.*, “Sprint acceleration mechanics: The major role of hamstrings in horizontal force production,” *Front. Physiol.*, vol. 6, p. 404, 2015.

[13] K. Furusawa *et al*, “The dynamics of ‘sprint’ running,” *Proc. R. Soc. Lond. Ser. B Contain. Pap. Biol. Character*, vol. 102, no. 713, pp. 29–42, 1927.

[14] P. Samozino *et al.*, “A simple method for measuring power, force, velocity properties, and mechanical effectiveness in sprint running: Simple method to compute sprint mechanics,” *Scand. J. Med. Sci. Sports*, p. n/a-n/a, Jun. 2015.

[15] N. Romero-Franco *et al.*, “Sprint performance and mechanical outputs computed with an iPhone app: Comparison with existing reference methods,” *Eur. J. Sport Sci.*, pp. 1–7, Nov. 2016.

[16] J. M. Neugebauer *et al*, “Ground reaction force estimates from ActiGraph GT3X+ hip accelerations,” *PLoS ONE*, vol. 9, no. 6, p. e99023, Jun. 2014.

[17] J. M. Neugebauer *et al*, “Estimating youth locomotion ground reaction forces using an accelerometer-based activity monitor,” *PLoS ONE*, vol. 7, no. 10, p. e48182, Oct. 2012.

[18] G. Logar and M. Munih, “Estimation of joint forces and moments for the in-run and take-off in ski jumping based on measurements with wearable inertial sensors,” *Sensors*, vol. 15, no. 5, pp. 11258–11276, May 2015.

[19] A. W. Garcia *et al*, “A comparison of accelerometers for predicting energy expenditure and vertical ground reaction force in school-age children,” *Meas. Phys. Educ. Exerc. Sci.*, vol. 8, no. 3, pp. 119–144, 2004.

[20] A. M. Sabatini, “Estimating three-dimensional orientation of human body parts by inertial/magnetic sensing,” *Sensors*, vol. 11, no. 12, pp. 1489–1525, Jan. 2011.

[21] J. Favre *et al*, “Ambulatory measurement of 3D knee joint angle,” *J. Biomech.*, vol. 41, no. 5, pp. 1029–1035, 2008.

[22] E. Bergamini *et al*, “Trunk inclination estimate during the sprint start using an inertial measurement unit: a validation study,” *J. Appl. Biomech*, vol. 29, no. 5, pp. 622-627, 2013.

[23] D. Jurman *et al*, “Calibration and data fusion solution for the miniature attitude and heading reference system,” *Sens. Actuators Phys.*, vol. 138, no. 2, pp. 411–420, Aug. 2007.

[24] E. Bergamini *et al*, “Estimation of temporal parameters during sprint running using a trunk-mounted inertial measurement unit,” *J. Biomech.*, vol. 45, no. 6, pp. 1123–1126, Apr. 2012.

[25] J. B. Lee *et al*, “The use of a single inertial sensor to identify stride, step, and stance durations of running gait,” *J. Sci. Med. Sport*, vol. 13, no. 2, pp. 270–273, Mar. 2010.

[26] A. J. Wixted *et al*, “Validation of trunk mounted inertial sensors for analysing running biomechanics under field conditions, using synchronously collected foot contact data,” *Sports Eng.*, vol. 12, no. 4, pp. 207–212, 2010.

[27] L. Parrington *et al*, “Validation of inertial measurement units for tracking 100m sprint data.,” *34th Int. Conf. Biomech. Sport*, 2016.

[28] R. S. McGinnis *et al*, “Quantifying the effects of load carriage and fatigue under load on sacral kinematics during countermovement vertical jump with IMU-based method,” *Sports Eng.*, vol. 19, no. 1, pp. 21–34, Mar. 2016.

[29] B. Milosevic and E. Farella, “Wearable inertial sensor for jump performance analysis,” in *Proceedings of the 2015 workshop on Wearable Systems and Applications (WearSys)*, 2015, pp. 15–20.

[30] P. Esser *et al*, “IMU: Inertial sensing of vertical CoM movement,” *J. Biomech.*, vol. 42, no. 10, pp. 1578–1581, Jul. 2009.

[31] R. Howard *et al*, “Estimation of force during vertical jumps using body fixed accelerometers,” in *25th IET Irish Signals Systems Conference 2014 and 2014 China-Ireland International Conference on Information and Communications Technologies (ISSC 2014/CIICT 2014)*, 2014, pp. 102–107.

[32] S. Yang *et al*, “Ambulatory running speed estimation using an inertial sensor,” *Gait Posture*, vol. 34, no. 4, pp. 462–466, Oct. 2011.

[33] N. E. Bezodis *et al*, “Alterations to the orientation of the ground reaction force vector affect sprint acceleration performance in team sports athletes,” *J. Sports Sci.*, pp. 1–8, Oct. 2016.

[34] R. Stanton *et al.*, “Validity of a smartphone-based application for determining sprinting performance,” *J. Sports Med.*, vol. 2016, 2016.

[35] R. Nagahara *et al*, “Kinematics of transition during human accelerated sprinting,” *Biol. Open*, vol. 3, no. 8, pp. 689–699, Aug. 2014.

[36] A. Higashihara *et al*, “Differences in activation properties of the hamstring muscles during overground sprinting,” *Gait Posture*, vol. 42, no. 3, pp. 360–364, Sep. 2015.

[37] A. Nummela *et al*, “EMG activities and ground reaction forces during fatigued and nonfatigued sprinting:,” *Med. Sci. Sports Exerc.*, vol. 26, no. 5, p. 605???609, May 1994.

[38] J. R. Baxter *et al*, “Ankle joint mechanics and foot proportions differ between human sprinters and non-sprinters,” *Proc. R. Soc. B Biol. Sci.*, vol. 279, no. 1735, pp. 2018–2024, May 2012.

[39] S. S. M. Lee and S. J. Piazza, “Built for speed: Musculoskeletal structure and sprinting ability,” *J. Exp. Biol.*, vol. 212, no. 22, pp. 3700–3707, Nov. 2009.

[40] R. Kram *et al*, “Force treadmill for measuring vertical and horizontal ground reaction forces,” *J. Appl. Physiol.*, vol. 85, no. 2, pp. 764–769, Aug. 1998.

[41] P. O. Riley *et al*, “A kinematics and kinetic comparison of overground and treadmill running,” *Med. Sci. Sports Exerc.*, vol. 40, no. 6, pp. 1093–1100, Jun. 2008.

[42] G. J. van Ingen Schenau, “Some fundamental aspects of the biomechanics of overground versus treadmill locomotion,” *Med. Sci. Sports Exerc.*, vol. 12, no. 4, pp. 257–261, 1980.

[43] I. Van Caekenberghe *et al*, “Mechanics of overground accelerated running vs. running on an accelerated treadmill,” *Gait Posture*, vol. 38, no. 1, pp. 125–131, May 2013.

[44] I. Van Caekenberghe *et al*, “Joint kinematics and kinetics of overground accelerated running versus running on an accelerated treadmill,” *J. R. Soc. Interface*, vol. 10, no. 84, pp. 20130222–20130222, May 2013.

[45] M. McKenna and P. E. Riches, “A comparison of sprinting kinematics on two types of treadmill and over-ground: Sprinting kinematics,” *Scand. J. Med. Sci. Sports*, vol. 17, no. 6, pp. 649–655, Mar. 2007.

[46] J.-B. Morin and P. Sève, “Sprint running performance: Comparison between treadmill and field conditions,” *Eur. J. Appl. Physiol.*, vol. 111, no. 8, pp. 1695–1703, Aug. 2011.

[47] J. B. Morin *et al*, “Direct measurement of power during one single sprint on treadmill,” *J. Biomech.*, vol. 43, no. 10, pp. 1970–1975, Jul. 2010.

[48] K. D. Simperingham *et al*, "Advances in sprint acceleration profiling for field-based team-sport athletes: Utility, reliability, validity and limitations," *Sports Med.*, Feb. 2016.

[49] H. K. A. Lakomy, "The use of a non-motorized treadmill for analysing sprint performance," *Ergonomics*, vol. 30, no. 4, pp. 627–637, Apr. 1987.

[50] S. M. Chelly and C. Denis, "Leg power and hopping stiffness: Relationship with sprint running performance:," *Med. Sci. Sports Exerc.*, pp. 326–333, Feb. 2001.

[51] F. Sousa *et al*, "Specific measurement of tethered running kinetics and its relationship to repeated sprint ability," *J. Hum. Kinet.*, vol. 49, pp. 245–256, Dec. 2015.

[52] P. E. di Prampero, "Sprint running: A new energetic approach," *J. Exp. Biol.*, vol. 208, no. 14, pp. 2809–2816, Jul. 2005.

[53] N. I. Volkov and V. I. Lapin, "Analysis of the velocity curve in sprint running," *Med. Sci. Sports*, vol. 11, no. 4, pp. 332–337, 1979.

[54] J.-B. Morin *et al*, "Spring-mass model characteristics during sprint running: Correlation with performance and fatigue-induced changes," *Int. J. Sports Med.*, vol. 27, no. 2, pp. 158–165, Feb. 2006.

[55] N. E. Bezodis *et al*, "Measurement error in estimates of sprint velocity from a laser displacement measurement device," *Int. J. Sports Med.*, vol. 33, no. 6, pp. 439–444, Jun. 2012.

[56] L. M. Arsac and E. Locatelli, "Modeling the energetics of 100-m running by using speed curves of world champions," *J. Appl. Physiol.*, vol. 92, no. 5, pp. 1781–1788, May 2002.

[57] J. Mendiguchia *et al.*, "Progression of mechanical properties during on-field sprint running after returning to sports from a hamstring muscle injury in soccer players," *Int. J. Sports Med.*, vol. 35, no. 08, pp. 690–695, Jan. 2014.

[58] J. Mendiguchia *et al.*, “Field monitoring of sprinting power-force-velocity profile before, during and after hamstring injury: Two case reports,” *J. Sports Sci.*, vol. 34, no. 6, pp. 535–541, Mar. 2016.

[59] J. J. Kavanagh and H. B. Menz, “Accelerometry: A technique for quantifying movement patterns during walking,” *Gait Posture*, vol. 28, no. 1, pp. 1–15, Jul. 2008.

[60] J. Wilson, “Position and motion sensors," in *Sensor Technology Handbook*, W. Kester, Burlington, MA: Elsevier Inc., 2005, ch. 6, pp. 321-409.

[61] W. Liberson, “A new application of quarts piezoelectric: piezoelectrographic walking and voluntary movement," *Hum Work.*, vol. 4, no. 2, pp. 196–202, 1936.

[62] G. Cavagna *et al*, “A three-directional accelerometer for analyzing body movements,” *J. Appl. Physiol.*, vol. 16, p. 191, Jan. 1961.

[63] G. A. Cavagna *et al*, “External work in walking,” *J. Appl. Physiol.*, vol. 18, no. 1, pp. 1–9, Jan. 1963.

[64] D. M. Pober, J. Staudenmayer *et al*, “Development of novel techniques to classify physical activity mode using accelerometers,” *Med. Sci. Sports Exerc.*, vol. 38, no. 9, pp. 1626–1634, Sep. 2006.

[65] S. E. Crouter *et al*, “A novel method for using accelerometer data to predict energy expenditure,” *J. Appl. Physiol. Bethesda Md 1985*, vol. 100, no. 4, pp. 1324–1331, Apr. 2006.

[66] M. del Rosario *et al*, “Tracking the evolution of smartphone sensing for monitoring human movement,” *Sensors*, vol. 15, no. 8, pp. 18901–18933, Jul. 2015.

[67] J. Bort-Roig *et al*, “Measuring and influencing physical activity with smartphone technology: A systematic review,” *Sports Med.*, vol. 44, no. 5, pp. 671–686, May 2014.

[68] S. Nishiguchi *et al.*, "Reliability and validity of gait analysis by Android-based smartphone," *Telemed. E-Health*, vol. 18, no. 4, pp. 292–296, May 2012.

[69] M. Yang *et al*, "Assessing the utility of smart mobile phones in gait pattern analysis," *Health Technol.*, vol. 2, no. 1, pp. 81–88, Apr. 2012.

[70] N. A. Capela *et al*, "Novel algorithm for a smartphone-based 6-minute walk test application: Algorithm, application development, and evaluation," *J. NeuroEngineering Rehabil.*, vol. 12, no. 1, p. 19, 2015.

[71] S. Mehner *et al*, "Location-independent fall detection with smartphone," 2013, pp. 1–8.

[72] M. Habib *et al*, "Smartphone-based solutions for fall detection and prevention: challenges and open issues," *Sensors*, vol. 14, no. 4, pp. 7181–7208, Apr. 2014.

[73] K. Orr *et al.*, "Validity of smartphone pedometer applications," *BMC Res. Notes*, vol. 8, no. 1, Dec. 2015.

[74] K. H. Schütte *et al*, "Wireless tri-axial trunk accelerometry detects deviations in dynamic center of mass motion due to running-induced fatigue," *PLOS ONE*, vol. 10, no. 10, p. e0141957, Oct. 2015.

[75] B. Purcell *et al*, "Use of accelerometers for detecting foot-ground contact time during running," in *Microelectronics, MEMS, and Nanotechnology*, 2005, pp. 603615–603615.

[76] R. Herren *et al*, "The prediction of speed and incline in outdoor running in humans using accelerometry," *Med. Sci. Sports Exerc.*, vol. 31, no. 7, pp. 1053–1059, Jul. 1999.

[77] B. J. Stetter *et al*, "A novel approach to determine strides, ice contact, and swing phases during ice hockey skating using a single accelerometer," *J. Appl. Biomech.*, vol. 32, no. 1, pp. 101–106, Feb. 2016.

[78] J. M. Schedel *et al*, “The biomechanic origin of sprint performance enhancement after one-week creatine supplementation,” *Jpn. J. Physiol.*, vol. 50, no. 2, pp. 273–276, Apr. 2000.

[79] R. S. McGinnis *et al.*, “Skin mounted accelerometer system for measuring knee range of motion,” in *Engineering in Medicine and Biology Society (EMBC), 2016 IEEE 38th Annual International Conference of the*, 2016, pp. 5298–5302.

[80] K. Sato *et al*, “Validation of an accelerometer for measuring sport performance,” *J. Strength Cond. Res. Natl. Strength Cond. Assoc.*, vol. 23, no. 1, pp. 341–347, Jan. 2009.

[81] S. R. Kathleen Janz, “Measuring children’s vertical ground reaction forces with accelerometry during walking, running, and jumping: The Iowa bone development study,” *Human Kinetics Journals*, 21-Apr-2010. [Online]. Available:

[82] A. V. Rowlands and V. H. Stiles, “Accelerometer counts and raw acceleration output in relation to mechanical loading,” *J. Biomech.*, vol. 45, no. 3, pp. 448–454, Feb. 2012.

[83] A. Pouliot-Laforte *et al*, “Validity of an accelerometer as a vertical ground reaction force measuring device in healthy children and adolescents and in children and adolescents with osteogenesis imperfecta type I,” *J Musculoskelet Neuronal Interact*, vol. 14, no. 2, pp. 155–161, 2014.

[84] A. Cerrito *et al*, “Reliability and validity of a smartphone-based application for the quantification of the sit-to-stand movement in healthy seniors,” *Gait Posture*, vol. 41, no. 2, pp. 409–413, Feb. 2015.

[85] E. Bergamini *et al*, “Estimating orientation using magnetic and inertial sensors and different sensor fusion approaches: Accuracy assessment in manual and locomotion tasks,” *Sensors*, vol. 14, no. 10, pp. 18625–18649, Oct. 2014.

[86] A. Lees *et al*, "Understanding how an arm swing enhances performance in the vertical jump," *J. Biomech.*, vol. 37, no. 12, pp. 1929–1940, Dec. 2004.

[87] I. Setuain *et al.*, "Vertical jumping biomechanical evaluation through the use of an inertial sensor-based technology," *J. Sports Sci.*, vol. 34, no. 9, pp. 843–851, May 2016.

[88] H. Halliday *et al*, *Fundamentals of Physics*, 9th ed. Hoboken, NJ: John Wiley & Sons, Inc., 2011.

[89] Carr, Joseph J., *Electronic Circuit Guidebook, Volume 1: Sensors*, vol. 1. Indianapolis, IN: PROMPT Publications, 1997.

[90] J. A. Barraza-Madrigal *et al*, "Posición y orientación instantánea de los segmentos corporales como un objeto arbitrario en el espacio 3D a través de la fusión de la información de acelerómetros y giroscopios," *Rev. Mex. Ing. Bioméd.*, vol. 35, no. 3, pp. 241–252, 2014.

[91] D. T.-P. Fong and Y.-Y. Chan, "The use of wearable inertial motion sensors in human lower limb biomechanics studies: A systematic review," *Sensors*, vol. 10, no. 12, pp. 11556–11565, Dec. 2010.

[92] J. Favre *et al*, "Functional calibration procedure for 3D knee joint angle description using inertial sensors," *J. Biomech.*, vol. 42, no. 14, pp. 2330–2335, Oct. 2009.

[93] J. Favre *et al*, "Quaternion-based fusion of gyroscopes and accelerometers to improve 3D angle measurement," *Electron Lett*, vol. 42, no. 11, pp. 612–614, 2006.

[94] G. Ligorio *et al*, "Assessing the performance of sensor fusion methods: Application to magnetic-inertial-based human body tracking," *Sensors*, vol. 16, no. 2, p. 153, Jan. 2016.

[95] G. Cooper *et al.*, "Inertial sensor-based knee flexion/extension angle estimation," *J. Biomech.*, vol. 42, no. 16, pp. 2678–2685, Dec. 2009.

[96] M. El-Gohary and J. McNames, “Human joint angle estimation with inertial sensors and validation with a robot arm,” *IEEE Trans. Biomed. Eng.*, vol. 62, no. 7, pp. 1759–1767, Jul. 2015.

[97] H. J. Luinge and P. H. Veltink, “Measuring orientation of human body segments using miniature gyroscopes and accelerometers,” *Med. Biol. Eng. Comput.*, vol. 43, no. 2, pp. 273–282, 2005.

[98] C. Mazzà *et al*, “An optimized Kalman filter for the estimate of trunk orientation from inertial sensors data during treadmill walking,” *Gait Posture*, vol. 35, no. 1, pp. 138–142, Jan. 2012.

[99] R. S. McGinnis *et al*, “Validation of complementary filter based imu data fusion for tracking torso angle and rifle orientation,” in *ASME 2014 International Mechanical Engineering Congress and Exposition*, vol. 3, 2014.

[100] A. Brennan *et al*, “Quantification of inertial sensor-based 3D joint angle measurement accuracy using an instrumented gimbal,” *Gait Posture*, vol. 34, no. 3, pp. 320–323, Jul. 2011.

[101] F. Buganè *et al*, “Estimation of pelvis kinematics in level walking based on a single inertial sensor positioned close to the sacrum: Validation on healthy subjects with stereophotogrammetric system,” *Biomed. Eng. Online*, vol. 13, no. 1, p. 146, 2014.

[102] H. Rouhani *et al*, “Measurement of multi-segment foot joint angles during gait using a wearable system,” *J. Biomech. Eng.*, vol. 134, no. 6, p. 061006, 2012.

[103] H. J. Luinge *et al*, “Ambulatory measurement of arm orientation,” *J. Biomech.*, vol. 40, no. 1, pp. 78–85, Jan. 2007.

[104] I. Skog and P. Händel, “Calibration of a MEMS inertial measurement unit,” in *XVII IMEKO World Congress*, Nov. 2006, pp. 1–6.

[105] S. P. Davidson *et al*, “Quantifying warfighter performance in a target acquisition and aiming task using wireless inertial sensors,” *Appl. Ergon.*, vol. 56, pp. 27–33, Sep. 2016.

[106] D. E. Lidstone *et al*, “Physiological and biomechanical responses to prolonged heavy load carriage during level treadmill walking in females,” *J. Appl. Biomech.*, pp. 1–27, Jan. 2017.

[107] S. M. Cain *et al*, “Quantifying performance and effects of load carriage during a challenging balancing task using an array of wireless inertial sensors,” *Gait Posture*, vol. 43, pp. 65–69, Jan. 2016.

[108] R. McGinnis and N. Perkins, “A highly miniaturized, wireless inertial measurement unit for characterizing the dynamics of pitched baseballs and softballs,” *SENSORS*, vol. 12, no. 9, pp. 11933–11945, Sep. 2012.

[109] J. B. Lee *et al*, “Identifying symmetry in running gait using a single inertial sensor,” *J. Sci. Med. Sport*, vol. 13, no. 5, pp. 559–563, Sep. 2010.

[110] W. L. Boehm and K. G. Gruben, “Post-stroke walking behaviors consistent with altered ground reaction force direction control advise new approaches to research and therapy,” *Transl. Stroke Res.*, vol. 7, no. 1, pp. 3–11, Feb. 2016.

[111] C. L. Christiansen *et al*, “Weight-bearing asymmetry during sit-stand transitions related to impairment and functional mobility after total knee arthroplasty,” *Arch. Phys. Med. Rehabil.*, vol. 92, no. 10, pp. 1624–1629, 2011.

[112] E. Kowalski and J. X. Li, “Lower limb joint angles and ground reaction forces in forefoot strike and rearfoot strike runners during overground downhill and uphill running,” *Sports Biomech.*, vol. 0, no. 0, pp. 1–16, Jun. 2016.

[113] G. Condello *et al*, “Biomechanical analysis of a change-of-direction task in college soccer players,” *Int. J. Sports Physiol. Perform.*, vol. 11, no. 1, pp. 96–101, Jan. 2016.

[114] D. W. T. Wundersitz *et al*, “Validity of an upper-body-mounted accelerometer to measure peak vertical and resultant force during running and change-of-direction tasks,” *Sports Biomech.*, vol. 12, no. 4, pp. 403–412, Nov. 2013.

[115] A. Krüger *et al*, “Determination of three-dimensional joint loading within the lower extremities in snowboarding,” *Proc. Inst. Mech. Eng. [H]*, vol. 226, no. 2, pp. 170–175, Feb. 2012.

[116] A. S. Jackson and M. L. Pollock, “Practical assessment of body composition,” *Phys. Sportsmed.*, vol. 13, no. 5, pp. 76–90, May 1985.

[117] R. E. Ostlund *et al*, “Relation between plasma leptin concentration and body fat, gender, diet, age, and metabolic covariates,” *J. Clin. Endocrinol. Metab.*, vol. 81, no. 11, pp. 3909–3913, Nov. 1996.

[118] R. Chakraverty *et al*, “Which spinal levels are identified by palpation of the iliac crests and the posterior superior iliac spines?,” *J. Anat.*, vol. 210, no. 2, pp. 232–236, Feb. 2007.

[119] H. Myklebust *et al*, “Validity of ski skating center-of-mass displacement measured by a single inertial measurement unit,” *J. Appl. Biomech.*, vol. 31, no. 6, pp. 492–498, Dec. 2015.

[120] L. G. Portney and M. P. Watkins, *Foundations of Clinical Research: Applications to Practice*, 2nd ed. Upper Saddle River, NJ: Prentice-Hall, Inc., 2000.

[121] D. Giavarina, “Understanding Bland Altman analysis,” *Biochem. Medica*, vol. 25, no. 2, pp. 141–151, 2015.

[122] J. Mercer *et al*, “Relationship between shock attenuation and stride length during running at different velocities,” *Eur. J. Appl. Physiol.*, vol. 87, no. 4–5, pp. 403–408, Jan. 2002.

[123] S. T. Jamison *et al*, “The effects of core muscle activation on dynamic trunk position and knee abduction moments: Implications for ACL injury,” *J. Biomech.*, vol. 46, no. 13, pp. 2236–2241, Sep. 2013.

[124] R. Wang *et al.*, “Isometric mid-thigh pull correlates with strength, sprint and agility performance in collegiate rugby union players,” *J. Strength Cond. Res. Natl. Strength Cond. Assoc.*, Mar. 2016.

[125] R. G. Lockie *et al*, “The effects of different speed training protocols on sprint acceleration kinematics and muscle strength and power in field sport athletes,” *J. Strength Cond. Res.*, vol. 26, no. 6, pp. 1539–1550, 2012.

[126] G. Roe *et al*, “Validity of 10 Hz GPS and timing gates for assessing maximum velocity in professional rugby union players,” *Int. J. Sports Physiol. Perform.*, pp. 1–14, Oct. 2016.

[127] M. Waldron *et al*, “Concurrent validity and test–retest reliability of a global positioning system (GPS) and timing gates to assess sprint performance variables,” *J. Sports Sci.*, vol. 29, no. 15, pp. 1613–1619, Dec. 2011.

[128] C. Petersen *et al*, “Validity and reliability of GPS units to monitor cricket-specific movement patterns,” *Int J Sports Physiol Perform*, vol. 4, no. 3, pp. 381–393, 2009.

[129] M. C. Varley *et al*, “Validity and reliability of GPS for measuring instantaneous velocity during acceleration, deceleration, and constant motion,” *J. Sports Sci.*, vol. 30, no. 2, pp. 121–127, Jan. 2012.

[130] G. Seco-Granados *et al*, “Challenges in Indoor Global Navigation Satellite Systems: Unveiling its core features in signal processing,” *IEEE Signal Process. Mag.*, vol. 29, no. 2, pp. 108–131, Mar. 2012.

[131] S. Godha and G. Lachapelle, “Foot mounted inertial system for pedestrian navigation,” *Meas. Sci. Technol.*, vol. 19, no. 7, p. 075202, Jul. 2008.

[132] J. B. Lee *et al*, “Inertial sensor, 3D and 2D assessment of stroke phases in freestyle swimming,” *Procedia Eng.*, vol. 13, pp. 148–153, 2011.

[133] W. H. K. de Vries *et al*, “Magnetic distortion in motion labs, implications for validating inertial magnetic sensors,” *Gait Posture*, vol. 29, no. 4, pp. 535–541, Jun. 2009.

[134] Y. Tian *et al*, “Accurate human navigation using wearable monocular visual and inertial sensors,” *IEEE Trans. Instrum. Meas.*, vol. 63, no. 1, pp. 203–213, Jan. 2014.

[135] A. Atrsaei *et al*, “Human arm motion tracking by orientation-based fusion of inertial sensors and kinect using unscented Kalman filter,” *J. Biomech. Eng.*, vol. 138, no. 9, p. 091005, 2016.

[136] J. B. Kuipers, *Quaternions and Rotation Sequences*. Princeton, NJ: Princeton University Press, 1999.

[137] J. A. Nichols *et al*, “Decoupling the wrist: A cadaveric experiment examining wrist kinematics following midcarpal fusion and scaphoid excision,” *J. Appl. Biomech.*, pp. 1–29, Oct. 2016.

[138] M. R. Cross *et al*, “Methods of power-force-velocity profiling during sprint running: A narrative review,” *Sports Med.*, pp. 1-15, Nov. 2016.

[139] R. H. Miller *et al*, “Limitations to maximum sprinting speed imposed by muscle mechanical properties,” *J. Biomech.*, vol. 45, no. 6, pp. 1092–1097, Apr. 2012.

[140] P. Samozino *et al*, “Optimal force–velocity profile in ballistic movements–Altius,” *Med. Sci. Sports Exerc.*, vol. 44, no. 2, pp. 313–322, Feb. 2012.

[141] M. Buchheit *et al.*, “Mechanical determinants of acceleration and maximal sprinting speed in highly trained young soccer players,” *J. Sports Sci.*, vol. 32, no. 20, pp. 1906–1913, Dec. 2014.

[142] J. Yu *et al.*, “The biomechanical insights into differences between the mid-acceleration and the maximum velocity phase of sprinting:,” *J. Strength Cond. Res.*, p. 1, Nov. 2015.

[143] A. Karatsidis *et al*, “Estimation of ground reaction forces and moments during gait using only inertial motion capture,” *Sensors*, vol. 17, no. 1, p. 75, Dec. 2016.

[144] J. M. Bland and D. G. Altman, “Agreement between methods of measurement with multiple observations per individual,” *J. Biopharm. Stat.*, vol. 17, no. 4, pp. 571–582, 2007.

[145] P. G. Weyand *et al*, “The biological limits to running speed are imposed from the ground up,” *J. Appl. Physiol.*, vol. 108, no. 4, pp. 950–961, Apr. 2010.

[146] M. Brughelli *et al*, “Effects of running velocity on running kinetics and kinematics,” *J. Strength Cond. Res.*, vol. 25, no. 4, pp. 933–939, 2011.

[147] R. S. McGinnis *et al*, “Inertial sensor and cluster analysis for discriminating agility run technique,” *IFAC-Pap.*, vol. 48, no. 20, pp. 423–428, Jan. 2015.

Appendix A: Quaternion Notation and Vector Rotations

For the studies described in Chapters 3 – 4, the anatomical frame (F_A), inertial world frame (F_w) (i.e the force plate frame in Chapter 3 and the track frame in Chapters 4 and 5), and sensor frame (F_S) are all right-handed and defined by the following axes (see Figure 4.1): $\hat{x}$ (anterior-posterior with the positive direction pointing forward), $\hat{y}$ (medial-lateral with the positive direction pointing left), and $\hat{z}$ (up-down with the positive direction pointing up). Vectors are denoted with bold lettering and the coordinate frame in which it is being referenced is given as a superscript (e.g., $\boldsymbol{u}_i^j$ refers to vector $\boldsymbol{u}_i$ measured in frame *j*). Finally, an *a priori* estimate of some variable *u* is denoted with the superscript u^-.

Any two unaligned frames may be aligned by a single rotation through an angle γ about an axis $\boldsymbol{U}$ (Figure 4.1) [136]. The quaternion (Q_γ) describing this orientation may be constructed using γ and $\boldsymbol{U}$ (given that $\boldsymbol{U}$ is of unit length) by [136]:

$$Q_\gamma = [q_0\ q_1\ q_2\ q_3]^T = \begin{bmatrix} cos\left(\frac{\gamma}{2}\right) \\ sin\left(\frac{\gamma}{2}\right)\boldsymbol{U} \end{bmatrix} \tag{A.1}$$

where $q_0 = cos\left(\frac{\gamma}{2}\right)$ is called the scalar part of the quaternion, $[q_1\ q_2\ q_3]^T = sin\left(\frac{\gamma}{2}\right)\boldsymbol{U}$ is called the vector part of the quaternion (denoted by $\boldsymbol{q}_v$), and the superscript T denotes the transpose operator. The quaternion product of any two quaternions, say *L* and *P* (denoted by $L \otimes P$), is defined as [136]:

$$L = [l_0\ \boldsymbol{l}_v]^T \tag{A.2}$$

$$P = [p_0\ \boldsymbol{p}_v]^T$$

$$L \otimes P = l_0 p_0 - \boldsymbol{l}_v \cdot \boldsymbol{p}_v + p_0 \boldsymbol{l}_v + q_0 \boldsymbol{l}_v + \boldsymbol{l}_v \times \boldsymbol{p}_v.$$

where $\cdot$ and $\times$ represent the scalar and cross products respectively. If Q_γ represents the orientation of F_S relative to F_w (that is if the axis and angle of Q_γ describe the composite rotation

that would align F_w with F_S), then any arbitrary vector measured in F_S ($\boldsymbol{u}^S$) may be expressed in terms of F_w ($\boldsymbol{u}^w$) by rotating F_S to be aligned with F_w according to [136]:

$$\boldsymbol{u}^w = Q_\gamma \otimes \boldsymbol{u}^S \otimes Q_\gamma^* \tag{A.3}$$

where Q_γ^* is the quaternion conjugate defined by $Q_\gamma^* = [q_0 \quad -\boldsymbol{q}_v]^T$ [136]. The rotation of $\boldsymbol{u}^S$ to $\boldsymbol{u}^w$ by Q_γ is the result in eq. (A.3) only if Q_γ is of unit length, which is the case as long as the axis of rotation used to construct Q_γ , $\boldsymbol{U}$ in eq. (A.1), is a unit vector [136]. The quaternion may be used to parametrize a rotation matrix (R), the construction of which is derived from eqs. (A.2) and (A.3). All vector rotations were performed using R according to [20, 136]:

$$\boldsymbol{u}^w = R\boldsymbol{u}^S \tag{A.4}$$

where:

$$R = \begin{bmatrix} q_0^2 + q_x^2 - q_y^2 - q_z^2 & 2(q_x q_y - q_z q_0) & 2(q_x q_z + q_y q_0) \\ 2(q_x q_y + q_z q_0) & q_0^2 - q_x^2 + q_y^2 - q_z^2 & 2(q_y q_z - q_x q_0) \\ 2(q_x q_z - q_y q_0) & 2(q_y q_z + q_x q_0) & q_0^2 - q_x^2 - q_y^2 + q_z^2 \end{bmatrix} \tag{A.5}$$

Instead of describing the orientation according to the single composite rotation Q_γ, one may also consider the following two successive rotations: first through an angle α about the F_w vertical axis ($\hat{z}_w = [0\ 0\ 1]^T$) (denoted by Q_α) followed by a second rotation through an angle β about an axis of unit length ($\boldsymbol{H}$) in the F_w horizontal plane (denoted by Q_β) such that:

$$Q_\alpha = \begin{bmatrix} cos\left(\frac{\alpha}{2}\right) \\ sin\left(\frac{\alpha}{2}\right)\hat{z}_w \end{bmatrix} \tag{A.6}$$

and:

$$Q_\beta = \begin{bmatrix} cos\left(\frac{\beta}{2}\right) \\ sin\left(\frac{\beta}{2}\right)\boldsymbol{H} \end{bmatrix} \tag{A.7}$$

Then α represents the IMU heading (angular deviation of the F_S and F_w horizontal plane axes when their vertical axes are aligned) and β represents the IMU attitude (angular deviation of the F_S and F_w vertical axes). The composite quaternion Q_γ is related to Q_α and Q_β by [136]:

$$Q_\gamma = Q_\alpha \otimes Q_\beta \tag{A.8}$$

The first estimate of the IMU orientation during the sprint is obtained by strapdown integration of the gyroscope angular rate signal starting from some initial orientation. Measurements during a static interval from the IMU magnetometer and accelerometer provide an estimate of the initial IMU heading and attitude respectively and thus the initial conditions from which gyroscope integration may begin. First, the accelerometer measurement of the gravity vector, which represents the coordinates of the F_w vertical axis in the IMU frame ($\hat{z}_w^S$), is used to determine the IMU attitude β by [93]:

$$\beta = \text{acos}(\hat{z}_w^S) \tag{A.9}$$

According to eq. (A.7), if one knows the axis $\boldsymbol{H}$ in the horizontal plane about which the sensor may have been rotated to assume this attitude, one can determine the quaternion Q_β. This axis $\boldsymbol{H}$ lies orthogonal to the plane defined by $\hat{z}_w^S$ and $\hat{z}_w^S$ and is thus given by the cross product [93]:

$$\boldsymbol{H} = \frac{\hat{z}_w^S \times \hat{z}_s^S}{\left\| \hat{z}_w^S \times \hat{z}_s^S \right\|} \tag{A.10}$$

The normalization in eq. (A.10) is necessary to make the quaternion Q_β of unit length. The local magnetic field vector ($\boldsymbol{B}$) can be used to estimate the heading of the IMU because $\boldsymbol{B}$ has a component in the horizontal plane of F_w [23]. First, the rotation matrix R_β constructed using the quaternion Q_β as in eq. (A.5) rotates the measurement of $\boldsymbol{B}$ in F_S ($\boldsymbol{B}^S$) to the horizontal plane ($\boldsymbol{B}_H$) according to:

$$\boldsymbol{B}_H = R_\beta \, \boldsymbol{B}^S \tag{A.11}$$

The x and y components of $\boldsymbol{B}_H$ ($B_{H,x}$ and $B_{H,y}$ respectively) then allow the determination of the IMU heading (α) relative to $\boldsymbol{B}_H$ by [23]:

$$\alpha = -atan2\left(\frac{B_{H,y}}{B_{H,x}}\right) \tag{A.12}$$

where $atan2$ returns the four-quadrant inverse tangent [106]. By eq. (A.6) and because eq. (A.12) provides the initial IMU heading estimate α, one may construct the quaternion Q_α. Then, because the quaternions Q_α and Q_β are known, one may estimate the initial IMU orientation at the beginning of the movement (i.e., the quaternion Q_γ) according to eq. (A.8). The estimate of the orientation at each instant k ($Q_{\gamma,k}$) during the movement is computed using the IMU gyroscope signal. The IMU's angular rate vector ($\boldsymbol{\omega}_S^S$) along with the time differential (dt) between two instants k and $k+1$ ($dt = t_{k+1} - t_k$) may be used to construct the incremental quaternion T_k that brings the IMU from the orientation at one instant ($Q_{\gamma,k}$) to the next ($Q_{\gamma,k+1}$) by [20, 136]:

$$T_k = \begin{bmatrix} \cos\left(\frac{\|\boldsymbol{\omega}_S^S\| dt}{2}\right) \\ sin\left(\frac{\|\boldsymbol{\omega}_S^S\| dt}{2}\right) \frac{\boldsymbol{\omega}_S^S}{\|\boldsymbol{\omega}_S^S\|} \end{bmatrix} \tag{A.13}$$

$$Q_{\gamma,k+1} = Q_{\gamma,k} \otimes T_k.$$

This provides an initial estimate of the IMU orientation throughout the entire movement.

Appendix B: Decomposition of Composite Quaternion

In Chapter 4, the first correction on the IMU estimate was given by assumption (I.); the heading of the runner (α) throughout the entire sprint should be mean 0. The first estimate of the quaternion, obtained by direct integration (see Appendix A), at any instant k during the sprint ($Q_{\gamma,k}^{-}$) is decomposed into two quaternions, $Q_{\beta,k}$ and $Q_{\alpha,k}^{-}$, such that $Q_{\gamma,k}^{-}$ is given by their quaternion product as shown in eq. (B.2). The derivation of the general decomposition may be found in [136] and will be given here in the context of utilizing the correction of assumption (I.). Let:

$$Q_\beta = b_0 + b_1\hat{\imath} + b_2\hat{\jmath} + b_3\hat{k} = \begin{bmatrix} cos\left(\frac{\beta}{2}\right) \\ sin\left(\frac{\beta}{2}\right)\boldsymbol{H} \end{bmatrix} \tag{B.1}$$

$$Q_\alpha^{-} = a_0 + a_1\hat{\imath} + a_2\hat{\jmath} + a_3\hat{k} = \begin{bmatrix} cos\left(\frac{\alpha^{-}}{2}\right) \\ sin\left(\frac{\alpha^{-}}{2}\right)\hat{z}_{\boldsymbol{w}} \end{bmatrix}$$

$$Q_\gamma^{-} = Q_\alpha^{-} \otimes Q_\beta = q_0 + q_1\hat{\imath} + q_2\hat{\jmath} + q_3\hat{k} = \begin{bmatrix} cos\left(\frac{\gamma^{-}}{2}\right) \\ sin\left(\frac{\gamma^{-}}{2}\right)\boldsymbol{U} \end{bmatrix}$$

Recall that Q_β has an axis of rotation ($\boldsymbol{H}$) in the horizontal plane ($\therefore b_3 = 0$) and that of Q_α^{-} is the vertical axis of F_T ($\hat{z}_{\boldsymbol{T}}$) ($\therefore a_1, a_2 = 0$). Thus:

$$Q_\beta = b_0 + b_1\hat{\imath} + b_2\hat{\jmath} \tag{B.2}$$

$$Q_\alpha^{-} = a_0 + a_3\hat{k}$$

The quaternion product yields:

$$Q_\alpha^{-} \otimes Q_\beta = a_0b_0 + (a_0b_1 - b_2a_3)\hat{\imath} + (a_0b_2 + b_1a_3)\hat{\jmath} + (b_0a_3)\hat{k} \tag{B.3}$$

and thus by eqs. (B.1) and (B.3):

$$q_0 = a_0 b_0 \tag{B.4}$$

$$q_1 = a_0 b_1 - b_2 a_3$$

$$q_2 = a_0 b_2 + b_1 a_3$$

$$q_3 = b_0 a_3$$

or in matrix form:

$$\begin{bmatrix} q_0 \\ q_3 \end{bmatrix} = A \begin{bmatrix} b_0 \\ 0 \end{bmatrix} \tag{B.5}$$

$$\begin{bmatrix} q_1 \\ q_2 \end{bmatrix} = A \begin{bmatrix} b_1 \\ b_2 \end{bmatrix}$$

$$A = \begin{bmatrix} a_0 & -a_3 \\ a_3 & a_0 \end{bmatrix}.$$

The inverse of A is its transpose and thus:

$$\begin{bmatrix} b_0 \\ 0 \end{bmatrix} = \begin{bmatrix} a_0 & a_3 \\ -a_3 & a_0 \end{bmatrix} \begin{bmatrix} q_0 \\ q_3 \end{bmatrix} \tag{B.6}$$

$$\begin{bmatrix} b_1 \\ b_2 \end{bmatrix} = \begin{bmatrix} a_0 & a_3 \\ -a_3 & a_0 \end{bmatrix} \begin{bmatrix} q_1 \\ q_2 \end{bmatrix}$$

which gives:

$$b_0 = a_0 q_0 + q_3 a_3 \tag{B.7}$$

$$0 = -q_0 a_3 + q_3 a_0$$

$$b_1 = a_0 q_1 + a_3 q_2$$

$$b_2 = -q_1 a_3 + q_2 a_0$$

Because Q_α^- describes a rotation through an angle α^-about the F_T vertical axis, the scalar part (a_0) and vector part (in this case a_3) are:

$$a_0 = cos\left(\frac{\alpha^-}{2}\right) \tag{B.8}$$

$$a_3 = sin\left(\frac{\alpha^-}{2}\right)$$

From eq. (B.7):

$$\frac{q_3}{q_0} = \frac{a_3}{a_0} \tag{B.9}$$

and because Q_γ^- is given from direct integration, by substituting eq. (B.8) into eq. (B.9) one can solve for the unknown α^-:

$$\alpha^- = atan\left(\frac{q_3}{q_0}\right) \tag{B.10}$$

and also Q_α^- by eq. (B.1). Then, by substituting eq. (B.10) and eq. (B.8) into eq. (B.7) one can obtain the unknowns b_0, b_1, and b_2, which allows the construction of the quaternion Q_β by eq. (B.1). Thus, given only the composite quaternion, one is able to derive the quaternions describing the heading and attitude of the IMU relative to the track frame.

Appendix C: IMU Calibration

Before data collection the accelerometer and magnetometer of the IMUs were calibrated according to a similar method used by Jurman et al. [23]. For the accelerometer, each sensor was placed in 24 different static orientations (four orientations differing by 90° rotations about the axis orthogonal to each of the six sides). For each orientation, 450 samples were acquired (one second). For the magnetometer, the sensor was rotated about each axis multiple times at a fixed location where the local magnetic field vector is constant for two minutes. The IMU determined resultant normalized acceleration in each of the 24 static orientations (u_s) should be one, representative of the world frame reference value (u^w) of gravity (1 g = 9.81 m/s^2). The normalized resultant magnetic field magnitude should also be one during the entire two-minute rotation trial for the magnetometer calibration, representative of the earth's magnetic field. The IMU vectors will be corrected by the bias vector ($\boldsymbol{b}$), rotated by an orthogonalization matrix (O) to compensate for the non-orthogonality of the sensor axes, and scaled by the sensitivity matrix (C) before the resultant magnitude is determined according to the following:

$$u^s = \|C \cdot O \cdot (\boldsymbol{u}^w - \boldsymbol{b})\| \tag{C.1}$$

$$O = \begin{bmatrix} 1 & 0 & 0 \\ \cos(\alpha_{xy}) & 1 & \cos(\alpha_{zy}) \\ \cos(\alpha_{xz}) & \cos(\alpha_{yz}) & 1 \end{bmatrix}, C = \begin{bmatrix} c_x & 0 & 0 \\ 0 & c_y & 0 \\ 0 & 0 & c_z \end{bmatrix}, \quad \boldsymbol{b} = \begin{bmatrix} b_x \\ b_y \\ b_z \end{bmatrix}$$

where α_{ij} is the angle between the i^{th} and j^{th} axes of the internal sensor, c_i is the scaling factor for the i^{th} axis, and b_i is the magnitude of bias for the i^{th} axis. The mean square error between u^s and

u^w for each orientation will serve as the objective function (M) to be minimized:

$$M = \frac{1}{n}\sum_{i=1}^{n}(u^w - u_i^s)^2 \tag{C.2}$$

The parameters of O, C, and $\boldsymbol{b}$ will be determined by unconstrained minimization of M. The initial guess for the parameters will be chosen such that O and C are both the 3x3 identity matrix and $\boldsymbol{b}$ is the zero vector.

Three Yost IMUs (Yost01, Yost02, Yost03) were used in the studies described in Chapters 3, 4, and 5. The results of the calibration trials are shown below.

Table C.1: Accelerometer and magnetometer calibration parameters for IMU Yost01

	Accelerometer	Magnetometer
c_x	1.0123	0.9836
c_y	0.9856	1.0025
c_z	0.9851	1.0386
α_{xy}	90.5032	89.8065
α_{zy}	91.0358	90.0603
α_{xz}	96.6318	92.3539
α_{yz}	91.0358	90.0603
b_x	0.0002	-0.0142
b_y	-0.0248	-0.029
b_z	-0.0567	-0.012

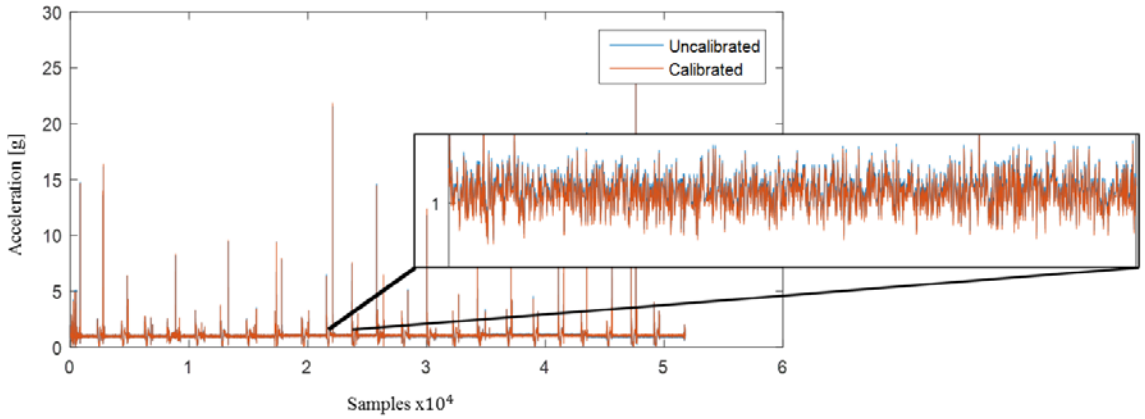

Figure C.1: Calibration of Yost01 accelerometer. The blue line is uncalibrated acceleration and the orange line is calibrated. The correct value should be one.

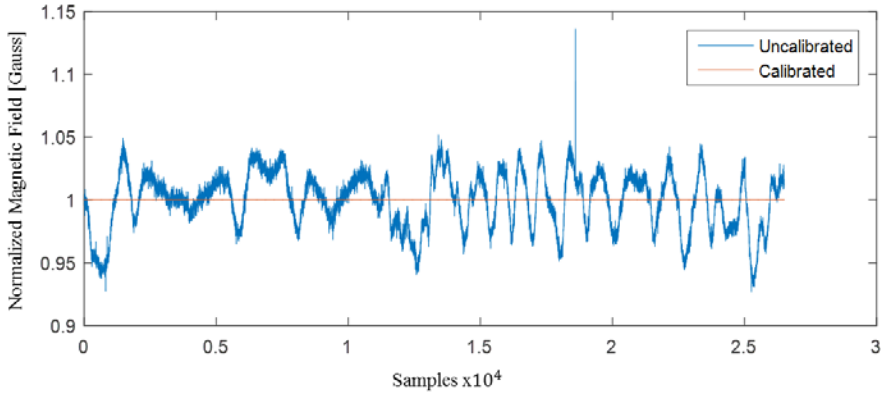

Figure C.2: Calibration of Yost01 magnetometer. The blue line is uncalibrated magnetometer output and the orange line is calibrated. The correct value should be one.

Table C.2: Accelerometer and magnetometer calibration parameters for IMU Yost02

	Accelerometer	Magnetometer
c_x	0.9927	1.0101
c_y	1.0074	1.0185
c_z	1.0231	1.0252
α_{xy}	90	90.7202
α_{zy}	90	88.9039
α_{xz}	90	90.3579
α_{yz}	90	88.9039
b_x	0.019	-0.0905
b_y	-0.0179	0.2285
b_z	-0.0338	-0.1544

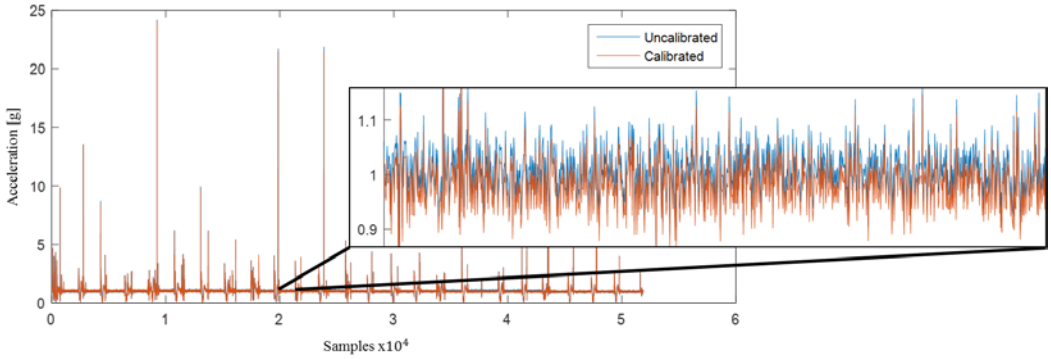

Figure C.3: Calibration of Yost02 accelerometer. The blue line is uncalibrated acceleration and the orange line is calibrated. The correct value should be one.

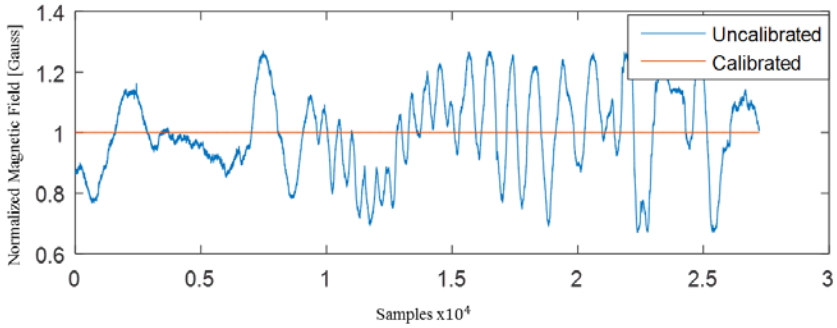

Figure C.4: Calibration of Yost02 magnetometer. The blue line is uncalibrated magnetometer output and the orange line is calibrated. The correct value should be one.

Table C.3: Accelerometer and magnetometer calibration parameters for IMU Yost03

	Accelerometer	Magnetometer
c_x	0.9945	0.9808
c_y	0.9865	1.0153
c_z	0.9883	1.0268
α_{xy}	94.3797	91.825
α_{zy}	88.8102	89.6357
α_{xz}	95.5681	91.7819
α_{yz}	88.8116	89.6356
b_x	-0.0017	-0.0169
b_y	0.0067	-0.0076
b_z	-0.0201	-0.0134

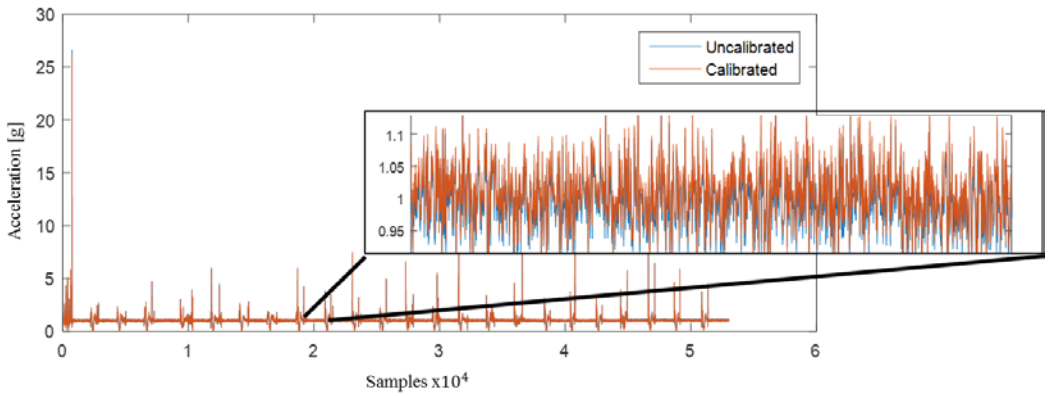

Figure C.5: Calibration of Yost03 accelerometer. The blue line is uncalibrated acceleration and the orange line is calibrated. The correct value should be one.

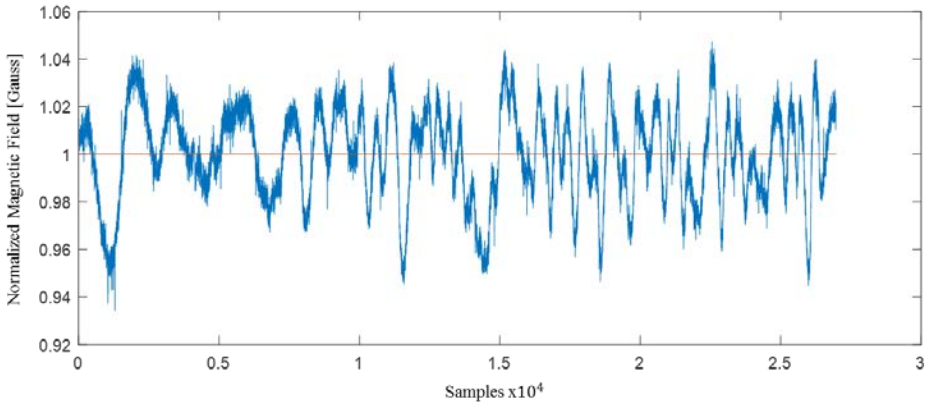

Figure C.6: Calibration of Yost03 magnetometer. The blue line is uncalibrated magnetometer output and the orange line is calibrated. The correct value should be one.

Vita

Reed Donovan Gurchiek was born in Nashville, Tennessee, to David and Donna Gurchiek. He graduated from Mount Juliet High School in Tennessee in June 2010. He entered Cumberland University to study Exercise Science in August 2010 and was awarded the Bachelor of Science degree in May 2015 with a minor in Mathematics. In the fall of 2015, he accepted a research assistantship in Exercise Science at Appalachian State University and began study toward a Master of Science degree. The M.S. was awarded May 2018.

Reed resides in Boone, NC with his wife and son and is finishing a second M.S. degree in Engineering Physics.